Title
Oriented Attachment of Cytochrome P450 2C9 to a Self-Assembled Monolayer on a Gold Electrode as a Biosensor Design

Author
Schneider, Elizabeth

Publication Date
2011

Peer reviewed|Thesis/dissertation

Oriented Attachment of Cytochrome P450 2C9 to a Self-Assembled Monolayer on a Gold Electrode as a Biosensor Design

by

Elizabeth Ann Schneider

A dissertation submitted in partial satisfaction of the

requirements for the degree of

Joint Doctor of Philosophy

with the University of California, San Francisco

in Bioengineering

in the

Graduate Division

of the

University of California, Berkeley

Committee in charge:

Professor Douglas S. Clark, Chair
Associate Professor Shuvo Roy
Professor Liwei Lin
Dr. Robert Kostecki

Fall 2011

Abstract

Oriented Attachment of Cytochrome P450 2C9 to a Self-Assembled Monolayer on a Gold Electrode as a Biosensor Design

by

Elizabeth Ann Schneider

Doctor of Philosophy in Bioengineering

University of California, Berkeley

Professor Douglas S. Clark, Chair

Cytochrome P450s (CYPs) are a family of enzymes implicated in the metabolism of drugs in the body. Consequently, P450 reactions are of high interest to the pharmaceutical industry, where lead compounds in drug development are screened as potential substrates of CYPs. The P450 reaction involves electron transfer to an iron heme via NADPH and the electron transfer partner enzyme P450 reductase (CPR). By immobilizing CYPs on an electrode however, NADPH and CPR are potentially no longer needed and the immobilized CYP can act as a biosensor by accepting electrons directly from the electrode. Such a biosensor could be used as an initial screening tool for CYP reactivity of pharmaceuticals in development. In this study, the drug-metabolizing enzyme CYP 2C9 was immobilized to a self-assembled monolayer (SAM) on a gold electrode in three different orientations to investigate the effect that orientation has on the direct electrochemistry of CYP and to evaluate oriented attachment of CYP to an electrode as a biosensor design. Three attachment methods were investigated: random attachment via amine coupling to a carboxy-terminated SAM, oriented attachment via C-terminal His-tag coupling to a Ni-NTA-functionalized SAM, and oriented attachment via maleimide/thiol coupling to a maleimide-functionalized SAM. Three 2C9 mutants (R125C, R132C, and K432C) were developed with a single cysteine mutation at the binding site for CPR on the side of the enzyme closest to the heme; attachment of these mutants to a gold electrode via maleimide/thiol coupling would orient the enzyme such that electron transfer occurs on the electrode in the same orientation that it does *in vivo* with CPR. Therefore, we expected oriented attachment via maleimide/thiol coupling to produce the most electroactive CYP biosensor. Electrochemical analysis and surface characterization of the SAMs on gold electrodes confirmed that electron transfer occurs through the SAMs, and activity assays of the 2C9 electrodes confirmed that wild-type 2C9 and the single Cys mutants R125C, R132C, and K432C were immobilized to the gold electrode via all three attachment methods. Cyclic voltammetry of the 2C9 electrodes revealed however, that direct electron transfer to 2C9 was not possible for all three attachment methods. Similar redox processes were observed for both the 2C9 electrodes and no-enzyme electrodes modified only with SAMs, suggesting that the redox process observed on the 2C9 electrodes is related to the underlying SAM. Thus, we were unable to make any conclusions regarding the effectiveness of oriented attachment in creating a 2C9 biosensor. However, to our knowledge, there are no examples in the literature of the oriented attachment of 2C9 to an electrode via coupling of an engineered cysteine to a maleimide-functionalized SAM on gold and therefore this study represents the first attempt towards such an electrode system.

This dissertation is dedicated to the power

of the mind to overcome adversity.

TABLE OF CONTENTS

List of Figures iv

List of Tables vii

Chapter 1
Cytochrome P450 Enzymes and the Development of CYP Biosensors 1

1.1 Introduction 1
1.2 Electrode Immobilization Strategies 3
1.2.1 Adsorption to Bare Electrodes 4
1.2.2 Layer-by-Layer Adsorption 6
1.2.3 Adsorption to Thin Films 7
1.2.4 Screen-printed Electrodes 9
1.2.5 Encapsulation in Polymers or Gels 10
1.2.6 Covalent Attachment to Self-Assembled Monolayers (SAMs) on Gold 11
1.3 Characterization of CYP Electrodes 14
1.4 Future Directions 16
1.5 Conclusion 17
1.6 References 19

Chapter 2
Development and Characterization of the Cytochrome P450 2C9 Mutants R125C, R132C, and K432C for Oriented Attachment to a Gold Electrode 25

2.1 Introduction 25
2.2 Materials and Methods 28
2.2.1 Materials 28
2.2.2 Methods 28
2.3 Results and Discussion 32
2.3.1 Expression and Purification of Wild-type CYP2C9 and Mutants 32
2.3.2 Enzyme Activity Assays with Vivid® BOMCC 37
2.3.3 Substrate Binding Difference Spectra with Tolbutamide 40
2.3.4 Kinetic Activity Assays with Tolbutamide 43
2.3.5 Conjugation with Texas Red® C2 Maleimide 45
2.4 Conclusion 49
2.5 References 51

Chapter 3
Surface Characterization and Electrochemical Analysis of Cytochrome P450 2C9 Immobilized to a Self-Assembled Monolayer on a Gold Electrode 55

3.1 Introduction 55
3.2 Materials and Methods 57
3.2.1 Materials 57

3.2.2 Methods 58
3.3 Results and Discussion 63
3.3.1 Surface Characterization of Gold Electrodes 63
3.3.2 Surface Characterization of MPA and Cystamine SAMs on Gold 65
3.3.3 Reaction of Sulfo-SMCC and N-Succinimidyl-3-maleimidopropionate with BODIPY® FL-L-cystine 67
3.3.4 Enzyme Activity of 2C9 Electrodes with Vivid® BOMCC 69
3.3.5 FT-IR Characterization 70
3.3.6 Cyclic Voltammetry of Ferrocene on MPA and Cystamine SAMs on Gold Electrodes 73
3.3.7 Cyclic Voltammetry of 2C9 Electrodes 75
3.3.8 Chronoamperometry with the Mediator Phenosafranine 85
3.3.9 HPLC Analysis of Phenosafranine Mediator Experiment 87
3.4 Conclusion 88
3.5 References 90

Chapter 4
Closing Summary and Future Directions **92**

4.1 Closing Summary 92
4.2 Future Directions 94

LIST OF FIGURES

Chapter 1

Figure 1.1 Schematic of a Cytochrome P450 Biosensor 2
Figure 1.2 Electrode Immobilization Strategies for the Creation of CYP Biosensors 4

Chapter 2

Figure 2.1 Schematic of Random and Site-Specific Attachment of CYP to an Electrode 25
Figure 2.2 Ribbon Diagram of the Crystal Structure of CYP2C9 26
Figure 2.3 Electrostatic Potential Map of the Proximal Side of CYP2C9 33
Figure 2.4 Solvent Accessible Surface Area of the Proximal Side of CYP2C9 33
Figure 2.5 Coomassie-Stained SDS-PAGE Gel of Purified wt 2C9, R125C, R132C, and K432C 34
Figure 2.6 Coomassie-Stained SDS-PAGE Gel of Purified SCF-R125C, SCF-R132C, and SFC-K432C 34
Figure 2.7 Absorption and Difference Spectra of wt 2C9 and the Single 2C9 Mutants R125C, R132C, and K432C in the Presence of Sodium Dithionite and Carbon Monoxide (CO) 36
Figure 2.8 Absorption and Difference Spectra of wt 2C9 and the Triple 2C9 mutants SCF-R125C and SFC-K432C in the Presence of Sodium Dithionite and Carbon Monoxide (CO) 37
Figure 2.9 Schematic of the Reaction between CYP2C9 and Vivid® BOMCC 38
Figure 2.10 Specific Activities of wt 2C9 and the Single 2C9 Mutants R125C, R132C, and K432C Measured in the Reconstitution and Peroxide-Supported Activity Assays. 39
Figure 2.11 Specific Activities of the Single 2C9 Mutants R125C and K432C and the Triple 2C9 Mutants SCF-R125C and SCF-K432C Measured in Reconstitution and Peroxide-Supported Activity Assays. 40
Figure 2.12 Schematic of the reaction of CYP2C9 with Tolbutamide to form 4-Hydroxytolbutamide 41
Figure 2.13 Substrate Binding Difference Spectra of wt 2C9, R125C, R132C, and K432C 41
Figure 2.14 Raw Data and Best Fit Lines for Saturation Binding of Tolbutamide to wt 2C9, R125C, R132C, and K432C 42
Figure 2.15 Raw Data and Best Fit Lines to the Michaelis-Menten Equation for Plots of Initial Product Formation Rate as a Function of Tolbutamide Concentration for wt 2C9, R125C, R132C, and K432C 44
Figure 2.16 Absorption Spectrum of Texas Red® C2 Maleimide 46
Figure 2.17 Absorption Spectra of wt 2C9, R125C, R132C, and K432C Conjugated to Texas Red® C2 Maleimide. 46
Figure 2.18 Fluorescent Scan of an SDS-PAGE Gel of wt 2C9, R125C, R132C, and K432C Conjugated to Texas Red® C2 Maleimide 47
Figure 2.19 Deconvoluted ESI Mass Spectra of Unmodified wt 2C9, R125C, R132C, and K432C 48
Figure 2.20 Deconvoluted ESI Mass Spectra of R125C, R132C, and K432C Conjugated to Texas Red® C2 Maleimide 49

Chapter 3

Figure 3.1 Schematic of Three Different Attachment Methods Used to Immobilize CYP2C9 on a Gold Electrode 57
Figure 3.2 Custom-Machined Electrochemical Cell 58
Figure 3.3 AFM Image of Gold-Coated Glass Slide Used as a Gold Working Electrode 64
Figure 3.4 CV Scan of a Polycrystalline Gold Electrode in 0.1 M H_2SO_4 at a Scan Rate of 50 mV/s 65
Figure 3.5 QCM-D Measurement of the Surface Coverage of MPA and Cystamine SAMs on Gold 66
Figure 3.6 Reductive Desorption of MPA and Cystamine SAMs on Gold Electrodes 67
Figure 3.7 The Amine-Reactive Maleimide Compounds Sulfo-SMCC and N-Succinimidyl-3-maleimidopropionate 68
Figure 3.8 Absorption Spectrum of BODIPY® FL-L-cystine in the Presence of the Reducing Agent TCEP and 50 mM KPi (pH 7.4) 68
Figure 3.9 Absorption Spectra of the Fluorophore BODIPY® FL Conjugated to Maleimide Glass Slides Functionalized via Sulfo-SMCC or N-Succinimidyl-3-maleimidopropionate 69
Figure 3.10 Activity Assays with Vivid® BOMCC of 2C9 Electrodes Made with Three Different Attachment Methods 70
Figure 3.11 Grazing Angle Incidence FT-IR Spectra Collected for Bare Gold, Maleimide, and R132C Electrodes 72
Figure 3.12 Covalent Attachment of Aminoferrocene and Ferrocenecarboxylic acid to (A) an MPA SAM and (B) a Cystamine SAM on Gold Electrodes 73
Figure 3.13 CV Scans and Plots of Peak Current versus Scan Rate for Ferrocene Covalently Coupled to an MPA and Cystamine SAM on Gold Electrodes 75
Figure 3.14 Representative Anaerobic CV of CYP2C9 Immobilized to an Electrode via Amine Coupling to a Long-Chain SAM on Gold 77
Figure 3.15 Representative Anaeraboic and Aerobic CVs of CYP2C9 Immobilized to an Electrode via Amine Coupling to a Long-Chain SAM on Gold 77
Figure 3.16 Anaerobic CVs of wt 2C9 and R132C Electrodes Made Using Random Attachment via Amine Coupling, Oriented Attachment via Ni-NTA/His-tag Coupling, and Oriented Attachment via Maleimide/Thiol Coupling, along with Anaerobic CVs of MPA SAM, Ni-NTA, and Maleimide Electrodes as No-Enzyme Controls 79
Figure 3.17 CV Scans of an MPA SAM Electrode and 2C9 and R132C Electrodes Immobilized by Random Attachment via Amine Coupling Taken in Anaerobic Buffer, Aerobic Buffer, and Aerobic Buffer containing 500 μM Tolbutamide 80
Figure 3.18 CV Scans of a Ni-NTA Electrode and 2C9 and R132C Electrodes Immobilized by Oriented Attachment via Ni-NTA/His-tag Coupling Taken in Anaerobic Buffer, Aerobic Buffer, and Aerobic Buffer containing 500 μM Tolbutamide 81
Figure 3.19 CV Scans of a Maleimide Electrode and 2C9 and R132C Electrodes Made with Oriented Attachment via Maleimide/Thiol Coupling Taken in Anaerobic Buffer, Aerobic Buffer, and Aerobic Buffer with 500 μM Tolbutamide 82
Figure 3.20 Aerobic CV Scans and Plots of Peak Current versus Scan Rate for Gold Electrodes Modified with MPA SAM, Ni-NTA, and Maleimide 83

Figure 3.21 CVs of a Bare Gold Electrode in Aerobic Buffer with and without 800 μM Tolbutamide 84
Figure 3.22 The Structure and Redox Potential of the Mediator Compound Phenosafranine 86
Figure 3.23 Schematic of Indirect Electrochemical Catalysis of Tolbutamide by CYP2C9 and the Mediator Phenosafranine 86
Figure 3.24 Chronoamperometry of the R132C Electrode in 1.2 mM Phenosafranine with Increasing Concentrations of Tolbutamide 87
Figure 3.25 Concentration of Tolbutamide in the Electrolyte versus Time for Electrolysis with the R132C and Maleimide Electrodes and the Mediator Phenosafraine 88

Chapter 4

Figure 4.1 Schematic of Oriented Attachment of 2C9 to Maleimide-Functionalized AuNPs on a Mixed SAM of 6HT and 7MHA on a Gold Electrode 95

LIST OF TABLES

Chapter 2

Table 2.1 Fitted values for the Apparent Michaelis-Menten Constant (K_M^{app}) and Turnover Rate (k_{cat}) for CuOOH-Supported Catalysis of Tolbutamide with wt 2C9, R125C, R132C, and K432C, along with the Tolbutamide Dissociation Constants (K_D) as Reference 45

Chapter 3

Table 3.1 Electroactive Surface Concentrations of Species Undergoing Reduction and Oxidation on Gold Electrodes Modified with MPA SAM, Ni-NTA, and Maleimide 84

Chapter 1. Cytochrome P450 Enzymes and the Development of CYP Biosensors

1.1 Introduction

Cytochrome P450s (CYPs) are a large family of heme-containing monooxygenase enzymes implicated in the metabolism of drugs and foreign chemicals in the body. Although there are 57 known CYP genes in humans[1], only five CYPs (CYP1A2, 2C9, 2C19, 2D6, and 3A4) are responsible for approximately 95% of the CYP-mediated drug metabolism in the body[2], with the remaining CYP enzymes being involved in steroidogenesis and fatty acid oxidation. Drug clearance is affected by CYP activity, as CYPs catalyze the hydroxylation, epoxidation, and N-, S-, and O-demethylation of drug molecules, allowing for second-phase metabolism and excretion from the body. Consequently, P450 reactions are of high interest to the pharmaceutical industry, where lead compounds in drug development are screened as potential substrates of CYPs. Knowing the P450 substrate profile of a drug allows for the prediction of harmful drug-drug or food-drug interactions, which are often caused by the interference of CYP metabolism via inhibition or induction of a specific P450 isozyme. In addition to metabolizing drugs, CYPs are also involved in the activation of polycyclic aromatic hydrocarbons, toxins, carcinogens, and other small molecule substrates, making them ideal for use in bioremediation systems.

Currently, the development of a screen for CYP activity of drug candidates is hindered by the lack of a method that matches the throughput achieved in other steps of the drug development process, such as combinatorial library generation and high-throughput bioactivity screening[3,4]. LC-MS/MS analysis of CYP metabolites remains the gold standard in industry for CYP activity screens but the throughput is limited by the number of samples that can be run in parallel and the analysis time. High-throughput fluorescent-based assays do exist; however, these assays are often an indirect measure of CYP activity as an inhibition of fluorescence in the presence of a fluorogenic substrate and a candidate substrate is taken as an indication of activity[5]. A recently developed high-throughput assay measures CYP activity directly using by measuring reaction species via fluorescence but this assay requires multiple reagents and enzymes and setting up the assay can be time consuming[6]. In addition, laboratory or industrial use of CYPs is limited by the need for NADPH as the electron donor in the catalytic cycle. This is a major limitation of using CYPs for high-throughput screening or organic synthesis as NADPH is expensive, decomposes over time due to hydrolysis, and is difficult to recover once it has been oxidized[7].

Mammalian CYPs are membrane bound and found primarily in the smooth endoplasmic reticulum or mitochondrial membrane of liver cells[8]. The catalytic mechanism of all CYPs is essentially the same; however, each enzyme has different substrate specificity. The catalytic cycle of CYPs involves a redox reaction at an iron-protoporphyrin IX heme. *In vivo*, CYPs require the use of an additional enzyme, cytochrome P450 reductase (CPR), to shuttle electrons from NADPH via FAD and FMN cofactors to the iron heme. The general electron transfer scheme can be represented by the following:

$$\text{Electrons from NADPH} \rightarrow \text{FAD} \rightarrow \text{FMN} \rightarrow \text{Ferric form of heme } (Fe^{3+})$$

Once reduced, the ferrous (Fe^{2+}) heme binds dioxygen and undergoes a second electron transfer, eventually forming an activated iron hydroperoxy intermediate ($Fe^{3+}-OOH^{-}$)[9]. One oxygen atom is reduced to form water, and the remaining ferryl-oxo species ($Fe^{4+}=O$) oxidizes the

substrate, regenerating the ferric form of the enzyme[9]. The iron heme is held in position by hydrogen bonds between heme propionates and the surrounding amino acid residues, and the iron itself is hexa-coordinated with a water molecule and a cysteine thiolate as the fifth and sixth ligands, respectively. In its resting state, the iron heme exists in the low-spin, ferric form with a relatively low redox potential between -400 and -170 mV[10-12]. Substrate binding is thought to trigger transfer of the first electron by displacing water as the fifth iron ligand, resulting in high-spin ferric iron and a shift in the redox potential to less negative values[9].

By immobilizing CYPs on an electrode NADPH and CPR are no longer needed as the electron donor and electron transfer partner enzyme, respectively, and the immobilized CYP can act as a biosensor by accepting electrons directly from the electrode, as shown in Figure 1.1. An increase in the current upon application of a potential can be correlated to catalytic activity of the enzyme against a candidate substrate. A CYP biosensor would be useful in the pharmaceutical industry as a tool for initial screens of drug candidates for reactivity with P450s and for potential drug-drug or food-drug interactions. Furthermore, the bioremediation potential of CYPs can be evaluated by screening environmental contaminants and pollutants for activity using such a biosensor. A high-throughput electrode array, fabricated using techniques found in semiconductor manufacturing, could even be used for personalized medicine by immobilizing CYP enzymes from an individual on the array and screening for CYP activity with different combinations of prescribed drugs.

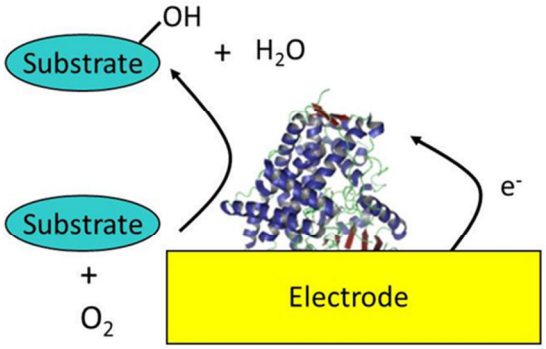

Figure 1.1 Schematic of a Cytochrome P450 Biosensor. Immobilization of CYPs on an electrode precludes the need for NADPH and cytochrome P450 reductase (CPR) and allows for transfer of electrons directly to the enzyme from the electrode. Measuring a current in the presence of a candidate substrate is a direct measure of drug reactivity, and thus the immobilized CYP can be used as a biosensor.

Since the publication in the mid- to late-1990s of several studies on the electrochemistry of the bacterial CYPs $P450_{CAM}$ and BM-3 in solution or on bare electrodes[13-15], there has been an explosion in the number of CYP biosensor studies in the literature over the last ten years. Although many of the initial studies on CYP biosensors were done using adsorption on bare electrodes as an immobilization strategy, it has become apparent that the electrode environment greatly affects CYP electroactivity. Immobilization of CYPs on an electrode modified with more protein-friendly materials prevents denaturation on the surface and has emerged as a better strategy for designing CYP biosensors. The types of electrodes and electrode modifications used in CYP biosensor studies vary, ranging from thin films with opposite charge adsorbed onto graphite to conductive polymers on noble metals such as gold and platinum. Most of these studies rely on a combination of electrochemical and analytical techniques to show that the CYP

biosensor is electroactive and can detect different drug compounds via electrochemically-driven catalysis. However, a number of recent studies characterizing the active site structure and redox potential of CYPs immobilized on electrodes have shown that much of the CYP protein immobilized on the electrode is in an inactive form and call into question the results from previous CYP biosensor studies[16-18]. In addition, some CYP biosensor studies are missing crucial substrate turnover data and instead rely on electrochemical experiments alone to prove the immobilized CYP is capable of electrochemically-driven catalysis[19].

With this in mind, this introduction focuses on the different electrode materials and immobilization strategies used to fabricate CYP biosensors, with special attention given towards characterization of the CYP electrode surface and electrochemically-mediated catalysis and detection of CYP substrates. An overview of electrode types and modifications will be discussed along with highlights of studies of particular interest. Primary attention will be given to CYP biosensors based on the human drug-metabolizing CYPs; however, some studies based on bacterial CYPs will be discussed as these studies served as a foundation for the development of mammalian CYP biosensors.

1.2 Electrode Immobilization Strategies

Various types of electrodes and electrode modifications have been used to fabricate CYP biosensors (Figure 1.2). Initial studies on the direct electrochemistry of CYPs employed adsorption to bare electrodes (primarily graphite) as an immobilization strategy but electrode modifications such as layer-by-layer assemblies of polyelectrolytes or thin films of lipid bilayers provide a more biomimetic environment and have been shown to enhance electron transfer to adsorbed CYPs. Screen-printed electrodes made of conductive pastes with enhancers such as gold nanoparticles have made miniaturization of CYP biosensors a reality while encapsulation in polymers or gels can stabilize CYPs on electrodes and enhance electron transfer if conductive polymers such as polypyrrole are used. Recently, covalent attachment to self-assembled monolayers (SAMs) on gold electrodes has been used as an immobilization strategy for creating CYP biosensors. The functionalization of SAMs with different chemical groups allows for site-specific attachment of CYPs at individual amino acid residues and control of the orientation of the immobilized enzyme.

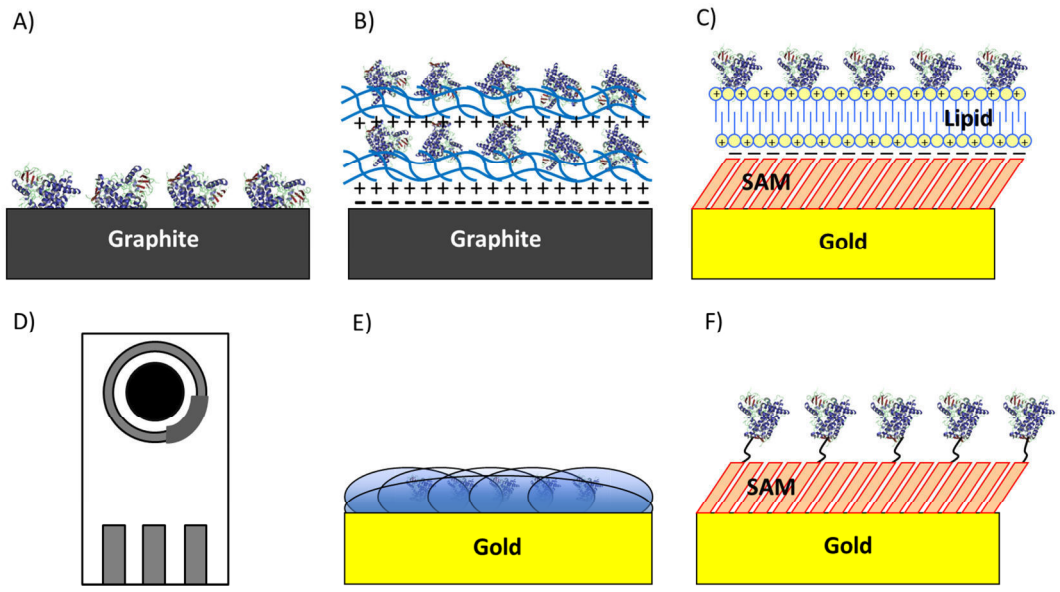

Figure 1.2 Electrode Immobilization Strategies for the Creation of CYP Biosensors. (A) Adsorption to bare electrodes. (B) Layer-by-layer (LbL) adsorption. (C) Adsorption to thin films. (D) Screen-printed electrodes. (E) Encapsulation in polymers or gels. (F) Covalent attachment to self-assembled monolayers (SAMs) on gold.

1.2.1 Adsorption to Bare Electrodes

Electrochemical investigations of the bacterial CYPs $P450_{CAM}$ (CYP101) and BM-3 (CYP102) on bare electrodes paved the way for current research on biosensors with drug-metabolizing CYPs. Electrochemically-driven catalysis with CYPs was initially investigated as a way to synthesize industrially relevant compounds without NAD(P)H or electron transfer partner enzymes. Initial studies employed a three electrode electrochemical cell with bacterial CYPs in solution to reduce the enzyme and initiate substrate turnover. Estabrook et al. used a mediator system with the soluble redox mediator cobalt(III) sepulchrate and a platinum wire working electrode to reduce BM-3 and other CYP fusion proteins, leading to a substrate turnover of 110 nmol/min/nmol P450 for the ω-hydroxylation of lauric acid by BM-3[13]. This turnover rate was significantly less than the turnover of lauric acid with NADPH and BM-3 (900 nmol/min/nmol P450), and the electrolytic reduction of molecular oxygen to hydrogen peroxide necessitated inclusion of the enzyme catalase to destroy accumulated peroxide and prevent destruction of the P450. A similar study on the electrochemical reduction of $P450_{CAM}$ in solution used an antimony-doped tin oxide-coated working electrode with the natural electron transfer partner enzyme putidaredoxin (Pdr) as a mediator[14]. Using this system, the authors were able to detect turnover of the $P450_{CAM}$ substrate camphor to the product 5-*exo*-camphor, and oxygen was supplied via water electrolysis at a platinum counter electrode. While neither of the abovementioned studies involved the physical immobilization of $P450_{CAM}$ and BM-3 on bare electrodes, the results from these indirect electrochemical systems validated that electrochemically-driven catalysis of CYPs was possible and sparked further research into the direct electrochemistry of CYPs and the construction of CYP biosensors.

The direct electrochemistry of CYPs adsorbed onto bare electrodes has been most successful with the bacterial P450s on graphite electrodes. There is limited information in the

literature on the direct electrochemistry of bacterial CYPs adsorbed on gold electrodes and even less evidence for the direct electrochemistry of mammalian CYPs adsorbed on bare electrodes. In 1996, Hill and co-workers observed the direct electrochemistry of $P450_{CAM}$ for the first time when it was adsorbed on a bare edge-plane pyrolytic graphite (EPG) electrode[20]. A pair of reversible redox peaks was seen in a cyclic voltammogram (CV) of the $P450_{CAM}$ electrode in buffer and an increase in the cathodic peak area in the presence of the substrate D-(+)-camphor suggested that the CYP electrode was capable of electrochemically-driven catalysis. The authors explained the facile adsorption of $P450_{CAM}$ to the negatively-charged EPG by noting that a patch of basic residues (Arg-72, Arg-112, Lys-344, and Arg-364) on the proximal side of the enzyme closest to the heme could interact with the electrode via electrostatics. A follow-up study by the same research group investigated the role of these residues and the possible orientation of $P450_{CAM}$ on a bare gold electrode by creating a $P450_{CAM}$ mutant with one surface cysteine engineered on the proximal side (K344C) and the rest of the native surface cysteines mutated to alanines [15]. The authors proposed that the well-known affinity of thiols for gold would lead to site-specific attachment of the $P450_{CAM}$ mutant at residue 344 and orientation of the enzyme on its proximal side. Adsorption of this mutant (designated SCF-K344C) to a bare gold electrode resulted in enhanced electroactivity compared to the WT enzyme and a surface cysteine-free mutant, as measured by the intensity of the cathodic peaks in the CVs. The results from this study suggest that the enhanced electroactivity of the SCF-K344C mutant may be due to orientation of the enzyme on the electrode surface. This is entirely plausible, as it is now known that a pocket of basic residues on the proximal sides of $P450_{CAM}$ and mammalian CYPs interacts with acidic residues on their respective electron transfer partner enzymes[21,22].

The limited success of bare electrode systems for the immobilization and direct electrochemistry of CYPs underscores the need for modification of the electrode surface to provide a suitable environment for electron transfer and prevent surface denaturation. Nevertheless, electrochemical studies of CYPs adsorbed onto bare electrodes continue to appear in the literature, and it is fairly well established that graphite electrodes such as glassy carbon (GC) and EPG are better able to promote the direct electrochemistry of CYPs than noble metal electrodes such as gold and platinum. The direct electrochemistry of the mammalian drug-metabolizing CYP2E1 was observed on a bare GC electrode in one of the first electrochemistry studies on a P450 enzyme from family 2[12]. Although a pair of reversible redox peaks was observed in CV scans with the GC/2E1 electrode, a faster electron transfer rate constant was observed with a modified gold electrode system (k_s = 10 s^{-1} versus 5 s^{-1} for the bare GC electrode), again suggesting that modification of the electrode surface enhances electron transfer. A more recent study of the cytochrome P450 enzyme CYP199A2 from the bacterium *Rhodopseudomonas palustris* adsorbed on a basal-plane pyrolytic graphite (BPG) electrode showed that the enzyme exhibited fast (k_s = 550 ± 50 s^{-1}) and quasi-reversible electron transfer with the electrode[23]. As with previous electrochemical studies on CYPs adsorbed to graphite electrodes, the interaction of CYP199A2 with the BPG electrode was thought to occur via an electrostatic interaction between basic residues on the proximal side of the enzyme and negatively charged residues on the electrode. Another study on the direct electrochemistry of CYPs on graphite electrodes poignantly illustrates the advantages conferred by modifying the electrode surface. Mazumdar and co-workers covalently immobilized $P450_{CAM}$ to a GC electrode modified with pyrene maleimide by targeting native cysteine residues on the surface of the enzyme[24]. Modifying the GC electrode with a conjugated ring system such as pyrene maleimide improved electron transfer between the electrode and $P450_{CAM}$ and resulted in an

electron transfer rate constant that was approximately 13 times greater than that for $P450_{CAM}$ adsorbed onto a bare GC electrode.

1.2.3 Layer-by-Layer Adsorption

One approach to modifying the electrode surface and providing a more protein-friendly environment for electrochemically-driven CYP catalysis is layer-by-layer (LbL) adsorption, a process by which multiple layers of oppositely-charged films and/or CYPs are built up on the electrode surface. Typical LbL adsorption procedures start by passivating the electrode surface with positive or negative charges. Graphite electrodes such as EPG, BPG, and GC already exhibit negative charges due to carbonyl and carboxyl groups introduced during oxidative activation of the graphite surface[25]. Noble metal electrodes such as gold and silver, however, must be functionalized with a charged self-assembled monolayer (SAM) or polyelectrolyte prior to build-up of an LbL structure. An advantage of the LbL technique over other immobilization methods such as covalent attachment is that multiple layers of enzyme can be built up on a single electrode, increasing the effective CYP concentration on the surface and the sensitivity of the biosensor. The Rusling laboratory at the University of Connecticut has pioneered the use of LbL adsorption for the direct electrochemistry of CYPs and the construction of CYP biosensors. In one of their first applications of the LbL technique, the Rusling group immobilized $P450_{CAM}$ on a gold electrode in multilayer films of either negatively charged poly(styrenesulfonate) (PSS) or positively charged poly(diallyldimethylammonium chloride) (PDDA)[26]. Multilayer films of $P450_{CAM}$/PDDA absorbed onto a gold electrode modified with a mercaptopropene sulfonic acid (MPS) SAM exhibited the highest turnover (9.3 h^{-1}) of the substrate styrene, as indicated by the formation of styrene oxide during electrolysis with the Au-MPS-$(P450_{CAM}/PDDA)_2$ electrode. Using a similar LbL technique, Joseph et al. made a CYP biosensor by immobilizing the human drug-metabolizing CYP3A4 on a gold electrode modified sequentially by MPS and PDDA[27]. CV scans of the Au/MPS/PDDA/3A4 electrode showed quasi-reversible redox peaks with a midpoint potential of 98 ± 5 mV vs. NHE, and the biosensor was able to detect the 3A4 drug substrates verapamil and midazolam. The authors noted a discrepancy between the measured 3A4 redox potential in their study and the more negative redox potentials found for other CYP biosensors in the literature but attributed this difference to the altered environment of the heme induced upon immobilization. In another study from the Rusling group, LbL adsorption was used to construct a CYP1A2 biosensor on carbon cloth (CC) electrodes by the alternate adsorption of PSS and 1A2[28]. The CC/PSS/$(CYP1A2/PSS)_2$ electrode exhibited nearly reversible electron transfer with a midpoint potential of -0.07 V vs. NHE and was able to catalyze the epoxidation of styrene at a turnover rate that was nearly 2.3 times that of 1A2-mediated epoxidation of styrene in solution with NADPH and CPR.

A number of unique CYP biosensor configurations have been realized using the LbL adsorption technique. Sultana et al. immobilized CYP1A2 and 3A4 microsomes onto rough PG electrodes using an LbL assembly of polyethylenimine (PEI) and PSS films[29]. CV scans of the multilayer films $[CYP1A2ms/PEI]_6$ and $[CYP3A4ms/PEI]_6$ on PG electrodes gave reversible reduction and oxidation peaks at approximately -0.49 V vs. SCE, and the authors were able to detect electrochemically-driven styrene epoxidation. The difference between the redox potential of the microsome films and that of recombinant 1A2 or 3A4 in polyion films (-0.49 V vs. SCE for microsomes vs. approximately -0.3 V vs. SCE for recombinant 1A2 or 3A4[28]) and the lack of

a redox potential shift in the presence of carbon monoxide suggested that the electroactivity seen in the 1A2 and 3A4 microsome films was due to reduction of CPR and not P450. The discovery that microsomes are as effective as recombinant CYPs in promoting direct electrochemistry on electrodes is encouraging for the development of CYP biosensors as microsomes are cheaper to make than recombinant CYPs and are already used in the pharmaceutical industry. A recent follow-up study of LbL films of either recombinant CYP1A2 or 2E1 and CPR/cytochrome b_5-containing microsomes on BPG electrodes revealed that electron transfer in the CYP electrodes followed the natural catalytic pathway with electron transfer occurring first to CPR and then from CPR to the P450[30]. Both 1A2 and 2E1 multilayers on BPG electrodes with CPR and b_5 exhibited reversible reduction and oxidation peaks in CV scans, and a PDDA/PSS/(CYP2E1/CPR+b_5) LbL film on a BPG electrode catalyzed the turnover of the substrate 4-(methylnitrosamino)-1-(3-pyridyl)-1-butanone (NNK) to 4-hydroxy-1-(3-pyridyl)-1-butanone (HPB) at a relative rate of 0.24 ± 0.04. Comparing this turnover rate to the turnover of NNK with 2E1 and NADPH/CPR in solution revealed that the multilayer 2E1 electrode was about 1.5 times more efficient at producing the HPB product.

1.2.4 Adsorption to Thin Films

There are numerous accounts in the literature of CYP biosensors constructed from thin films of lipid bilayers or polyelectrolytes absorbed onto electrodes, and the success of these studies has established the thin film technique as an alternative to LbL assembly for promoting CYP electroactivity. Depositing thin films on the electrode surface is typically accomplished by simple drop-casting or a Langmuir trough; drop casting results in a non-uniform or multilayer film while a Langmuir trough creates monolayers of uniform Langmuir-Blodgett (LB) films. One of the first studies on CYPs adsorbed to thin film modified electrodes investigated the direct electrochemistry of $P450_{CAM}$ adsorbed to a GC electrode modified with a solution of the clay colloid sodium montmorillonite. The authors created a pretreated sodium montmorillonite colloid (PSMC) by mixing sodium montmorillonite colloid with colloidal Pt and created a GC/PSMC/$P450_{CAM}$ electrode via the drop-casting method[31]. A pair of reversible redox peaks with a formal potential of -139 mV vs. NHE were observed in an anaerobic CV scan of the GC/PSMC/$P450_{CAM}$ electrode, and a linear relationship between the peak anodic and cathodic currents and the scan rate indicated a surface redox process. The calculated electron transfer rate constant was relatively fast, ranging from 5 to 152 s^{-1} for scan rates of 0.4 to 12 V/s, respectively, and the similarity of these rates to that for electron transfer *in vivo* from Pdr to $P450_{CAM}$ prompted the authors to speculate that the negatively charged clay mimics the electrostatics of Pdr and may orient the $P450_{CAM}$ for electron transfer. A similar study done more recently in 2004 by Shumyantseva et al. used a mixture of sodium montmorillonite colloid and the non-ionic detergent Tween 80 to immobilize the mammalian CYP 2B4 on a GC electrode[32]. The authors detected reversible reduction and oxidation peaks for the GC/Clay+Tween/2B4 electrode at a formal potential of -295 mV vs. Ag/AgCl but were not able to detect any redox activity with a GC/Clay/2B4 electrode, underlining the importance of the nonionic detergent for promoting electron transfer. Although the GC/Clay+Tween/2B4 electrode had the highest electron transfer rate constant (k_s >114 s^{-1}), the highest amount of electroactive 2B4 was achieved when the sodium montmorillonite clay, Tween and 2B4 were mixed together before deposition on the GC electrode, suggesting that surrounding the 2B4 with an ionic and lipophilic environment enhances its electroactivity. Using this immobilization strategy, the resulting 2B4 electrode was

able to amperometrically detect the drug substrates aminopyrine and benzphetamine, and catalytic turnover of aminopyrine was confirmed by quantifying formaldehyde, the product of aminopyrine-N-demethylation. The results from these studies suggest that thin films of clay nanoparticles can be used to build efficient CYP biosensors.

Thin films of lipid bilayers are especially attractive as they are thought to recapitulate the lipophilic environment of the smooth endoplasmic reticulum where most mammalian CYPs reside. The majority of CYP biosensor studies utilizing thin films of lipid bilayers on electrodes use the cationic lipid didodecyldimethylammonium bromide (DDAB) on GC or EPG electrodes, although phospholipids such as L-α-phosphatidylcholine dimyristoyl (DMPC) have been used in the past[33]. DDAB forms a stable lipid bilayer at room temperature and the positive charge on the ammonium ion allow it to interact electrostatically to negatively charged graphite electrodes. The Rusling group has pioneered the use of biomembrane-like films in CYP biosensors by using thin films of DDAB or DMPC to create electrochemically active $P450_{CAM}$ on PG electrodes[33]. Since then, numerous research groups have used the same approach to create electrochemically active mammalian CYPs. In 2005, Bernhardt and co-workers reported the direct electrochemistry of P450s from the 2C family for the first time using thin films of DDAB on EPG electrodes[34]. The human drug-metabolizing CYPs 2C9, 2C18, and 2C19 were immobilized separately on EPG electrodes by drop-casting a mixture of CYP and an aqueous dispersion of DDAB on EPG. For all three enzymes a single Fe^{III}/Fe^{II} redox potential was identified but the signal-to-background current was very weak and only a small (1-3%) amount of the total immobilized enzyme was electroactive. The authors also noted a peak-to-peak separation of 150 to 200 mV in the CV scans that was well above the theoretical 90 mV for a one-electron transfer to an adsorbed redox species and stated this discrepancy might be caused by the heterogeneity of CYP conformations in the DDAB film. A similar study published at the same time characterized the direct electrochemistry of CYP2C9 adsorbed on a DDAB-modified EPG electrode[35]. A pair of redox peaks centered at -41 mV vs. Ag/AgCl was seen for the GC/DDAB/2C9 electrode, and this redox process was found to be surface-confined based on the linear relationship between the peak anodic and cathodic currents and the scan rate. Although it was not determined whether or not the 2C9 electrode was capable of substrate turnover, an anodic shift in the redox potential in the presence of CO and the 2C9 substrates torsemide, tolbutamide, and warfarin suggested that the immobilized 2C9 was in a conformation that allowed for substrate binding. The authors noted that the measured redox potential of -41 mV for the GC/DDAB/2C9 electrode was much higher than the reported redox potentials in solution. This is the case for most CYP electrodes and is purported to be a result of conformation changes or dehydration induced upon immobilization. A recent study has extended the use of DDAB films on electrodes to the mitochondrial CYP27B1, which catalyzes the hydroxylation of 25-hydroxyvitamin D_3 ($25(OH)D_3$) to its active metabolite. Recombinant mouse CYP27B1 was adsorbed onto EPG disc electrodes modified with DDAB, and the EPG/DDAB/27B1electrode exhibited nearly symmetric redox peaks with a midpoint potential of -180 mV vs. Ag/AgCl[36]. Interestingly, no product formation was observed during electrolysis of the 27B1 electrode in the presence of $25(OH)D_3$; the authors proposed the DDAB may be blocking the enzyme's active site, a phenomenon that has been documented before with the surfactant SDS[37].

1.2.5 Screen-Printed Electrodes

Screen-printed electrodes are ideal for constructing CYP biosensors because screen-printing is inexpensive and a number of conductive additives such as rhodium graphite or gold nanoparticles can be mixed directly into the electrode paste. In addition, electrodes of many different sizes and configurations can be made using screen-printing, making the construction of a CYP biosensor array relatively simple. The Shumyantseva laboratory of the Institute of Biomedical Chemistry at the Russian Academy of Medical Sciences has been studying the direct electrochemistry of CYPs on screen-printed electrodes for some time, in particular the direct electrochemistry of CYP11A1 (P450scc), the CYP responsible for the side chain cleavage reaction of cholesterol. One of their first studies involved the immobilization of the riboflavin-P450 conjugates RfP4501A2, RfP4502B4, and RfP450scc on rhodium graphite screen-printed thick film electrodes[38]. The Rf-P450 conjugates were immobilized onto screen-printed electrodes by drop casting a solution of the Rf-P450, BSA, glutaraldehyde, sodium cholate, and phospholipid onto the electrode surface, and all three Rf-P450 electrodes were capable of electrochemically-driven turnover with their respective substrates. Amperometric responses were observed with the RfP4502B4 and RfP450scc electrodes in the presence of aminopyrine and cholesterol, respectively, showing that the CYP electrodes acted as biosensors. A related study used riboflavin-graphite screen-printed electrodes to construct a CYP1A2 biosensor. The 1A2 was immobilized on a screen-printed electrode by encapsulation in a glycerol and agarose gel matrix, and the resulting 1A2 electrode was able to electrochemically detect increasing concentrations of the drug clozapine[39]. Gold nanoparticles (AuNP) were used to enhance the electroactivity of P450scc on rhodium-graphite screen-printed electrodes in another study by Shumyantseva et al[40]. The reduction current of the P450scc electrode was significantly enhanced in the presence of the gold nanoparticles, and the authors suggested that the rough electrode surface imparted by the nanoparticles provided for more intimate electrical contact with the enzyme. Interestingly, the AuNP-P450scc electrode was more sensitive in detecting cholesterol than the aforementioned RfP450scc electrode, further suggesting that the gold nanoparticles enhanced the electroactivity of P450scc. The human drug-metabolizing CYP 2B4 was covalently immobilized on a screen-printed carbon electrode for the detection of cocaine in a recent study by Asturias-Arribas et al[41]. The 2B4 was amine-coupled using EDC/NHS to a screen-printed carbon electrode functionalized with carboxylic acid groups, and the resulting 2B4 biosensor accurately determined the concentration of cocaine in confiscated street cocaine samples.

Screen-printed electrodes have also been used in conjunction with the lipid DDAB to construct CYP biosensors. CYP2B4, 1A2, and 51b1 (sterol-14α-demethylase) were prepared on screen-printed graphite electrodes modified with a mixture of gold nanoparticles and DDAB in a study by Shumyantseva et al[42]. Aerobic CV scans of the DDAB/AuNP/2B4 and DDAB/Au-NP/1A2 electrodes showed midpoint potentials of -393 and -437 mV vs. Ag/AgCl, respectively, and the electrodes were sensitive to their respective substrates benzphetamine and lanosterol. A comparison between the DDAB/AuNP/2B4 and DDAB/2B4 electrodes revealed that the gold nanoparticles enhanced the observed reduction current in aerobic CV scans. In an interesting follow-up study, the same research group investigated the stoichiometry of electrochemically-driven benzphetamine catalysis with a DDAB/AuNP/2B4 electrode[43]. The authors tracked the formation of H_2O_2, consumption of O_2, and formation of the product formaldehyde over time to investigate the extent of uncoupling that occurs during electrolysis with the 2B4 electrode.

Uncoupling occurs when reduction of the P450 heme does not lead to product formation and instead results in the unproductive release of reactive oxygen species that short-cut the natural catalytic cycle. A bi-electrode scheme with a Prussian blue electrode and Clark oxygen electrode was used to electrochemically measure the formation of H_2O_2 and the consumption of O_2, respectively, with time. The results showed that although the electrochemical reduction of 2B4 does lead to uncoupling and the formation of H_2O_2, the electrochemically-derived stoichiometric coefficients for O_2, H_2O_2, and formaldehyde were similar to those from the NADPH/microsomal system. This suggests that, for the DDAB/AuNP/2B4 system, catalysis on an electrode is a comparable substitute to NADPH-mediated catalysis and can be used to study the electrochemistry of CYPs *in vitro*. This DDAB/AuNP system was extended to other CYPs and multiple substrates in a recent study, where CYP3A4 and 11A1 (P450ssc), in addition to 2B4 and 51bl, were immobilized on screen-printed graphite electrodes modified with DDAB and gold nanoparticles[44]. Multiple substrates and inhibitors were detected with the different CYP electrodes, implying that this novel DDAB/AuNP system could be a universal method for the construction of a screen-printed array of CYP biosensors.

1.2.6 Encapsulation in Polymers or Gels

A number of CYP biosensor studies have used encapsulation in polymers or gels to immobilize P450s on an electrode and enhance their electroactivity. The majority of these studies have used the conductive polymer polypyrrole to entrap the P450 on an electrode and enmesh it in a conductive matrix. $P450_{CAM}$ was immobilized in polypyrrole polymerized on an indium tin oxide (ITO) electrode in one of the first published examples of a CYP biosensor made using the encapsulation technique[45]. Polypyrrole was electropolymerized on the surface of the ITO electrode in the presence of various concentrations of $P450_{CAM}$, and the resulting $P450_{CAM}$ electrode was capable of electrochemically-driven catalysis as seen by the presence of hydroxycamphor in the electrolyte after controlled potential electrolysis with the substrate camphor. In a similar study, a quintuple P450 BM-3 mutant was immobilized in polypyrrole on Pt wire and GC electrodes, and both types of electrodes were capable of substrate turnover with the model substrate *p*-nitrophenoxycarboxylic acid (p-NCA)[46]. The authors compared two different types of polypyrrole polymerization procedures (chemical vs. electrochemical) for their effect on BM-3 activity and concluded that electropolymerization affected enzyme activity the least. In a more recent study, a CYP2B4 biosensor was constructed using a miniaturized three electrode chip made with photolithography, and the 2B4 was immobilized on a gold working electrode via encapsulation in polypyrrole[47]. Chronoamperograms of the 2B4 electrode polarized at 0.45 V vs. Ag/AgCl showed a current response proportional to the concentration of the substrate phenobarbital, and the 2B4 biosensor accurately determined the concentration of phenobarbital in a commercially available pharmaceutical. However, the authors did not assay for product in the electrolyte after electrolysis; therefore, it is unclear whether the detection of phenobarbital was due to electrochemically-driven 2B4 catalysis or an unrelated electrochemical process.

Hydrophilic gels such as agarose, chitosan, and sol-gels have also been used to encapsulate CYPs on electrodes and facilitate electron transfer. Additives such as nanoparticles or lipids can be added to gels to enhance the conductivity and/or stability of the immobilized CYP. Iwuoha et al. used a methyltriethoxysilane (MTEOS) sol-gel to encapsulate $P450_{CAM}$ on a GC electrode[48]. DDAB was added to the $P450_{CAM}$ prior to encapsulation and created a

biomembrane-like environment on the surface of the electrode. CV scans of the resulting GCE-[$P450_{CAM}$/DDAB/SG] electrode in phosphate buffer and in 90% acetonitrile revealed a pair of redox peaks, and the $P450_{CAM}$ biosensor was capable of detecting the substrates camphor and pyrene in aerobic phosphate buffer. Surprisingly, the authors noted that the biosensor exhibited faster reversible electron transfer in 90% acetonitrile than water and attributed this to the increased fluidity of DDAB in acetonitrile and relaxation of the sol-gel/enzyme layer. Sol-gel encapsulation also maintained the activity of the immobilized $P450_{CAM}$ as the biosensor remained stable for up to four weeks. The natural polysaccharide chitosan mixed with gold nanoparticles was used to encapsulate the human drug-metabolizing enzyme CYP 2B6 on a GC electrode; the resulting 2B6 electrode was used as a biosensor to amperometrically detect the drugs lidocaine, cyclophosphamide, and bupropion[49]. The gold nanoparticles were prepared in a chitosan solution and mixed with the P450 prior to drop-casting on the surface of the GC electrode. The authors observed enhanced peak currents for the GC/AuNP-chitosan/2B6 electrode when compared to a GC/2B6 electrode, suggesting that the gold nanoparticles and chitosan film facilitated facile electron transfer to the P450. Absorption spectra of a glass slide coated with a AuNP-chitosan/2B6 film revealed that the absorption band for colloidal gold was red-shifted from 536 to 541 nm, indicating an interaction between the enzyme and the gold nanoparticles. Electrospray ionization mass spectrometry (ESI-MS) detected the catalytic product hydroxybupropion after controlled potential electrolysis confirmed the 2B6 electrode was capable of substrate turnover.

1.2.7 Covalent Attachment to Self-Assembled Monolayers on Gold

Covalent attachment of CYPs to gold electrodes via SAMs has proven to be a robust and simple technique for creating CYP biosensors. Long or short chain n-alkanethiols form an ordered monolayer, or SAM, on gold due to the high affinity of sulfhydryl groups (-SH) for gold and favorable van der Waals interactions between the alkane chains. SAMs with various termini can be used to modify gold electrodes with functional groups such as carboxyls, amines, and maleimides to facilitate different immobilization chemistries. No clear consensus exists in the CYP biosensor literature on whether short or long chain SAMs are better at promoting electron transfer but it is well known that short chain SAMs create a diffuse and less ordered monolayer whereas long chain SAMs create a densely packed and well-ordered monolayer. Many CYP biosensor studies with SAMs in the literature use long chain alkanethiols such as 11-mercaptoundecanoic acid (MUA) or hexanoic acid but there are examples of shorter chain thiols such as dithio-bismaleimidoethane (DTME) or mercaptopropionic acid (MPA) being used to immobilize CYPs[50] and glucose oxidase[51], respectively. Longer chain SAMs may help stabilize the immobilized CYP and prevent surface denaturation however there is a trade-off in electroactivity as the electron transfer rate constant decreases exponentially with the chain length, *n*, of the SAM[52]. A recent study illustrated this phenomenon quite well; Zhang and co-workers compared the surface coverage and electron transfer resistance of MUA and MPA SAMs on gold nanopillar modified electrodes using CV and electrochemical impedance spectroscopy (EIS)[53]. The MUA SAM had the higher surface coverage at 62.2% but its electron transfer resistance (209 kΩ) was approximately 33 times that of the MPA SAM, and a glucose oxidase (GOx) biosensor made from the MPA coated electrode was six times more sensitive at detecting glucose than one made with an MUA coated electrode.

Several different immobilization chemistries have been used to covalently attach CYPs to SAMs formed on gold electrodes. The most common immobilization chemistry is amine coupling and uses the reagents EDC (1-Ethyl-3-[3-dimethylaminopropyl]carbodiimide hydrochloride) and NHS (N-hydroxysuccinimide) to attach the P450 to a carboxy-terminated SAM on gold via surface exposed amine groups (lysine residues). Although this attachment chemistry is fairly simple and widely used, the immobilized CYP is tethered to the electrode in a random orientation based on the number and reactivity of surface exposed amines. Nevertheless, different research groups have covalently coupled CYPs to carboxy SAMs on gold via amine coupling and observed electroactivity even though the immobilized CYP may not be oriented for electron transfer. CYP2C9 was immobilized to a gold electrode via amine coupling to a mixed SAM of 3:1 octanethiol (OT) and MUA. An anaerobic CV scan of the Au/OT-MUA/2C9 electrode revealed quasi-reversible reduction and oxidation peaks at a formal potential of -0.49 and -0.42 V vs. Ag/AgCl, respectively, and detection of the metabolite 7-hydroxywarfarin in the electrolyte after controlled potential electrolysis with the 2C9 substrate warfarin confirmed that the 2C9 biosensor was capable of electrochemically-driven catalysis[54]. More recently, Fantuzzi et al. used amine coupling to a mixed SAM of 1:1 6-hexanethiol (6HT) and 7-mercaptoheptanoic acid (7MHA) to immobilize a fusion protein of CYP3A4 and flavodoxin (FLD) to gold electrodes made via photolithography[55]. Fusing 3A4 with the flavodoxin from *Desulfovibrio vulgaris* was shown earlier by the same research group to improve the coupling efficiency of 3A4 on gold and GC electrodes[56]. A microfluidic cell made of the Au/6HT-7MHA/3A4-FLD electrode, a screen-printed carbon counter electrode, and a screen-printed Ag/AgCl reference electrode was used to detect the 3A4 substrates quinidine, nifedipine, alosetron, and ondansetron, and the K_M values for these substrates were determined. Although there was some variability between the microfluidically-measured K_M values and K_M values in the literature, the relative ranking of the substrates from low to high K_M matched that seen in the literature, suggesting that the 3A4-FLD biosensor could be used as an initial screen for 3A4 reactivity of test compounds. A follow-up study used the same immobilization strategy with 6HT and 7MHA SAMs to attach polymorphic variants of CYP2C9 to gold electrodes in an eight-electrode array[57]. As in the aforementioned studies with 3A4, the variants 2C9*1 (wild-type), 2C9*2 (R144C), and 2C9*3 (I359L) were fused separately to the flavodoxin from *D. vulgaris*. A commercially available strip of micro-machined electrodes in 300 μL wells formed an eight-electrode array, and the 2C9 biosensors were used to measure the K_M and k_{cat} values of the substrate warfarin with the different 2C9 variants. The amperometrically-determined K_M values were notably smaller than those in the literature however a relative ranking of the 2C9 variants based on electrochemically-driven formation of the product hydroxywarfarin matched that seen in the literature.

Oriented attachment of CYPs to SAMs on gold electrodes has been done via site-specific attachment at certain residues. Martin and Johnson oriented his-tagged bovine P450c17 at the C-terminus on a gold electrode by modifying an MPA SAM on gold with nickel-charged Acbztacn (1-acetato-4-benzyl-triazacyclononane), an alternative to Ni-NTA[58]. Surface plasmon resonance experiments revealed that the Ni-Acbztacn surface did not experience any metal leaching over a 24 hour period, and the presence of redox peaks in an anaerobic CV scan of the Au/Ni-Acbztacn/P450c17 electrode in the presence of DDAB showed that the immobilized P450c17 was electroactive. SAMs modified with maleimide groups have been used to site-specifically attach CYPs to electrodes at cysteine residues (thiols). One of the first examples of this immobilization strategy was the covalent attachment of CYP2E1 to a gold electrode[12]. A gold electrode was modified sequentially with a cystamine SAM (CYSAM) and an amine-reactive

maleimide, and recombinant 2E1 was incubated overnight on the maleimide-functionalized electrode to create a 2E1 biosensor. The authors compared the Au/CYSAM/MALIM/2E1 electrode to 2E1 electrodes made with bare GC, GC/DDAB, GC/PDDA, and Au/MPA/PDDA electrodes and found that the maleimide modified electrode resulted in the highest electron transfer rate constant (10 ± 0.5 s^{-1}). Analysis of the crystal structure of 2E1 revealed the presence of two surface cysteines, C261 and C268, on the proximal face of the enzyme with 37 and 25% surface exposure, respectively, and the authors suggested that attachment at these residues may have resulted in oriented attachment of 2E1 on the proximal side and enhanced electron transfer to the heme. A related study by the same research group characterized the electrocatalytic response of recombinant 2E1 mutants attached specifically at C261 or C268 on gold electrodes modified with a DTME SAM[50]. MUT261 and MUT268 were created by mutating all the surface cysteine residues to serines save for C261 and C268, respectively. After 30 minutes of electrolysis in the presence of the 2E1 substrate *p*-nitrophenol, the amount of product *p*-nitrocatechol in the electrolyte was determined spectrophotometrically for the different 2E1 electrodes. The MUT261 and MUT268 electrodes produced, respectively, 2.6 and 2.1 times as much *p*-nitrocatechol as the wild-type 2E1 electrode, suggesting that orienting the enzyme on the electrode enhanced its electroactivity. A maleimide-functionalized SAM was also used to immobilize the CYP2D6 polymorphic variants 2D6*1 (wild-type), 2D6*2, and 2D6*17 on a gold electrode[57]. An eight-electrode array of gold electrodes was modified sequentially with a 6-aminohexanethiol SAM and N-succinimidyl-3-maleimidopropionate to create maleimide functionalized electrodes. N-succinimidyl-3-maleimidopropionate was identified in an earlier study by the same research group as being superior to DTME for functionalization of gold electrodes with maleimide groups and therefore was used in place of DTME[59]. The resulting 2D6 biosensors were used to measure the K_M and k_{cat} values of the different 2D6 variants with the substrate bufuralol, and the polymorphic variants were distinguishable from one another by their different K_M and k_{cat} values, which were found to be in agreement with results from the literature. However, unlike the aforementioned studies with 2E1, the authors did not comment on which residues on 2D6 most likely reacted with the maleimide surface and whether or not the 2D6 variants were oriented on the electrode surface.

Few studies have directly compared the electrochemical response of CYPs adsorbed on graphite electrodes to that of CYPs covalently attached to SAMs on gold electrodes. However, an interesting study by Dodhia et al. published in 2008 compared the electrochemical response of CYP3A4 fusion proteins immobilized on GC and gold electrodes via a PDDA thin film and maleimide-functionalized SAM, respectively[56]. CYP3A4 was fused to either the heme domain of P450 BM-3 (BMP) or the flavodoxin from *D. vulgaris* (FLD) in an attempt to improve the electroactivity of the immobilized CYP. For covalent attachment to gold, the gold electrode was modified sequentially with a cystamine SAM and N-succinimidyl-3-maleimidopropionate to create a maleimide surface, and attachment of the 3A4-BMR and 3A4-FLD enzymes presumably occurred at surface exposed cysteine residues. The authors assessed the electroactivity of the different 3A4 electrodes by comparing the electron transfer rate constants, amounts of product formed during electrolysis, and the coupling efficiencies for each system. 3A4 electrodes made using the GC/PDDA system exhibited much higher electron transfer rate constants (200 to 400 s^{-1}) than those made from Au/CYSAM/MALIM electrodes (0.6 to 3.7 s^{-1}), suggesting that graphite electrodes enhance electron transfer to immobilized CYPs. This is not surprising, given there are many accounts in the literature of fast electron transfer to CYPs on graphite electrodes such as GC, EPG, and PG. What is surprising about this study is that during electrolysis with the

3A4 substrate erythromycin, 3A4 electrodes made using the Au/CYSAM/MALIM system produced, on average, the product formaldehyde at a rate 2.7 times that of the GC/PDDA/3A4 electrodes. In addition, the Au/CYSAM/MALIM/3A4 electrodes exhibited coupling efficiencies that were at least two times higher than that seen with the GC/PDDA/3A4 electrodes, and for the best case of 3A4-FLD on maleimide-gold, the coupling efficiency at 19.9% was similar to that for CYP3A4 and NADPH/CPR *in vitro*[60]. Taken together, the results from this study suggest that covalent attachment of CYPs to SAMs on gold electrodes, in particular oriented attachment via maleimide/thiol coupling, produces an electroactive CYP that behaves much like it does in solution with NADPH/CPR.

1.3 Characterization of CYP Electrodes

The majority of CYP biosensor studies use electrochemical techniques such as cyclic voltammetry or chronoamperometry to show that the immobilized CYP is electroactive and capable of substrate turnover. However, little information exists on the conformation of CYPs immobilized on electrodes and the effect, if any, that structural changes induced by immobilization have on catalysis. There is some evidence to suggest that CYPs undergo a conformational change upon electrode immobilization that results in the formation of P420, an inactive CYP species characterized by absorption of the reduced ferrous enzyme at 420 nm. Formation of P420 is thought to occur via structural changes in the enzyme that result in protonation of the axial thiolate ligand and perturbation of the electronic environment of the heme[61]. Formation of P420 has been induced by increases in temperature[62] and/or pressure[63] and exposure to neutral salts[64], detergents[65], organic solvents[66], and high/low pH buffers[67]. In a study by Hill and co-workers, immobilization of the bacterial P450 BM-3 in thin films of the surfactant DDAB was found to induce formation of the inactive P420 species over time[17]. A difference spectrum of the reduced (Fe^{II}) BM-3 bound to CO revealed the presence of a 420 nm peak after a two minute incubation in a DDAB dispersion. A CV scan at 25 mV/s of a BPG/DDAB/BM-3 electrode showed well-defined, reversible redox peaks centered at -260 mV vs. SCE, suggesting that even though some of the enzyme was in the inactive P420 form electron transfer to and from the iron heme was still possible. The authors noted that the BM-3 Fe^{III}/Fe^{II} redox potential in DDAB was approximately 300 mV more positive than the redox potential in solution and attributed this anodic potential shift to stabilization of the ferrous (Fe^{II}) heme in the P420 state. In a similar study, Gilardi and co-workers investigated the effects of the polycations PEI and PDDA on the absorption spectra of the heme domain of P450 BM-3 (BMP) immobilized on mesoporous tin-oxide (SnO_2) electrodes[68]. Using cyclic voltabsorptometry, the authors were able to measure the absorption spectra of immobilized BM-3 during cyclic voltammetry. Electrochemical reduction of the SnO_2/PEI/BMP electrode in the presence of CO resulted in the formation of the inactive P420 species while no P420 was detected during reduction of the SnO_2/PDDA/BMP electrode. PDDA seemed to inhibit formation of the inactive P420 form and stabilize the Fe^{II}-CO complex in an active conformation. This result is in stark contrast to the finding that DDAB induces formation of P420 upon immobilization of BM-3 on an electrode, and the fact that both PEI and DDAB have been used in CYP biosensor studies calls into question the results from these studies and whether or not the electrochemical responses seen with these sensors were actually from inactive P420 instead of active CYP.

Formation of the inactive P420 species has also been observed for bacterial and mammalian CYPs immobilized to SAMs on electrodes. Surface-enhanced resonance Raman

spectroscopy (SERRS) of $P450_{CAM}$ adsorbed to an MUA SAM on a silver (Ag) electrode revealed that both the ferric and ferrous states of the enzyme were predominantly in the P420 form[16]. The authors attributed the formation of the inactive P420 to the high electric field experienced at the surface of the SAM and attempted to mitigate this by increasing the ionic strength, introducing methyl-terminated alkanethiols into the SAM, decreasing the pH, or by amine coupling the CYP to the carboxylate SAM. Unfortunately none of these methods resulted in stabilization of the native P450 state, suggesting that electric field-induced conformational changes were solely responsible for the formation of inactive P420. Increasing the number of methylene units, *n*, of the carboxylate SAM on Ag resulted in a positive shift in the redox potential of the immobilized CYP, most likely due to a stabilizing effect of the longer chain SAMs on the ferrous form of the enzyme. Shortening the length of the ω-carboxylate SAM had the opposite effect: the redox potential exhibited a negative shift. In this case, the authors proposed that the high electric field closer to the electrode surface stabilizes the positively charged ferric form of the enzyme, resulting in a more negative redox potential. A similar study used SERRS to investigate the active site structure, substrate binding, and redox activity of the drug-metabolizing CYP 2D6 adsorbed to an MUA SAM on a silver electrode[18]. SERRS spectra revealed that the enzyme retained its native structure upon immobilization and was able to reversibly bind the substrate dextromethorphan. Electrochemical reduction of the 2D6 enzyme however, was not possible as SERRS spectra taken of the Ag/MUA/2D6 electrode polarized at negative potentials contained marker bands at 1371 and 1360 cm^{-1} for the oxidized and P420 forms of the enzyme, respectively. Based on these results, the authors concluded that electrodes coated with an MUA SAM were not suitable for the direct electrochemistry of 2D6. This is an interesting result, considering that MUA coated gold electrodes promoted the direct electrochemistry and electrochemically-driven catalysis of CYP2C9 in a previous study[54].

Atomic force microscopy (AFM) and scanning tunneling microscopy (STM) can also be used to characterize the surface of CYP electrodes but few CYP biosensor studies in the literature have taken advantage of these techniques. AFM can be used to assess the morphology and conformation of enzyme on the electrode surface while STM with electrochemical control (EC-STM) is especially useful as it allows for imaging of the electrode surface at different applied potentials. EC-STM images of an electroactive enzyme taken at potentials near the enzyme redox potential exhibit a markedly higher contrast than images taken at potentials far from the enzyme redox potential[69]. Thus, the quality and contrast of EC-STM images can be used to estimate the electroactivity and redox potential of an electrode-immobilized CYP. A study by Davis et al. used STM to probe the conformation of a $P450_{CAM}$ mutant (SCF-K344C) adsorbed to a gold electrode[70]. The authors mutated all the surface-exposed cysteines on $P450_{CAM}$ to chemically inert alanines and mutated one lysine residue (K344) on the proximal side of the enzyme closest to the heme to a cysteine. STM images of the SCF-K344C mutant on gold revealed an ordered and compact monolayer of enzyme on the surface whereas images of the wild-type enzyme showed a random and unstructured monolayer, suggesting that the specific cysteine mutation of the SCF-K344C mutant oriented the enzyme on the surface of the electrode. Gilardi and co-workers used a similar immobilization approach to immobilize a CYP2E1 fusion protein on a maleimide-functionalized SAM on gold, and the authors used tapping-mode AFM (TMAFM) to image a monolayer of 2E1 on the electrode[19]. The same research group also used TMAFM to image single-cysteine mutants of the BM-3 heme domain BMP immobilized on gold electrodes via a maleimide-functionalized SAM[59]. Two surface cysteines, C156 and C62, were mutated individually to serines (C156S and C62S) such that attachment to the maleimide gold

electrode occurred at only one surface cysteine residue. TMAFM images of wild-type BMP, C156S, and C62S immobilized on the maleimide-coated gold electrode showed that immobilization of the C156S mutant at residue C62 resulted in a stable and well-ordered monolayer. An analysis of the crystal structure of BMP revealed that residues C62 and C156 had a solvent accessibility of 11.6 and 1.0 $Å^2$, respectively. The authors proposed that the increased solvent accessibility of residue C62 allowed for enhanced binding of the C156S mutant to maleimide gold.

1.4 Future Directions

CYP biosensors are increasingly being made from microfabricated electrodes or nanostructured materials such as multi-walled carbon nanotubes (MWCNTs) or gold nanoparticles. Microfabricated CYP biosensors and array-based systems integrated with microfluidics are bringing portable CYP biosensors closer to reality while nanostructured electrodes increase the active surface area for electron transfer and allow for more intimate contact with the immobilized CYP. Combining nanostructured materials with microfabricated electrode arrays, one can imagine the creation of a portable CYP biosensor chip for use at a doctor's office or patient's bedside for personalized medicine. MWCNTs were used by Carrara et al. to promote the direct electrochemistry of P450scc on rhodium graphite screen-printed electrodes[71]. The MWCNTs were deposited on the rhodium-graphite electrodes by drop casting, and aerobic CV scans of the MWCNT-modified P450scc electrode showed a marked increase in the cathodic current when compared to a P450scc electrode modified with gold nanoparticles. The MWCNT-modified P450scc electrode behaved as a biosensor for the amperometric detection of cholesterol; its sensitivity of 1.12 $\mu A/(mM \cdot mm^2)$ was similar to that of a P450scc biosensor made with gold nanoparticles but the carbon nanotubes considerably improved the linearity of the cholesterol response. In a more recent study, De Micheli and co-workers used MWCNT-modified screen-printed electrodes to create CYP biosensors from the drug-metabolizing CYPs 3A4, 2B4, and 2C9[72]. The authors compared the sensitivity of 3A4 biosensors made with bare or MWCNT electrodes to the drug cyclophosphamide and found that incorporation of the MWCNTs greatly enhanced the sensitivity of the sensor. A MWCNT-modified 3A4 electrode exhibited a limit of detection of 12 μM for the detection of cyclophosphamide, down from 59 μM for a 3A4 biosensor made with a bare graphite electrode. Similar results were found for MWCNT-based biosensors made with 2B4 and 2C9, and the low detection limits of these biosensors enabled determination of drug concentrations in human plasma. In addition, a new mathematical model was developed to de-convolute the biosensor response from multiple drugs in a mixture, paving the way for detection of multiple drugs in human plasma samples.

Quantum dots and nanostructured gold are also being used to create novel CYP biosensors. Komatsu and co-workers discovered that the nanostructured surface of sputtered gold electrodes enhanced the electroactivity of CYP3A4 adsorbed to the surface via a naphthalene thiolate SAM[73]. Using these nanostructured gold electrodes, the authors measured an electron transfer rate constant of $340 \pm 40\ s^{-1}$ for electron transfer to 3A4. Substrate turnover was not assessed; however, a positive potential shift of the 3A4 redox potential in the presence of the 3A4 substrate testosterone suggested that the electrode-immobilized 3A4 was capable of substrate binding. In a follow-up study, the same research group examined the direct electron electrochemistry of 3A4 further by immobilizing 3A4 microsomes on gold nanodome arrays

made using microfabrication[74]. Gold nanodome arrays were made using anodized aluminum foil as a template, and AFM images of nanodomes made under optimal conditions showed an organized array of nanostructures that were approximately 150 nm in diameter. Microsomes containing 3A4 were adsorbed on a naphthalene thiolate SAM on the gold nanodomes, and aerobic CV scans of the nanodome-modified 3A4 electrode showed that the nanostructures led to an enhanced cathodic current when compared to a 3A4 electrode made using gold without nanostructures. A recent study by Ndangili et al. also examined the effects of a nanostructured surface on the direct electrochemistry of CYPs but used ZnSe quantum dots instead of gold nanodome arrays or gold nanoparticles[75]. The authors used amine coupling to conjugate ZnSe quantum dots coated with an MPA SAM to a gold disk electrode modified with a cystamine SAM. Recombinant CYP3A4 was then amine coupled to unreacted carboxyl groups on the immobilized ZnSe quantum dots to create a nanostructured 3A4 biosensor. The particle diameter of the MPA-ZnSe quantum dots was estimated from UV absorption to be 3.40 nm, much smaller than the gold nanodomes prepared in the aforementioned study. An aerobic CV scan of the Au/CYSAM/ZnSe/3A4 electrode revealed a reduction peak at -200 mV vs. Ag/AgCl while a more negative reduction potential was observed for a Au/CYSAM/3A4 electrode without quantum dots. This positive shift in the reduction potential with ZnSe quantum dots was attributed to the ability of quantum dots to confine electrons and thus lower the activation energy for electron transfer[76]. The Au/CYSAM/ZnSe/3A4 electrode behaved as a biosensor for the detection of the hormone 17β-estradiol (E2); a plot of the current response as a function of E2 concentration followed Michaelis-Menten kinetics. Not surprisingly, the nanostructured electrode surface imparted by the ZnSe quantum dots enhanced the electrocatalytic response of the 3A4 biosensor to E2.

1.5 Conclusion

The future for CYP biosensors clearly lies in the development of miniaturized systems made from nanostructured materials. Site-specific attachment and orientation of CYPs on the electrode surface is also gaining ground as a popular immobilization strategy due to the enhanced electroactivity seen when the enzyme is attached at the proximal side and thus in a productive orientation for electron transfer. Miniaturized systems, such as the microfluidic device recently developed by Gilardi and co-workers with CYP3A4[55], may eventually lead to the development of portable CYP biosensor chips for diagnostic or clinical use. Nanostructured electrodes are gradually becoming the system of choice for the construction of CYP biosensors and it is likely that there will be more examples of these systems in the future. Gold nanoparticles are especially attractive as they are easy to make, can be functionalized with various chemistries, and have been shown to serve as "excellent electron transfer relays" for the direct electrochemistry of enzymes[77]. Direct attachment of the buried CYP heme to the electrode also remains a possibility. This has already been done for glucose oxidase biosensors[78], although the direction of electron transfer occurs from the cofactor to the electrode as opposed to CYP biosensors where electron transfer occurs from the electrode to the cofactor. With the right chemistry, this approach might be used in the future to directly wire CYPs to an electrode.

In less than two decades, the state-of-the art for CYP biosensors has gone from adsorption to bare electrodes to immobilization on electrodes modified with novel nanostructured materials such as gold nanoparticles and quantum dots. It is clear from previous studies on the direct electrochemistry of CYPs that engineering the electrode surface is crucial

for promoting electroactivity and electrochemically-derived catalysis. Although modification of the electrode surface has produced CYP electrode systems that undergo very fast electron transfer, it is not yet clear if electrochemically-driven CYP catalysis mimics electron transfer and catalysis in solution or even *in vivo*. Many questions remain about the nature of electron transfer from the electrode to the buried P450 heme and what effects, if any, direct electrochemistry has on the conformation of CYPs and the electronic environment of the heme. The discovery of inactive P420 in some electrode systems warrants rigorous surface characterization as an additional tool for analysis of CYP biosensors. Whether or not these issues matter for a given CYP biosensor is unclear and may depend on the application. On one hand, a CYP biosensor developed to be an initial screening tool for CYP reactivity of lead candidates in drug development may not need to be 100% accurate as long as the relative ranking of compound activities follows that seen in *in vivo* studies. On the other hand, a CYP biosensor designed to entirely replace *in vivo* models—a so-called patient-on-a-chip—needs to behave identical to *in vivo* CYP metabolism, in which case the nature of electron transfer to the CYP its conformation becomes paramount.

1.6 References

1. Nebert, D.W., Russell, D.W. Clinical importance of the cytochromes P450. *The Lancet* (2002) 360:1155-1162.
2. Williams, J.A., Hyland, R., Jones, B.C., Smith, D.A., Hurst, S., Goosen, T.C., Peterkin, V., Koup, J.R., Ball, S.E. Drug-drug interactions for UDP-glucuronosyltransferase substrates: a pharmacokinetic explanation for typically observed low exposure (AUC_i/AUC) ratios. *Drug Metab. Dispos.* (2004) 32:1201-1208.
3. Ansede, J.H., Thakker, D.R. High-throughput screening for stability and inhibitory activity of compounds toward cytochrome P450-mediated metabolism. *J. Pharma. Science* (2003) 93:239-255.
4. Kumar, R.A., Clark, Douglas S. High-throughput screening of biocatalytic activity: applications in drug discovery. *Curr. Opin. Chem. Bio.* (2006) 10:162-268.
5. Trubetskoy, O.V., Gibson, J.R., Marks, B.D. Highly miniaturized formats for in vitro drug metabolism assays using Vivid® fluorescent substrates and recombinant human cytochrome P450 enzymes. *J. Biomol. Screen.* (2005) 10:56-66.
6. Traylor, M.J., Ryan, J.D., Arnon, E.S., Dordick, J.S., Clark, D.S. Rapid and quantitative measurement of metabolic stability without chromatography or mass spectrometry. *JACS* (2011) 133:14476-14479.
7. Udit, A.K., Gray, H.B. Electrochemistry of heme-thiolate proteins. *Biochem. Biophys. Res. Commun.* (2005) 338:470-476.
8. Anzenbacher, P., Anzenbacherová, E. Cytochromes P450 and metabolism of xenobiotics. *Cell. Mol. Life Sci.* (2001) 58:737-747.
9. Denisov, I.G., Makris, T.M., Sligar, S.G., Schlichting, I. Stucture and chemistry of cytochrome P450. *Chem. Rev.* (2005) 105:2253-2277.
10. Williams-Smith, D.L., Cammack, R. Oxidation-reduction potentials of cytochromes-P450 and ferredoxin in the bovine adrenal: their modification by substrates and inhibitors. *Biochim. Biophys. Acta* (1977) 499:432-442.
11. Guengerich, F.P., Ballou, D.P., Coon, M.J.J. Purified liver microsomal cytochrome P-450: electron accepting properties and oxidation-reduction potential. *J. Biol. Chem.* (1975) 250:7405-7414.
12. Fantuzzi, A., Fairhead, M., Gilardi, G. Direct electrochemistry of immobilized human cytochrome P450 2E1. *JACS* (2004) 126:5040-5041.
13. Estabrook, R.W., Faulkner, K.M., Seth, M.S., Fisher, C.W. Application of electrochemistry for P450-catalyzed reactions. *Methods Enzymol.* (1996) 272: 44-51.
14. Reipa, V., Mayhew, M.P., Vilker, V. A direct electrode-driven P450 cycle for biocatalysis. *PNAS* (1997) 94:13554-13558.
15. Kam-Wing Lo, K., Wong, L., Hill, A.O. Surface-modified mutants of cytochrome $P450_{cam}$: enzymatic properties and electrochemistry. *FEBS Letters* (1999) 451:342-346.
16. Todorovic, S., Jung, C., Hildebrandt, P., Murgida, D.H. Conformational transitions and redox potential shifts of cytochrome P450 induced by immobilization. *J. Biol. Inorg. Chem.* (2006) 11:119-127.

17. Udit, A.K., Hagen, K.D., Goldman, P.J., Star, Andrew., Gillan, J.M., Gray, H.B., Hill, M.G. Spectroscopy and electrochemistry of cytochrome P450 BM3-surfactant film assemblies. *JACS* (2006) 128:10320-10325.
18. Bonifacio, A., Millo, D., Keizers, P.H.J., Boegschoten, R., Commandeur, J.N.M., Vermeulen, NPE., Gooijer, C., van der Zwan, G. Active-site structure, binding and redox activity of the heme-thiolate enzyme CYP2D6 immobilized on coated Ag electrodes: a surface-enhanced resonance Raman scattering study. *J. Biol. Inorg. Chem.* (2008) 13:85-96.
19. Sadeghi, S.J., Fantuzzi, A., Gilardi, G. Breakthrough in P450 bioelectrochemistry and future perspectives. *Biochim. Biophys. Acta* (2011) 1814:237-248.
20. Kazlauskaite, J., Westlake, A.C.G., Wong, L., Hill, H.A.O. Direct electrochemistry of cytochrome P450cam. *Chem. Commun.* (1996) 18:2189-2190.
21. Lewis, D.F.V., Hlavica, P. Interactions between redox partners in various cytochrome P450 systems: functional and structural aspects. *Biochim. Biophys. Acta* (2000) 1460:353-374.
22. Hlavica, P., Schulze, J., Lewis D.F.V. Functional interaction of cytochrome P450 with its redox partners: a critical assessment and update of the topology of predicted contact regions. *J. Inorg. Biochem.* (2003) 96: 279-297.
23. Fleming, B.D., Bell, S.G., Wong, L., Bond, A.M. The electrochemistry of a heme-containing enzyme, CYP199A2, adsorbed directly onto a pyrolytic graphite electrode. *J. Electroanal. Chem.* (2007) 611:149-154.
24. Mhaske, S.D., Ray, M., Mazumdar, S. Covalent linkage of CYP101 with the electrode enhances the electrocatalytic activity of the enzyme: vectorial electron transport from the electrode. *Inorg. Chim. Acta* (2010) 363:2804-2811.
25. Noked, M., Soffer, A., Aurbach, D. The electrochemistry of activated carbonaceous materials: past, present, and future. *J. Solid State Electrochem.* (2011) 15:1563-1578.
26. Lvov, Y.M., Lu, Z., Schenkman, J., Zu, X., Rusling, J.F. Direct electrochemistry of myoglobin and cytochrome P450cam in alternate layer-by-layer films with DNA and other polyions. *JACS* (1998) 120:4073-4080.
27. Joseph, S., Rusling, J.F., Lvov, Y.M., Friedberg, T., Fuhr, U. An amperometric biosensor with human CYP3A4 as a novel drug screening tool. *Biochem. Pharmacol.* (2003) 65:1817-1826.
28. Estavillo, C., Lu Z., Jansson, I., Schenkman, J.B., Rusling, J.F. Epoxidation of styrene by human cyt P450 1A2 by thin film electrolysis and peroxide activation compared to solution reactions. *Biophys. Chem.* (2003) 104:291-296.
29. Sultana, N., Schenkman, J.B., Rusling, J.F. Protein film electrochemistry of microsomes genetically enriched in human cytochrome P450 monooxygenases. *JACS* (2005) 127:13460-13461.
30. Krishnan, S., Wasalathanthri, D., Zhao, L., Schenkman, J.B., Rusling, J.F. Efficient bioelectronic actuation of the natural catalytic pathway of human metabolic cytochrome P450s. *JACS* (2011) 133:1459-1465.
31. Lei, C., Wollenberger, U., Jung, C., Scheller, F.W. Clay-bridged electron transfer between cytochrome $P450_{CAM}$ and electrode. *Biochem. Biophys. Res. Commun.* (2000) 268:740-744.
32. Shumyantseva, V., Ivanov, Y.D., Bistolas, N., Scheller, F.W., Archakov, A.I., Wollenberger, U. Direct electron transfer of cytochrome P450 2B4 at electrodes

modified with nonionic detergent and colloidal clay nanoparticles. *Anal. Chem.* (2004) 76:6046-6052.
33. Zhang, Z., Nassar, A.F., Lu, Z., Schenkman, J.B., Rusling, J.F. Direct electron injection from electrodes in $P450_{CAM}$ in biomembrane-like films. *Faraday Trans.* (1997) 93:1769-1774.
34. Shukla, A., Gillam, E.M., Mitchell, D.J., Bernhardt, P.V. Direct electrochemistry of enzymes from the cytochrome P450 2C family. *Electrochem. Commun.* (2005) 7:437-442.
35. Johnson, D.L., Lewis, B.C., Elliot, D.J., Miners, J.O., Martin, L.L. Electrochemical characterization of the human cytochrome P450 CYP2C9. *Biochem. Pharmacol.* (2005) 69:1533-1541.
36. Rhieu, S.Y., Ludwig, D.R., Siu, V.S., Palmore, G.T.R. Direct electrochemistry of cytochrome P450 27B1 in surfactant films. *Electrochem. Commun.* (2009) 11:1857-1860.
37. Udit, A.K., Hill, M.G., Gray, H.B. Electrochemistry of cytochrome P450 BM-3 in sodium dodecyl sulfate films. *Langmuir* (2006) 22:10854-10857.
38. Shumyantseva, V.V., Bulko, T.V., Usanov, S.A., Schmid, R.D., Nicolini, C., Archakov, A.I. Construction and characterization of bioelectrocatalytic sensors based on cytochromes P450. *J. Inorg. Biochem.* (2001) 87:185-190.
39. Antonini M., Ghisellini, P., Pastorino, L., Paternolli, C., Nicolini, C. Preliminary electrochemical characterization of the cytochrome P4501A2-clozapine interaction. IEE Proc.-Nanobiotechnology (2003) 150:31-34.
40. Shumyantseva, V.V., Carrara, S., Bavastrello, V. Riley, J.D., Bulko, T.V., Skryabin, K.G., Archakov, A.I., Nicolini, C. Direct electron transfer between cytochrome P450scc and gold nanoparticles on screen-printed rhodium-graphite electrodes. *Biosens. Bioelectron.* (2005) 21:217-222.
41. Asturias-Arribas, L., Alonso-Lomillo, M.A., Domínguez-Renedo, O., Arcos-Martínez, M.J. CYP450 biosensors based on screen-printed carbon electrodes for the determination of cocaine. *Anal. Chim. Acta* (2011) 685:15-20.
42. Shumyantseva, V.V., Bulko, T.V., Rudakov, Y.O., Kuznetsova, G.P., Samenkova, N.F., Lisitsa, A.V., Karuzina, I.I., Archakov, A.I. Electrochemical properties of cytochroms P450 using nanostructured electrodes: direct electron transfer and electro catalysis. *J. Inorgan. Biochem.* (2007) 101:859-865.
43. Rudakov, Y.O., Shumyantseva, V.V., Bulko, T.V., Suprun, E.V., Kuznetsova, G.P., Samenkova, N.F., Archakov, A.I. Stoichiometry of electrocatalytic cycle of cytochrome P450 2B4. *J. Inorgan. Biochem.* (2008) 102:2020-2025.
44. Shumyantseva, V.V., Bulko, T.V., Suprun, E.V., Chalenko, Y.M., Yu.Vagin, M., Rudakov, Y.O., Shatskaya, M.A., Archakov, A.I. Electrochemical investigations of cytochrome P450. *Biochim. Biophys. Acta Proteins & Proteomics* (2011) 1814:94-101.
45. Sugihara, N., Ogoma, Y., Abe, K., Kondo, Y., Akaike, T. Immobilization of cytochrome P-450 and electrochemical control over its activity. *Polym. Adv. Tech.* (1998) 9:307-313.
46. Holtmann, D., Mangold, K., Schrader, J. Entrapment of cytochrome P450 BM-3 in polypyrrole for electrochemically-driven biocatalysis. *Biotechnol. Lett.* (2009) 31:765-770.

47. Alonso-Lomillo, M.A., Gonzalo-Ruiz, J., Domínguez-Renedo, O., Muñoz, F.J., Arcos-Martínez, M.J. CYP450 biosensors based on gold chips for antiepileptic drugs determination. *Biosens Bioelectron.* (2008) 23:1733-1737.
48. Iwuoha, E.I., Kane, S., Anita, C.O., Smyth, M., Ortiz de Montellano, P.R., Fuhr, U. Reactivities of organic phase biosensors 3: electrochemical study of cytochrome P450cam immobilized in a methyltriethoxysilane sol-gel. *Electroanalysis* (2000) 12:980-986.
49. Liu, S., Peng, L., Yang, X., Wu, Y., He, L. Electrochemistry of cytochrome P450 enzyme on nanoparticle-containing membrane-coated electrode and its applications for drug sensing. *Anal. Biochem.* (2008) 375:209-216.
50. Mak, L.H., Sadeghi, S.J., Fantuzzi, A., Gilardi, G. Control of human cytochrome P450 2E1 electrocatalytic response as a result of unique orientation on gold electrodes. *Anal. Chem.* (2010) 82:5357-5362.
51. Shervedani, R.K., Hatefi-Mehrjardi, A. Comparative electrochemical behavior of glucose oxidase covalently immobilized on mono-, di-, and tetra-carboxylic acid functional Au-thiol SAMs via anhydride derivatization route. *Sens. Act. B* (2009) 137:195-204.
52. Nikki, K.,Gregory, B. Electrochemistry of redox-active protein films immobilized on self-assembled monolayers of organothiols. In: Rusling, James, ed. Surfactant Science Series. Biomolecular Films. Vol. 111. New York, NY. Marcel Dekker Inc. (2003)
53. Anandan, V., Gangadharan, R., Zhang, G. Role of SAM chain length in enhancing the sensitivity of nanopillar modified electrodes for glucose detection. *Sensors* (2009) 9:1295-1305.
54. Yang, M., Kabulski, J.L., Wollenberg, L. Chen, X., Subramanian, M., Tracy, T.S., Lederman, D., Gannett, P.M., Wu, N. Electrocatalytic drug metabolism by CYP2C9 bonded to a self-assembled monolayer-modified electrode. *Drug Metab. Disp.* (2009) 37:892-899.
55. Fantuzzi, A., Capria, E., Mak, L.H., Dodhia, V.R., Sadeghi, S.J., Collins, S., Somers, G., Huq, E., Gilardi, G. An electrochemical microfluidic platform for human P450 drug metabolism profiling. *Anal. Chem.* (2010) 82:10222-10227.
56. Dodhia, V.R., Sassone, C., Fantuzzi, A., Di Nardo, G., Sadeghi, S.J., Gilardi, G. Modulating the coupling efficiency of human cytochrome P450 CYP3A4 at electrode surfaces through protein engineering. *Electrochem. Commun.* (2008) 10:1744-1747.
57. Panicco, P., Dodhia, V.R., Fantuzzi, A., Gilardi, G. Enzyme-based amperometric platform to determine the polymorphic response in drug metabolism by cytochromes P450. *Anal. Chem.* (2011) 83:2179-2186.
58. Johnson, D.L, Martin, L.L. Controlling protein orientation at interfaces using histidine tags: an alternative to Ni/NTA. *JACS* (2005) 127:2018-2019.
59. Ferroro, V.E.V., Andolfi, L., Di Nardo, G., Sadeghi, S.J., Fantuzzi, A., Cannistraro, S., Gilardi, G. Protein and electrode engineering for the covalent immobilization of P450 BMP on gold. *Anal. Chem.* (2008) 80:8438-8446.
60. Perret, A., Pompon, D. Electron shuttle between membrane-bound cytochrome P450 3A4 and b_5 rules uncoupling mechanism. *Biochemistry* (1998) 37:11412-11424.

61. Perera, R., Sono, M., Sigman, J.A., Pfister, T.D., Lu, Y., Dawson, J.H. Neutral thiol as a proximal ligand to ferrous heme iron: implications for heme proteins that lose cysteine thiolate ligation on reduction. *PNAS* (2003) 100:3641-3646.
62. Mouro, C., Jung, C., Bondon, A., Simonneaux, G. Comparative fourier transform infrared studies of the secondary structure and the CO heme ligand environment in cytochrome P-450cam and cytochrome P-20cam. *Biochemistry* (1997) 36:8125-8134.
63. Hui Bon Hoa, G., Di Primo, C., Dondaire, I., Sligar, S., Gunsalus, I.C., Douzou, P. Conformational changes of cytochromes P-450cam and P-450lin induced by high pressure. *Biochemistry* (1989) 28:651-656.
64. Imai, Y., Sato, R. Conversion of P-450 to P-420 by neutral salts and some other reagents. *Eur. J. Biochem.* (1967) 1:419-426.
65. Omura, T., Sato, R. The carbon monoxide-binding pigment of liver microsomes. *J. Biol. Chem.* (1964) 239:2370-2378.
66. Yu, C.A., Gunsalus, I.C. Cytochrome P-450$_{cam}$: II. Interconversion with P-420. *J. Biol. Chem.* (1974) 249:102-106.
67. O'Keefe, D.H., Ebel, R.E., Peterson, J.A., Maxwell, J.C., Caughey, W.S. An infrared spectroscopic study of carbon monoxide binding to ferrous cytochrome P-450. *Biochemistry* (1978) 17:5845-5852.
68. Panicco, P., Astuti, Y., Fantuzzi, A., Durrant, J.R., Gilardi, G. P450 versus P420: correlation between cyclic voltammetry and visible absorption spectroscopy of the immobilized heme domain of cytochrome P450 BM3. *J. Phys. Chem. B* (2008) 112:14063-14068.
69. Bonanni, B., Andolfi, L., Bizzarri, A.R., Cannistraro, S. Functional metalloproteins integrated with conductive substrates: Detecting single molecules and sensing individual recognition events. *J. Phys. Chem. B* (2007) 111:5062-5075.
70. Davis, J.J., Djuricic, D., Lo, K.K.W., Wallace, E.N.K., Wong, L., Hill, H.A.O. A scanning tunnelling study of immobilized cytochrome P450$_{cam}$. *Faraday Discuss.* (2000) 116:15-22.
71. Carrara, S., Shumyantseva, V.V., Archakov, A.I., Samori, B. Screen-printed electrodes based on carbon nanotubes and cytochrome P450scc for highly sensitive cholesterol biosensors. *Biosens. Bioelectron.* (2008) 24:148-150.
72. Cararra, S., Cavallini, A., Erokhin, V., De Micheli, G. Multi-panel drugs detection in human serum for personalized therapy. *Biosens. Bioelectron.* (2011) 26:3914-3919.
73. Mie, Y., Ikegami, M., Komatsu, Y. Gold sputtered electrode surfaces enhance direct electron transfer reactions of human cytochrome P450s. *Electrochem. Commun.* (2010) 12:860-683.
74. Ikegami, M., Mie, Y., Hirano, Y., Suzuki, M., Komatsu, Y. Size-controlled fabrication of gold nanodome arrays and its application to enzyme electrodes. *Colloids and Surfaces A: Physicochem. Eng. Aspects* (2011) 384:388-392.
75. Ndangili, P.M., Jijana, A.M., Baker, P.G.L., Iwuoha, E.I. 3-Mercaptopropionic acid capped ZnSe quantum dot-cytochrome P450 3A4 enzyme biotransducer for 17β-estradiol. *J. Electroanal. Chem.* (2011) 653:67-74.
76. Liu, M., Shi, G., Zhang, L., Cheng, Y., Jin, L. Quantum dots modified electrode and its application in electroanalysis of hemoglobin. *Electrochem. Commun.* (2006) 8:305-310.

77. Jensen, P.S., Chi, Q., Grumsen, F.B., Abad, J.M., Horsewell, A., Schiffrin, D.J., Ulstrup, J. Gold nanoparticle assisted assembly of a heme protein for enhancement of long-range interfacial electron transfer. *J. Phys. Chem. C* (2007) 111:6124-6132.
78. Zayats, M., Katz, E., Willner, I. Electrical-contacting of flavoenzymes and NAD(P)+-dependent enzymes by reconstitution and affinity interactions on phenylboronic acid monolayers associated with Au-electrodes. *JACS* (2002) 124:14724-14735.

Chapter 2. Development and Characterization of the Cytochrome P450 2C9 Mutants R125C, R132C, and K432C for Oriented Attachment to a Gold Electrode

2.1 Introduction

By immobilizing cytochrome P450s (CYPs) on an electrode NADPH and cytochrome P450 reductase (CPR) are no longer needed as the electron donor and electron transfer partner enzyme, respectively, and CYP can accept electrons directly from the electrode. If the immobilized CYP is electroactive on the electrode, an increase in current in the presence of a substrate can be correlated to CYP activity and thus the CYP electrode can behave as a biosensor. Numerous immobilization strategies, ranging from direct adsorption[1] to covalent attachment to a self-assembled monolayer (SAM)[2], are found in the literature for the attachment of CYPs to electrodes; however, it is becoming clear that the orientation of the enzyme on the electrode surface affects the efficiency of electron transfer. Amine coupling a CYP via the reagents EDC (1-ethyl-3-[3-dimethylaminopropyl]carbodiimide hydrochloride) and NHS (N-hydroxysuccinimide) to a carboxy-terminated SAM on a gold electrode is a robust and widely used immobilization technique. However, as seen in Figure 2.1A, this leads to a random orientation of the P450 on the electrode surface as attachment occurs randomly at surface-exposed amines (lysine residues). Site-specific attachment, unlike amine coupling, exploits the reactivity of a particular residue and can be used to immobilize a P450 on an electrode surface in a particular orientation. Figure 2.1B shows one approach to site-specific attachment; an engineered thiol (cysteine residue) on the surface of a P450 enzyme can react specifically to a maleimide-terminated SAM on a gold electrode. The location of the engineered cysteine (Cys) residue determines the orientation of the enzyme on the electrode. An analysis of the crystal structure (Figure 2.2) of the mammalian CYP 2C9, a model drug-metabolizing CYP, reveals that CYPs have two distinct faces: the proximal side of the enzyme where the reductase enzyme binds and electron transfer occurs *in vivo* and the distal side that contains the substrate binding pocket. Thus, engineering a Cys residue on the proximal side of CYP and coupling to a maleimide SAM on gold would orient the proximal side on the electrode surface and ensure the enzyme is oriented as it is for *in vivo* electron transfer.

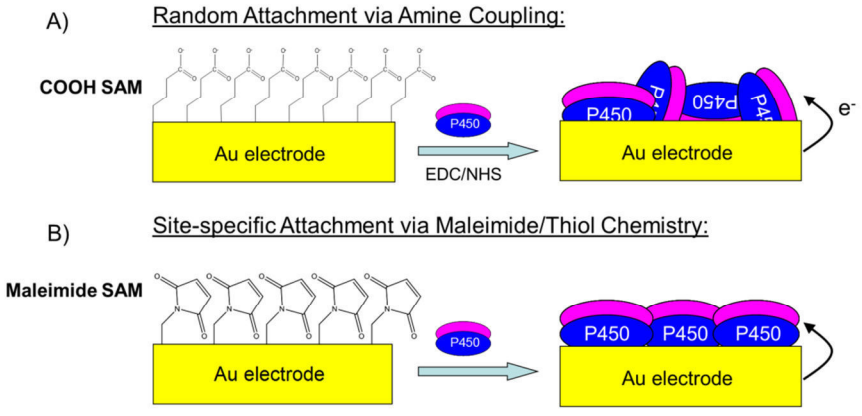

Figure 2.1 Schematic of Random and Site-Specific Attachment of CYP to an Electrode. (A) Amine coupling via EDC/NHS to a carboxy-terminated SAM on a gold electrode leads to a random orientation on the electrode as attachment occurs randomly at surface-exposed amines (lysine residues). (B) Site-specific attachment of CYP can occur via maleimide/thiol chemistry. An engineered Cys residue on the surface of the CYP reacts specifically to a maleimide-terminated SAM on gold, orienting the CYP on the electrode based on the location of the engineered Cys residue.

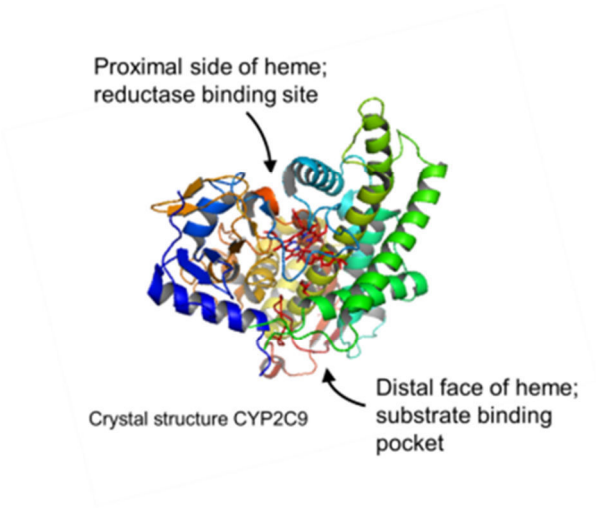

Figure 2.2 Ribbon Diagram of the Crystal Structure of CYP2C9. The heme is closest to the surface on the proximal side where cytochrome P450 reductase (CPR) binds and electron transfer occurs *in vivo*, and the distal face of the enzyme is where substrate binding occurs. The image was made in PyMol using the 1R90 crystal structure of 2C9 deposited in the Protein Data Bank (PDB)[3].

Site-specific and oriented attachment has been investigated as an electrode immobilization strategy for the bacterial cytochromes $P450_{CAM}$ (CYP101) and BM-3 (CYP102). Hill and co-workers observed the direct electrochemistry of the bacterial cytochrome $P450_{CAM}$ adsorbed to a bare edge-plane pyrolytic graphite (EPG) electrode and suggested that a patch of positively-charged residues on the proximal face of the enzyme (R72, R112, K433, and R364) was able to interact via electrostatics to the negatively-charged EPG electrode[4]. In a follow-up study, the authors explored the role of these residues and the proximal-side orientation of $P450_{CAM}$ on a bare gold electrode by creating a $P450_{CAM}$ mutant with an engineered Cys residue (K344C) on the proximal side and the rest of the surface Cys residues mutated to alanines[5]. This $P450_{CAM}$ mutant, designated SCF-K344C, exhibited enhanced electroactivity on a bare gold electrode when compared to electrodes made with either wild-type $P450_{CAM}$ or a surface cysteine free (SCF) mutant. The well-known affinity of thiols for gold most likely led to site-specific adsorption of the SCF-K344C mutant on the proximal side and orientation of the enzyme on the electrode surface. Mutagenesis studies have shown that K344 is involved in the binding of putidaredoxin, the electron transfer partner enzyme for $P450_{CAM}$[6]; thus attachment of $P450_{CAM}$ at residue 344 immobilizes the enzyme on the electrode such that electron transfer occurs in the same orientation as it does *in vivo*. Ferrero et al. oriented the heme domain of P450 BM-3 (BMP) on a maleimide-functionalized SAM on a gold electrode via attachment at the native surface Cys residues C62 and C156[7]. The authors developed the single-Cys mutants C62S and C156S for immobilizing BMP at residues C156 and C62, respectively and characterized the resulting electrodes using tapping-mode atomic force microscopy (TMAFM) and cyclic voltammetry (CV). TMAFM images showed that immobilization of the C156S mutant resulted in a stable and well-ordered enzyme monolayer while immobilization of the C62S mutant did not. An analysis of the crystal structure of BMP revealed that the surface exposure of residue 62 was more than 10 times greater than that of residue 156, suggesting that the increased accessibility of residue 62 enabled facile attachment of the C156S mutant. Although this study resulted in the site-specific attachment of BMP on an electrode, it is unclear whether or not the

enzyme was oriented for electron transfer as no information was given on the location of residues C62 and C156 on BMP.

Gilardi and co-workers have immobilized the human drug-metabolizing CYPs 2D6[8], 2E1[2,9], and 3A4[10] to maleimide-functionalized gold electrodes using site-specific attachment at *native* surface Cys residues. In one of their first studies utilizing this method, 2E1 was immobilized to a gold electrode modified sequentially with a cystamine SAM (CYSAM) and an amine-reactive maleimide (MALIM)[2]. A 2E1 electrode made using this system exhibited the fastest electron transfer rate constant ($10 \pm 0.5\ s^{-1}$) when compared to 2E1 electrodes made with either glassy carbon (GC) or gold electrodes modified with polyelectrolytes, and the Au/CYSAM/MALIM/2E1 electrode behaved as a biosensor for detection of the 2E1 substrate *p*-nitrophenol. A 3D model of 2E1 revealed that out of four surface Cys residues, C261 and C268 had the highest surface exposures at 37 and 25%, respectively, and were on the proximal side of the heme; therefore, the authors proposed that attachment most likely occurred at C261 or C268 and the enzyme may have been oriented for electron transfer on the proximal side. In a subsequent study, the same research group developed 2E1 mutants with only one surface Cys at either residue 261 (MUT261) or 268 (MUT268) by mutating the remaining surface Cys residues to serines[9]. The authors covalently coupled these mutants and wild-type (wt) 2E1 to a gold electrode modified with a dithio-bismaleimidoethane (DTME) SAM and measured the amount of the product *p*-nitrocatechol produced by each electrode during electrolysis with the substrate *p*-nitrophenol. Electrodes made with MUT261 and MUT268 produced approximately 2.6 and 2.1 times, respectively, as much product as the wt 2E1 electrode, suggesting that site-specific attachment at residues 261 and 268 on the proximal side resulted in more efficient electrocatalysis. In another study from the Gilardi group, a fusion protein made from CYP3A4 and the flavodoxin (FLD) from *Desulfovibrio vulgaris* was covalently coupled to a gold electrode modified with a maleimide-SAM[10]. A comparison to a 3A4 electrode made via adsorption to a thin film on graphite revealed that the Au/CYSAM/MALIM/3A4-FLD electrode produced, on average, 2.7 times more formaldehyde during electrolysis with the 3A4 substrate erythromycin even though it exhibited the lowest electron transfer rate constant. Taken together, the results from these studies suggest that site-specific attachment of CYPs at Cys residues, in particular those on the proximal side of the heme, is a viable method for constructing CYP biosensors and may immobilize the enzyme in an electroactive orientation.

In the present study, the cytochrome P450 2C9 (CYP2C9) mutants R125C, R132C, and K432C were developed and characterized for the site-specific attachment of 2C9 to a maleimide-functionalized SAM on a gold electrode. CYP2C9 is used as a model enzyme because it metabolizes the second-largest number of drugs after CYP3A4 and therefore is an important drug-metabolizing CYP[11]. Typical 2C9 substrates are small lipophilic anions that act as weak acids and include the anticoagulant warfarin, the first-generation anti-hypoglycemic agent tolbutamide, and non-steroidal anti-inflammatory drugs (NSAIDs) such as ibuprofen and naproxen[12]. There are very few examples of the direct electrochemistry of 2C9 on an electrode[8,13-15], and, to our knowledge, there are no published studies on the site-specific attachment of 2C9 to a gold electrode via an engineered Cys residue. The mutations R125C, R132C, and K432C were chosen based on their sequence alignment with residues on the proximal side of CYP2B4 that were reported to be involved in the binding of P450 reductase[16,17]. Immobilization of 2C9 on an electrode at these residues would presumably orient the enzyme

such that electron transfer occurs at the proximal side of the heme, mimicking *in vivo* electron transfer.

2.2 Materials and Methods

2.2.1 Materials

Vivid® BOMCC, recombinant human cytochrome b_5, recombinant cytochrome P450 oxidoreductase, TCEP (tris-(2-carboxyethyl)phosphine, hydrochloride), and Texas Red® C2 maleimide were purchased from Invitrogen (Life Technologies, Carlsbad, CA). Diclofenac sodium salt, tolbutamide, sodium cholate, sodium dithionite, 5-aminolevulinic acid hydrochloride, imidazole, cumene hydroperoxide, NADPH (β-nicotinamide dinucleotide phosphate) and PS (L-α-phosphatidyl-L-serine from *Glycine Max* (soybean)) were purchased from Sigma-Aldrich (St. Louis, MO). 4-hydroxytolbutamide was purchased from Cayman Chemical (Ann Arbor, MI), and CHAPS was purchased from Fisher Scientific (Pittsburgh, PA). DLPC (1,2-dilauroyl-*sn*-glycero-3-phosphocholine) and DOPC (1,2-dioleoyl-*sn*-glycero-3-phosphocholine) lipids were purchased from Avanti Polar Lipids Inc. (Alabaster, AL). IPTG (Isopropyl-b-D-Thiogalactopyranoside) was purchased from Apex BioResearch Products (San Diego, CA). All other chemicals or reagents used were of the highest available quality and were from Sigma-Aldrich or Fisher Scientific unless stated otherwise.

2.2.2 Methods

Expression and Purification of Wild-type CYP2C9 and Mutants

The pcWori(+) expression plasmid pCW-CYP2C9Δ3-20(6xHis) was kindly provided by Professor John O. Miners (Flinders University School of Medicine, Adelaide, Australia) and contained a truncated version of the CYP2C9 gene (N-terminal residues 3-20 are deleted) modified by a 6x Histidine-tag on the C-terminus. The single 2C9 mutants R125C, R132C, and K432C were generated by site-directed mutagenesis using the Quikchange® Lightning Mutagenesis Kit (Stratagene, La Jolla, CA), and the mutagenesis PCR reactions were carried out as per the manufacturer's instructions. PCR primers for the R125C mutant were as follows: forward 5'-ATGGAAGGAGATCCGGTGCTTCTCCCTCATGACGC-3' and reverse 5'−GCGTCATGAGGGAGAAGCACCGGATCTCCTTCCAT-3'. PCR primers for the R132C mutant were as follows: forward 5'-CTCCCTCATGACGCTGTGCAATTTTGGGATGGGGA-3' and reverse 5'-TCCCCATCCCAAAATTGCACAGCGTCATGAGGGAG-3'. PCR primers for the K432C mutant were as follows: forward 5'-TACTTCATGCCTTTCTCAGCAGGAT GCCGGATTTGTGTGGGAGAA-3' and reverse 5'-TTCTCCCACACAAATCCGGCATCCTG CTGAGAAAGGCATGAAGTA-3'. Triple 2C9 mutants with only one surface cysteine, designated SCF-R125C, SCF-R132C, and SCF-K432C, were generated by site-directed mutagenesis of the R125C, R132C, and K432C plasmid DNA using the Quikchange® Lightning Mutagenesis Kit; the native surface cysteines C338 and C372 were both mutated to serines. PCR primers for the C338S mutation were as follows: forward 5'-AACCGGAGCCCCTC CATGCAAGACAGG-3' and reverse 5'-CCTGTCTTGCATGGAGGGGCTCCGGTT-3'. PCR primers for the C372S mutation were as follows: forward 5'-CTGCCCCATGCAGTGAC

CTCCGACATTAAATTCAGAAACTA-3' and reverse 5'-TAGTTTCTGAATTTAATGTCGG AGGTCACTGCATGGGGCAG-3'.

Plasmids containg wild-type (wt) CYP2C9 and mutants were transformed into DH5α *E. coli* cells, and starter cultures (75 ml) were grown overnight with shaking at 37°C in LB broth containing ampicillin (100 μg/ml). These starter cultures were used to inoculate one liter expression cultures of Terrific Broth (TB) containing 100 μg/ml ampicillin. Expression cultures were grown with shaking at 37°C until the OD at 660 nm reached 0.7 or higher, at which point expression was induced by the addition of 1 mM IPTG and 0.5 mM of the heme precursor α-aminolevulinic acid. Induced cultures were grown with shaking at 30°C for 40 hours. Cells were harvested by centrifugation at 5,000 rpm for 10 mins at 4°C, and crude DH5α membranes containing the six-his-tagged wild-type CYP2C9 and mutants were prepared according to an established protocol[18]. Membranes were solubilized overnight at 4°C in a potassium phosphate buffer containing CHAPS (100 mM KPi, 6 mM $Mg(CH_3COO)_2$, 0.1 mM DTT, 20% glycerol, 0.5% CHAPS, pH 7.6), and solubilized membranes were centrifuged at 31,000 rpm for 30 mins at 4°C to remove any residual solids.

Wild-type his-tagged CYP2C9 and mutants were purified from solubilized DH5α membranes using a 5 ml Ni Sepharose™ column (HisTrap HP, GE Healthcare Bio-Sciences, Piscataway, NJ) and a modified version of an established protocol[14]. All purification steps were done at 4°C. Columns were equilibrated with equilibration buffer (100 mM KPi, 0.1 mM DTT, 20% glycerol, 0.5% CHAPS, pH 7.6) at a flow rate of 5 ml/min prior to loading solubilized membranes. Non-specifically bound protein was removed from the column by a series of three washes for 10 mins each at a flow rate of 5 ml/min (Wash Buffer #1: 100 mM KPi, 0.1 mM DTT, 20% glycerol, pH 7.6; Wash Buffer #2: 100 mM KPi, 0.1 mM DTT, 20 mM imidazole, 20% glycerol, pH 7.6; Wash Buffer #3: 100 mM KPi, 0.1 mM DTT, 50 mM imidazole, 20% glycerol, pH 7.6). His-tagged CYP2C9 and mutants were eluted by flowing elution buffer (100 mM KPi, 0.1 mM DTT, 500 mM imidazole, 20% glycerol, pH 7.6) through the column at a flow rate of 5 ml/min. Elution fractions containing wt or mutant 2C9 (judged by the presence of an absorption peak at 418 nm for low-spin ferric (Fe^{3+}) heme) were pooled and dialyzed at 4°C overnight in potassium phosphate buffer without CHAPS (100 mM KPi, 0.1 mM DTT, 1 mM EDTA, 10% glycerol, pH 7.6) and stored at -80°C. The concentrations of wt 2C9 and mutants were determined spectrophotometrically using the CO difference spectra method[19], and their purities were determined to be greater than 90% by visual inspection of a Coomassie-stained SDS-PAGE gel.

Enzyme Activity Assays with Vivid® BOMCC

Specific activities of the recombinant wt 2C9 and mutants were measured with the fluorogenic substrate Vivid® BOMCC using either a reconstitution assay with NADPH, cytochrome b_5, and cytochrome P450 reductase or a peroxide-supported assay with cumene hydroxperoxide. The reconstitution assay conditions were similar to those used by Yamazaki et al[20]. Briefly, 46 nM CYP2C9 was incubated for 20 mins at room temperature with 50 nM each of cytochrome b_5 and cytochrome P450 reductase, 500 μM sodium cholate, and 20 μg/ml of a lipid mix (a 1:1:1 mixture of DLPC:DOPC:PS) in 50 mM KPi, pH 7.4, and the reaction was initiated by the addition of 25 μM Vivid® BOMCC and 100 μM NADPH. For the peroxide-

supported assay, 46 nM CYP2C9 was incubated for 20 mins at room temperature with 500 μM sodium cholate and 20 μg/ml of a lipid mix (a 1:1:1 mixture of DLPC:DOPC:PS) in 50 mM KPi, pH 7.4, and the reaction was initiated by the addition of 25 μM Vivid® BOMCC and 500 μM cumene hydroperoxide. Reconstitution and peroxide-supported reactions were followed by fluorescently monitoring the formation of the Vivid® Blue product (excitation 409 nm, emission 460 nm) over a two hour time period in a SPECTRAMax M2 plate reader (Molecular Devices LLC, Sunnyvale, CA). Specific activities were taken as the average initial rate of five replicates divided by the CYP concentration.

Substrate Binding Difference Spectra with Tolbutamide

The dissociation constants for tolbutamide of wt 2C9 and the mutants R125C, R132C, and K432C were measured using substrate binding difference spectroscopy. A 2 μM solution of P450 containing 868 μg/ml lipid mix (a 1:1:1 mix of DLPC, DOPC, and PS) in 50 mM KPi, 10% glycerol, and 0.5% sodium cholate, pH 7.4 was split into two 1.0 ml quartz cuvettes, and the cuvettes were placed in a double beam spectrophotometer (Lambda 650 UV/Vis spectrophotometer, PerkinElmer, Waltham, MA). Aliquots of 25 mM tolbutamide dissolved in dimethylsulfoxide (DMSO) were added one at a time to one cuvette while a same-volume vehicle blank (DMSO only) was added to the second reference cuvette. After an incubation time of 10 mins, a difference spectrum was taken from 300 to 550 nm. Plots of substrate binding were made by plotting the difference between the absorbance of high-spin (370-390 nm) and low-spin (415-420 nm) Fe^{3+} in the difference spectra as a function of the tolbutamide concentration. Dissociation constants (K_D) for wt 2C9 and the mutants R125C, R132C, and K432C were calculated by fitting the raw data in the substrate binding plots to a 1:1 saturation binding equation using non-linear regression.

Kinetic Activity Assays with Tolbutamide

For kinetic assays with tolbutamide, either 1 μM (for R125C, R132C, and K432C) or 2 μM (for wt 2C9) recombinant P450 was incubated in 50 mM KPi, pH 7.4 with 500 μM cumene hydroperoxide and either 20, 50, 100, 200, 300, 500, or 800 μM tolbutamide. The cumene hydroperoxide and tolbutamide were added individually to the reaction from 100x stock solutions dissolved in methanol or dimethylsulfoxide, respectively, and the reaction was initiated by the addition of cumene hydroperoxide. The final percentage of organic solvent in all reactions was 2.0% (v/v). Reactions were incubated for a total time of 15 minutes and an aliquot of 200 μl was removed at 0, 5, 10, and 15 minutes for HPLC analysis of the product 4-hydroxytolbutamide. Timepoint samples were diluted 1:1 with the internal standard (500 μM diclofenac dissolved in methanol) and immediately vortexed and stored at -20°C. Samples were prepared for HPLC analysis by centrifugation at 14,000 x g for 10 mins at room temperature, followed by filtration through a 0.2 μm nylon membrane (Acrodisc® Syringe Filters, Pall Life Sciences, Ann Arbor, MI). A 4-hydroxytolbutamide calibration curve was prepared by diluting 5, 10, 20, and 50 μM 4-hydroxytolbutamide (dissolved in dimethylsulfoxide) 1:1 with the internal standard (500 μM diclofenac dissolved in methanol). For each kinetic assay, 20 μl each of the calibration curve samples and timepoint samples were injected separately at a flow rate of 0.4 ml/min onto a C18 HPLC column (Prevail C18 3u, 150 mm x 3.0 mm, Grace Discovery Sciences, Deerfield, IL) connected to an Agilent 1200 series liquid chromatograph (LC) system

with a UV/Vis detector, and the eluate was monitored at 236 nm. Solvent A was 95% H_2O and 5% MeOH with 0.05% formic acid and Solvent B was 100% MeOH with 0.05% formic acid. The following linear gradient was used: 0-8 mins: 50% Solvent B, 8-15 mins: 90% Solvent B, 16 -25 mins: 50% Solvent B. The area of the 4-hydroxytolbutamide peak relative to that of the internal standard peak (the relative response) was calculated for each timepoint sample and compared to the calibration curve to calculate the concentration of 4-hydroxytolbutamide in each timepoint sample. The initial rate of reaction for each tolbutamide concentration was found from the slope of a linear fit to the 4-hydroxytolbutamide concentration versus time plot. The apparent Michaelis constants (K_M) and V_{max} values for wild-type CYP2C9 and the mutants were found by fitting the initial rate versus tolbutamide concentration data to the Michaelis-Menten equation using non-linear regression. The reported apparent K_M and k_{cat} values are the average values obtained from three replicate experiments performed on three different days, and the reported errors are the standard deviations.

Conjugation of Wild-type CYP2C9 and Mutants to Texas Red® C2 Maleimide

For conjugation of wt 2C9 and the mutants R125C, R132C, and K432C to a maleimide-containing fluorophore, a concentrated Texas Red® C2 maleimide solution in DMSO was added at a molar excess of approximately 4.3 to a concentrated solution of P450 in 50 mM KPi, pH 8.0. After a two-hour incubation at room temperature, a NAP-5 size exclusion column (GE Healthcare Bio-Sciences, Piscataway, NJ) was used to separate free dye from protein-bound dye. Conjugation of the Texas Red® C2 maleimide to wild-type 2C9 and mutants was confirmed qualitatively by SDS-PAGE and visible absorption at 418 and 595 nm wavelengths for low-spin ferric (Fe^{3+}) heme and Texas Red, respectively.

Texas Red-CYP conjugates and unconjugated CYPs were analyzed using an Agilent 1200 series liquid chromatograph (LC; Santa Clara, CA) connected in-line to an LTQ Orbitrap XL hybrid mass spectrometer equipped with an Ion Max electrospray ionization source (ESI; Thermo-Fisher Scientific, Waltham, MA). The LC was equipped with a C8 guard column and a C8 analytical column (75 x 0.5 mm) and used a 100 μl sample loop. Solvent A was water with 0.1% (v/v) formic acid and solvent B was acetonitrile with 0.1% (v/v) formic acid. Samples were loaded in 0.3 mL polypropylene snap-top vials sealed with rubber septa and were kept in the Agilent 1200 autosampler tray prior to analysis. Approximately 100 to 200 pmoles of protein samples were injected separately onto the column. Analyte trapping after injection was performed for five minutes in 99.5% A at a flow rate of 90 μl/min. The elution program consisted of a linear gradient from 30 to 95% B over a time period of 19.5 minutes, 95% B for five minutes, a linear gradient to 0.5% B for 0.5 minutes, followed by 0.5% B for 9.5 minutes. A flow rate of 90 μl/min was used during elution. The temperature of the column and sample compartments was maintained at 35°C and 10°C, respectively. Solvent blanks of Milli-Q water were run between samples, and the autosampler needle was rinsed with Milli-Q water between samples to avoid cross-contamination.

PEEK tubing (0.005" i.d. x 1/16" o.d., Western Analytical, Lake Elsinore, CA) was used to connect the LC column exit to the mass spectrometer ion source. External mass calibration was done prior to analysis with the standard LTQ calibration mixture containing caffeine, the peptide MRFA, and Ultramark 1621 dissolved in a solution of 51% acetonitrile, 25% methanol, 23% water, and 1% acetic acid (v/v). ESI source parameters were as follows: ion transfer

capillary temperature 275°C, normalized sheath gas (nitrogen) flow rate 25%, ESI voltage 2.5 kV, ion transfer capillary voltage 33 V, and tube lens voltage 125 V. Mass spectra were recorded, in profile format, in the positive ion mode in the range m/z = 500 to 2000 using the Orbitrap mass analyzer with a full automatic MS gain control target setting of 5 x 10^5 charges and a resolution setting of 6 x 10^4 (at m/z = 400, FWHM). Xcalibur software (version 4.1, Thermo) was used to process raw mass chromatograms and spectra, and ProMass software (version 2.5 SR-1, Novatia, Monmouth Junction, NJ) was used to deconvolute measured charge state distributions using default "small protein" parameters and a background subtraction factor of 1.5.

2.3 Results and Discussion

2.3.1 Expression and Purification of Wild-type CYP2C9 and Mutants

Site-directed mutagenesis studies have shown that the interaction between CYP and P450 reductase occurs via electrostatics; basic residues on the proximal side of the CYP interact with acidic residues on P450 reductase[21,22]. An electrostatic potential map of the proximal side of CYP2C9 (Figure 2.3) reveals a pocket of positively charged residues centered in the middle of the enzyme that most likely interacts with negatively charged residues on P450 reductase. Upon closer inspection (Figure 2.4), these positively charged residues were revealed to be R125, R132, and K432. These residues align, respectively, with residues R126, R133, and K433 on the proximal side of CYP2B4, a drug-metabolizing CYP in the same family (Family 2). Residues R126, R133, and K433 on 2B4 were shown in a previous study to mediate binding of P450 reductase[16]; thus residues R125, R132, and K432 on 2C9 were chosen for individual mutation to cysteines. These single mutants were designated as R125C, R132C, and K432C. There are two native surface cysteines, C338 and C372, on 2C9 that could react with maleimide groups on an electrode. However, the solvent accessible surface area of C338 and C372 is very low (25.0 and 53.2 $Å^2$, respectively) compared to that of R125, R132, and K432 (125.1, 142.0, and 82.5 $Å^2$, respectively), making it unlikely that these native surface Cys residues would react. Nonetheless, additional 2C9 mutants bearing only one surface cysteine were made to ensure oriented attachment of 2C9 to a gold electrode. Residues R125, R132, and K432 were mutated individually to cysteines and residues C338 and C372 were both mutated to serines. These triple 2C9 mutants were designated as SCF-R125C, SCF-R132C, and SCF-K432C (SCF stands for Surface Cysteine Free) and contain only one surface Cys at residues 125, 132, and 432, respectively.

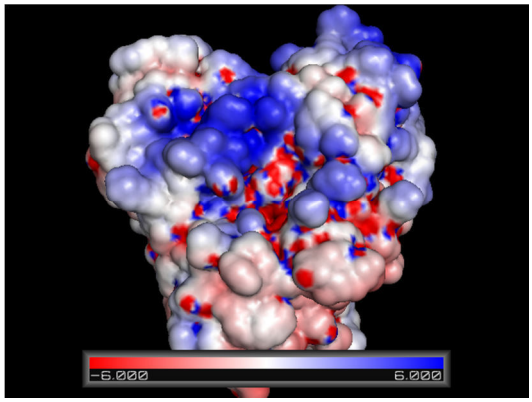

Figure 2.3 Electrostatic Potential Map of the Proximal Side of CYP2C9. An electrostatic potential map of the proximal side of 2C9 reveals a patch of positively charged residues in the center. Electrostatic potential is colored red (negatively charged residues) to blue (positively charged residues), and the image was made in PyMol using the 1R90 crystal structure of 2C9 deposited in the PDB[3].

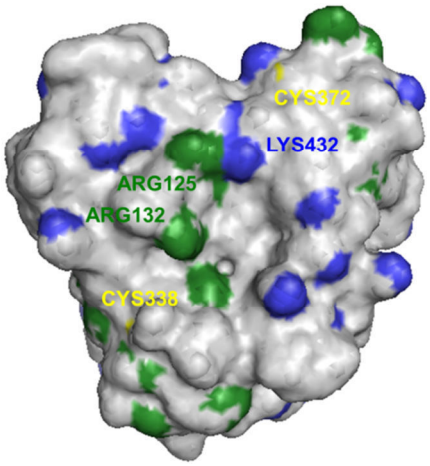

Figure 2.4 Solvent Accessible Surface Area of the Proximal Side of CYP2C9. A map of the solvent accessible surface area of the proximal side of 2C9 shows that the positively charged patch seen in the electrostatic potential map is made up of residues R125, R132, and K432. Two native surface cysteines, C338 and C372, are also barely visible on the proximal side of 2C9. Arginines, lysines, and cysteines are colored green, blue, and yellow, respectively, and the image was made in PyMol using the 1R9O crystal structure of 2C9 deposited in the PDB[3].

Site-directed mutagenesis of recombinant, his-tagged 2C9 in the pcWori(+) expression plasmid was used to make all the 2C9 mutants, and sequencing of mutant DNA confirmed the correct placement of the desired mutations. His-tagged wild-type (wt) 2C9, single mutants (R125C, R132C, and K432C) and triple mutants (SCF-R125C, SCF-R132C, and SCF-K432C) were expressed in DH5α *E. coli* and purified using a Ni-NTA column. Wt-2C9, R125C, R132C, and K432C expressed and purified well, as seen in a Coomassie-stained SDS-PAGE gel of elution fractions depicted in Figure 2.5. SCF-R125C, SCF-R132C, and SCF-K432C all expressed; however, SCF-R132C did not purify well. As shown in Figure 2.6, there was no detectable SCF-R132C protein in a Coomassie-stained SDS-PAGE gel of elution fractions. It is unclear why SCF-R132C did not purify and further attempts to purify this mutant were not carried out. It is possible that the enzyme denatured during purification due to instability. Absorption spectroscopy of the elution and flow-through fractions obtained during purification of the SCF-R132C mutant indicated that there was no P450 present in either of these fractions.

However, DH5α cell pellets harvested after expression of SCF-R132C were dark brown from the iron heme, suggesting that SCF-R132C was present in the *E. coli* cell lysate before further purification.

Figure 2.5 Coomassie-Stained SDS-PAGE Gel of Purified wt 2C9, R125C, R132C, and K432C. Lanes 1 thru 5 are K432C, R132C, R125C, wt-2C9, and protein ladder, respectively. The 50 kDa marker is labeled, and the molecular weight of recombinant 2C9 is approximately 55 kDa.

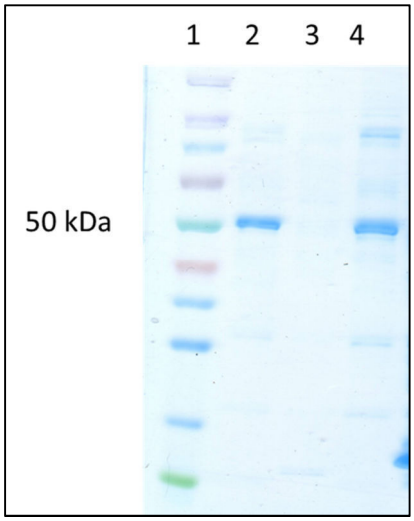

Figure 2.6 Coomassie-Stained SDS-PAGE Gel of Purified SCF-R125C, SCF-R132C, and SFC-K432C. Lanes 1 thru 4 are protein ladder, SCF-R125C, SCF-R132C, and SCF-K432C, respectively. The 50 kDa marker is labeled, and the molecular weight of recombinant 2C9 is approximately 55 kDa.

Visible absorption spectrophotometry was used to further characterize wt 2C9 and the single (R125C, R132C, and K432C) and triple (SCF-R125C and SCF-K432C) 2C9 mutants. CYP enzymes are known for their characteristic absorption at 450 nm in the presence of carbon monoxide (CO) and a reducing agent, hence the 'P450' name. Low-spin, reduced ferrous heme (Fe^{2+}) binds to CO tightly, resulting in a shift in the absorption peak from 418 to 450 nm[19]. Thus, absorption spectra of wt 2C9 and the single/triple mutants were taken in the presence of CO and a reducing agent to assess whether or not the enzymes were properly folded and contained heme. Figure 2.7 shows the absorption and difference spectra of wt 2C9 and the single

mutants R125C, R132C, and K432C in the presence of the reductant sodium dithionite and CO. There is a clear peak at 450 nm in both the absorption and difference spectra of wt 2C9 and the single 2C9 mutants, suggesting that these enzymes are properly folded and contain the iron heme. A small shoulder at approximately 420 nm is also visible in the absorption spectra for both wt 2C9 and the single 2C9 mutants and indicates that some of the CYP enzyme in these samples was in an inactive form known as P420. P420, named for the presence of an absorption peak at 420 nm, is an inactive form of the enzyme that is thought to be brought about by protonation of the axial cysteine thiolate heme ligand[23]. Formation of P420 has been shown to occur via increases in temperature[24] and/or pressure[25] and exposure to neutral salts[26], detergents[19], organic solvents[27], and high/low pH buffers[28]. Thus, the extent of formation of P420 is an indication of how stable a particular CYP is. A comparison of the absorption spectra for wt 2C9 and the single 2C9 mutants reveals roughly the same degree of P420 formation in all samples. One can conclude that Cys mutations at residues R125, R132, and K432 minimally affect the immediate environment of the iron heme because the resulting mutants appear to have the same absorption spectrum as wt 2C9. This is surprising, as residues R125 and K432 are one residue away, respectively, from R124 and R433, which stabilize the iron heme via hydrogen bonds to the heme propionates[29]. In addition, residue K432 is three residues away from C435, which acts as the axial ligand to the iron heme[28].

Figure 2.8 shows the absorption and difference spectra for wt 2C9 and the triple mutants SCF-R125C and SCF-K432C in the presence of sodium dithionite and CO. There is a clear peak at 450 nm in the absorption spectra of the triple mutants, suggesting that they are properly folded, contain heme, and are able to bind CO. However, a comparison with the absorption spectrum of wt 2C9 reveals that there is more P420 formation in the triple mutants, suggesting that the additional mutations C338S and C372S perturb the structure of the enzyme and induce protonation of the axial cysteine thiolate. An analysis of the crystal structure of 2C9 shows that both C338 and C372 are partially buried in the interior of the protein; thus, changing these residues to serines may disrupt polar interactions with interior residues and alter the conformation of the enzyme.

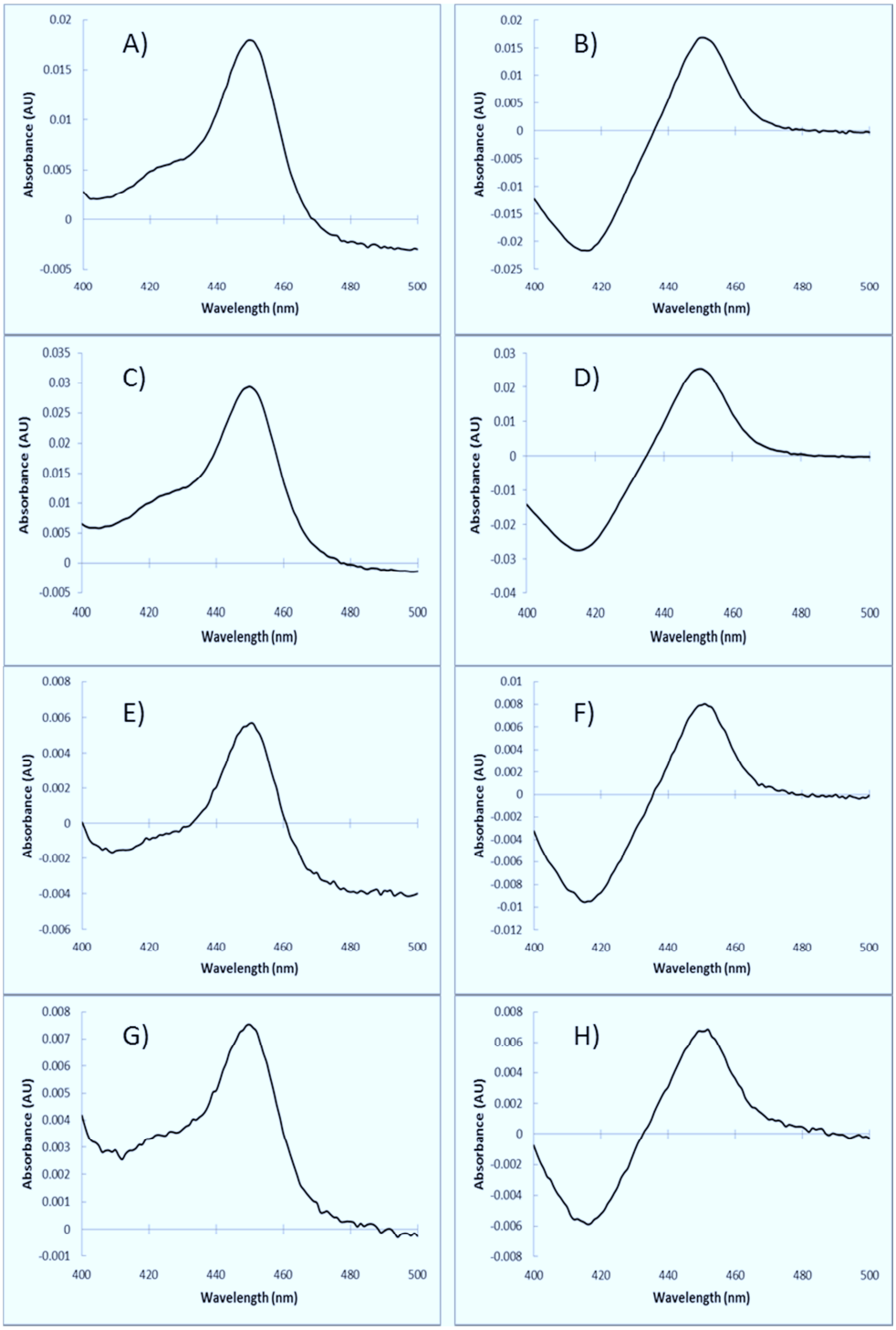

Figure 2.7 Absorption and Difference Spectra of wt 2C9 and the Single 2C9 Mutants R125C, R132C, and K432C in the Presence of Sodium Dithionite and Carbon Monoxide (CO). CO difference spectra were taken as the difference between the absorption spectrum of reduced, CO-bound CYP and oxidized CYP without CO. (A) Absorption spectrum of wt 2C9. (B) Difference spectrum of wt 2C9. (C) Absorption spectrum of R125C. (D) Difference spectrum of R125C. (E) Absorption spectrum of R132C. (F) Difference spectrum of R132C. (G) Absorption spectrum of K432C. (H) Difference spectrum of K432C.

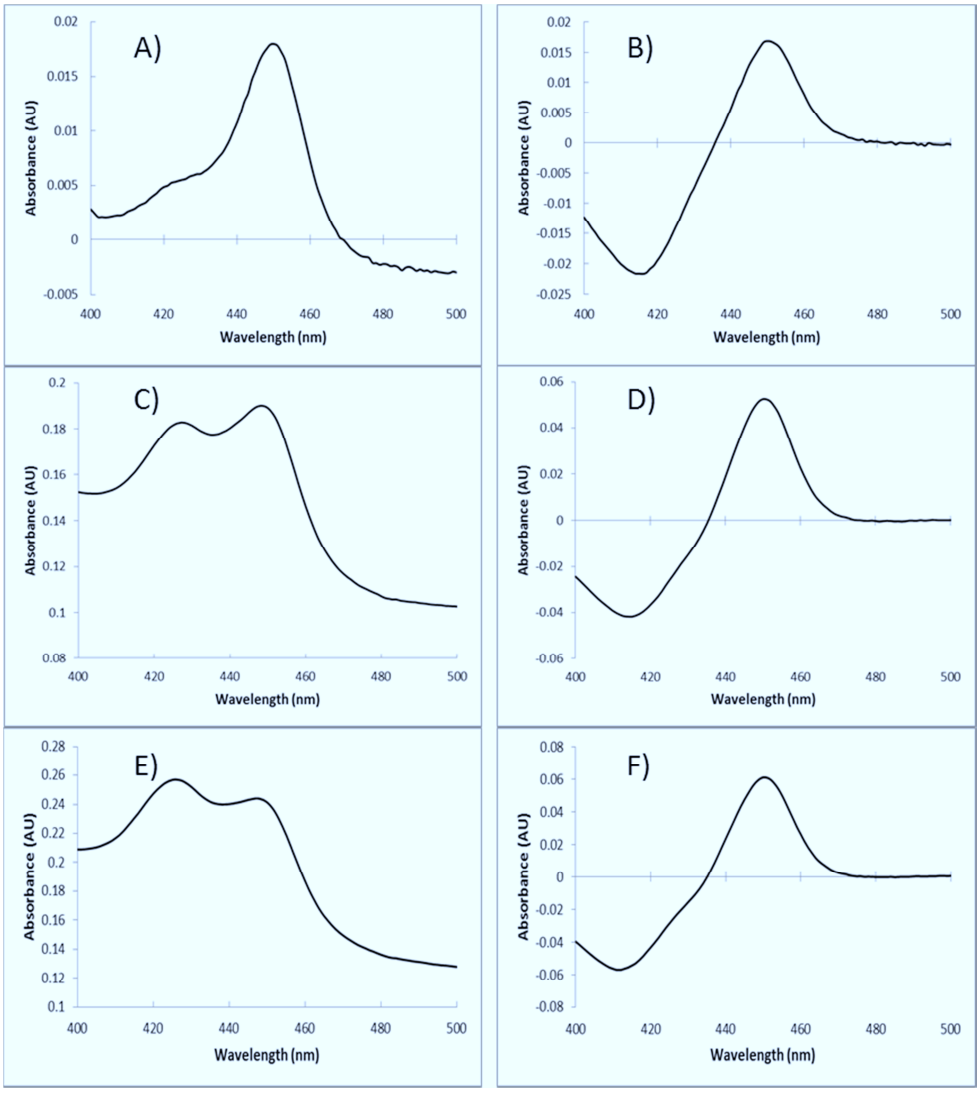

Figure 2.8 Absorption and Difference Spectra of wt 2C9 and the Triple 2C9 mutants SCF-R125C and SFC-K432C in the Presence of Sodium Dithionite and Carbon Monoxide (CO). CO difference spectra were taken as the difference between the absorption spectrum of reduced, CO-bound CYP and oxidized CYP without CO. (A) Absorption spectrum of wt 2C9. (B) Difference spectrum of wt 2C9. (C) Absorption spectrum of SCF-R125C. (D) Difference spectrum of SCF-R125C. (E) Absorption spectrum of SCF-K432C. (F) Difference spectrum of SCF-K432C.

2.3.2 Enzyme Activity Assays with Vivid® BOMCC

Specific activities of wt 2C9 and the single/triple 2C9 mutants were measured with the fluorogenic substrate Vivid® BOMCC. As shown in Figure 2.9, Vivid® BOMCC reacts with 2C9 to form the highly fluorescent product Vivid® Blue; the activity of wt 2C9 and the single/triple mutants was therefore assessed by following the fluorescence of the Vivid® Blue product (excitation 409 nm, emission 460 nm) over time. Two kinds of activity assays were performed. In one assay termed a reconstitution activity assay, recombinant 2C9 was reconstituted in lipid with the electron transfer partner enzymes CPR and cytochrome b_5 (b_5) and NADPH was used as the electron donor. In a second assay termed a peroxide-supported activity assay, the organic hydroperoxide cumene hydroperoxide (CuOOH) was used as the electron donor in lieu of NADPH, CPR, and b_5. Peroxides such as H_2O_2 or CuOOH have been used in

previous studies as an electron donor for the direct activation of bacterial and mammalian CYPs for catalysis and can be used in place of CPR and NAD(P)H[30-34].

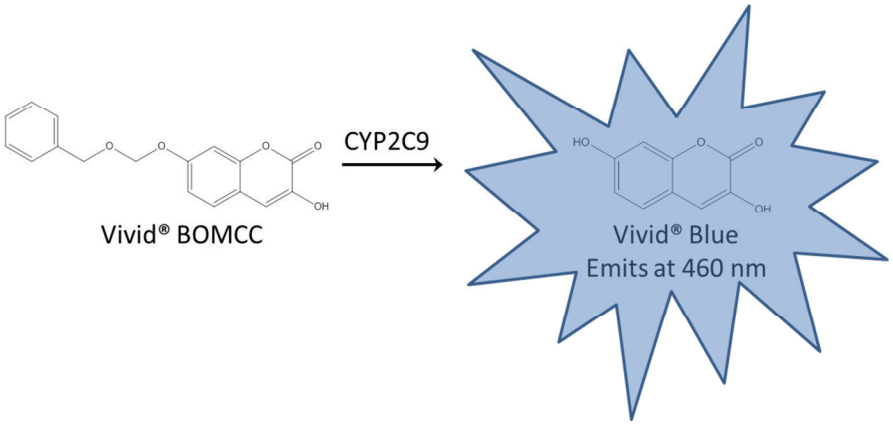

Figure 2.9 Schematic of the Reaction between CYP2C9 and Vivid® BOMCC. Reaction of CYP2C9 with Vivid® BOMCC results in formation of the highly fluorescent product Vivid® Blue, which excites at 409 nm and emits at 460 nm.

The specific activities of wt 2C9 and the single mutants R125C, R132C, and K432 measured from the reconstitution and peroxide-supported activity assays with Vivid® BOMCC are shown in Figure 2.10. The mutants R125C, R132C, and K432C had significantly lower activity than wt 2C9 when they were reconstituted with CPR/b_5 and NADPH; however, this loss in activity was recovered when CuOOH was used in lieu of CPR/b_5 and NADPH. This suggests that residues R125, R132, and K432 are indeed involved in binding of P450 reductase and/or b_5 and site-specific attachment of 2C9 to a maleimide-gold electrode at these residues will most likely immobilize the enzyme in an electroactive orientation. Similar results have been found for the naturally occurring 2C9 mutant R144C (CYP2C9*2); the authors similarly concluded that the surface residue R144 was involved in binding P450 reductase[35]. In the peroxide-supported assay, the specific activities of wt 2C9 and the single 2C9 mutants from low to high follows the order K432C < wt 2C9 < R125C < R132C. R132C had the highest specific activity at 777.7 ± 15.4 Rfu/min/μM P450, and K432C had the lowest specific activity at 427.4 ± 24.4 Rfu/min/μM P450. The specific activity of R125C in the peroxide-supported activity assay (622.2 ± 29.7 Rfu/min/μM P450) was very similar to that of wt 2C9 (567.3 ± 19.0 Rfu/min/μM P450).

Although the visible absorption spectra of reduced and CO-bound K432C suggest that the mutation K432C does not appreciably affect stability of the iron heme, the results from the peroxide-supported activity assay suggest otherwise; the mutation appears to negatively affect catalysis with Vivid® BOMCC. As mentioned earlier, residue K432 is close to residues R433 and C435, which are involved in stabilization and ligation, respectively, of the iron heme. The mutation K432C may alter the conformation of these residues and in turn perturb nearby residues involved in substrate binding or catalysis. The single mutation R132C resulted in a 37% increase in specific activity over wt 2C9. The R132C mutant was consistently more active than wt 2C9 each time the peroxide-supported activity assay with Vivid® BOMCC was performed. Residue R132 is located on the surface of 2C9 in the loop region between helices C and D in the crystal structure and at first glance does not appear to be involved in substrate binding[3]; thus, it is strange that mutation R132C has such a marked effect on enzyme activity with Vivid® BOMCC. In a previous study, the mutation R132Q, a polymorphic variant of 2C9 (CYP2C9*33) identified

in Japanese, resulted in a five-fold lower catalytic activity towards the substrate diclofenac when the enzyme was expressed in a baculovirus-insect cell system[36,37]. The results from this study suggest that residue R132 may be involved in substrate binding or catalysis but it is more likely that the mutation R132Q, like the mutation R132C in the present study, adversely affects the interaction of 2C9 with P450 reductase and/or b_5. It is unclear from our results exactly how the mutation R132C affects catalytic activity with Vivid® BOMCC. The activity of the R125C mutant is very similar to that of wt 2C9 in the peroxide-supported assay; therefore, it appears that incorporation of a Cys at residue 125 does not affect its inherent catalytic activity if a surrogate electron donor is used in place of CPR/NADPH. A polymorphic variant of 2C9 identified in an Indian individual (CYP2C9*14) contained the mutation R125H and, when expressed in *E. coli*, exhibited a greater than 90% decrease in catalytic activity and an increase in K_M with the substrate tolbutamide[38]. This decrease in catalytic activity seen with the mutant R125H may be due to altered binding of P450 reductase and/or b_5, as seen in the present study with the mutant R125C, but the increase in K_M with tolbutamide suggests that residue R125 may also be involved in substrate binding.

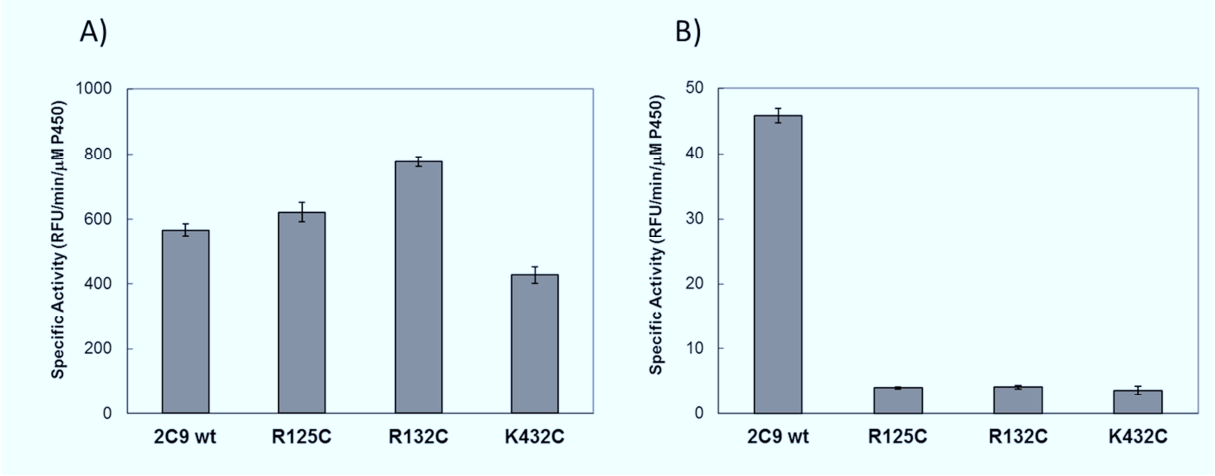

Figure 2.10 Specific Activities of wt 2C9 and the Single 2C9 Mutants R125C, R132C, and K432C Measured in the Reconstitution and Peroxide-Supported Activity Assays. The specific activities of wt 2C9 and the mutants R125C, R132C, and K432C measured in (A) a reconstitution activity assay with 50 nM each of P450 reductase and cytochrome b_5 and 25 µM Vivid® BOMCC and (B) a peroxide-supported activity assay with 500 µM CuOOH and 25 µM Vivid® BOMCC. A concentration of 46 nM P450 was used for both the reconstitution and peroxide-supported activity assays.

Figure 2.11 shows the specific activities measured in the reconstitution and peroxide-supported activity assays with Vivid® BOMCC for the triple 2C9 mutants SCF-R125C and SCF-K432C, along with those for the single 2C9 mutants R125C and K432C for comparison. The specific activities of SCF-R125C and SCF-K432C in the reconstitution activity assay are approximately 99% lower than the values obtained with the peroxide-supported activity assay, suggesting, like the results from activity assays of the single 2C9 mutants R125C and K432C, that residues R125 and K432 are involved in binding P450 reductase and/or b_5. However, unlike the single mutants R125C and K432C, the triple mutants SCF-R125C and SCF-K432C exhibit markedly lower activities when CuOOH is used as a surrogate electron donor in lieu of P450 reductase, b_5, and NADPH. This suggests that the additional mutations C338S and C372S adversely affect substrate binding and/or catalysis, at least with Vivid® BOMCC. These findings corroborate the results obtained earlier with absorption spectroscopy. The presence of more

P420 in the absorption spectra of reduced and CO-bound SCF-R125C and SCF-K432C suggested that the additional mutations C338S and C372S perturb the 2C9 structure such that the axial cysteine thiolate becomes protonated. Now, additional information obtained from activity assays with these triple 2C9 mutants shows that, in addition to altering the environment of the heme, the mutations C338S and C372S affect catalysis. Despite the fact that the triple mutants SCF-R125C and SCF-K432C contained only one reactive cysteine and would be immobilized on an electrode in only one orientation, their low activity and apparent instability deemed them unsuitable for use in a 2C9 electrode. Thus, only the single 2C9 mutants R125C, R132C, and K432C were further characterized and considered for immobilization on an electrode.

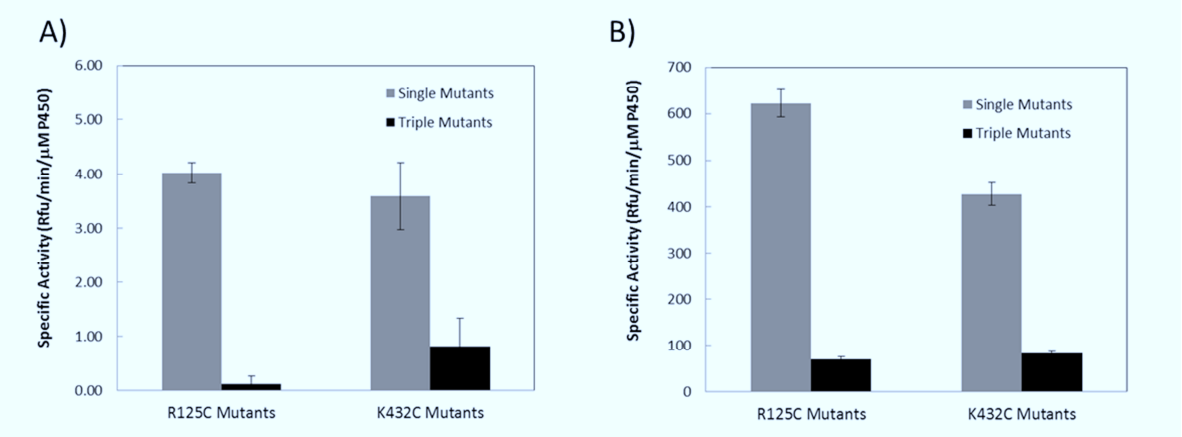

Figure 2.11 Specific Activities of the Single 2C9 Mutants R125C and K432C and the Triple 2C9 Mutants SCF-R125C and SCF-K432C Measured in Reconstitution and Peroxide-Supported Activity Assays. The specific activities of the single (R125C and K432C, shown in grey) and triple (SCF-R125C and SCF-K432C, shown in black) 2C9 mutants in (A) a reconstitution activity assay with 50 nM each of P450 reductase and cytochrome b_5 and 25 µM Vivid® BOMCC and (B) a peroxide-supported assay with 500 µM CuOOH and 25 µM Vivid® BOMCC. A concentration of 46 nM P450 was used for both the reconstitution and peroxide-supported activity assays.

2.3.3 Substrate Binding Difference Spectra with Tolbutamide

The effect of the mutations R125C, R132C, and K432C on binding of the 2C9 substrate tolbutamide were analyzed via substrate binding difference spectroscopy. It is well established in the literature that substrate binding to CYPs displaces a water molecule as the sixth ligand to the iron heme[39]. For some CYPs, this substrate-induced displacement of water is accompanied by a spin shift in the iron heme from low-spin (LS) to high-spin (HS) ferric (Fe^{3+}) iron[39]. This spin-shift is characterized by a change in the absorption wavelength of the ferric heme; HS ferric heme absorbs at approximately 390 nm while LS ferric heme absorbs at approximately 418 nm. Tracking this shift in absorbance from 418 to 390 nm upon substrate binding, or collecting a difference spectra, allows one to follow substrate binding and obtain a dissociation constant (K_D) for the substrate. Tolbutamide, a first-generation anti-hypoglycemic agent, is widely used as a marker substrate for 2C9 activity in *in vitro* activity assays and is almost exclusively metabolized *in vivo* by 2C9 to the product 4-hydroxytolbutamide, as seen in Figure 2.12[40]. Figure 2.13 shows the substrate binding difference spectra obtained by incubating wt 2C9, R125C, R132C, and K432C with increasing concentrations of tolbutamide. As seen in Figure 2.13, the absorption wavelength for HS ferric heme varies amongst wt 2C9 and the single 2C9 mutants from approximately 375 nm for the R132C mutant to 390 nm for the K432C mutant. The absorption peak for LS ferric heme however, is nearly constant at approximately 415 to 420 nm amongst all

the 2C9 variants. The fact that the absorbance of LS ferric heme decreases upon incubation with increasing concentrations of tolbutamide indicates a shift to HS ferric heme and that wt 2C9 and the single 2C9 mutants R125C, R132C, and K432C bind tolbutamide. However, the variation in the absorption peak for HS ferric heme seen in the various difference spectra indicates that tolbutamide binding alters the chemical environment of the heme to varying degrees in wt 2C9 and the single 2C9 mutants.

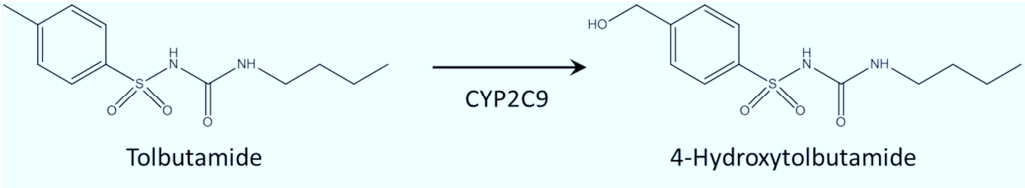

Figure 2.12 Schematic of the reaction of CYP2C9 with Tolbutamide to form 4-Hydroxytolbutamide

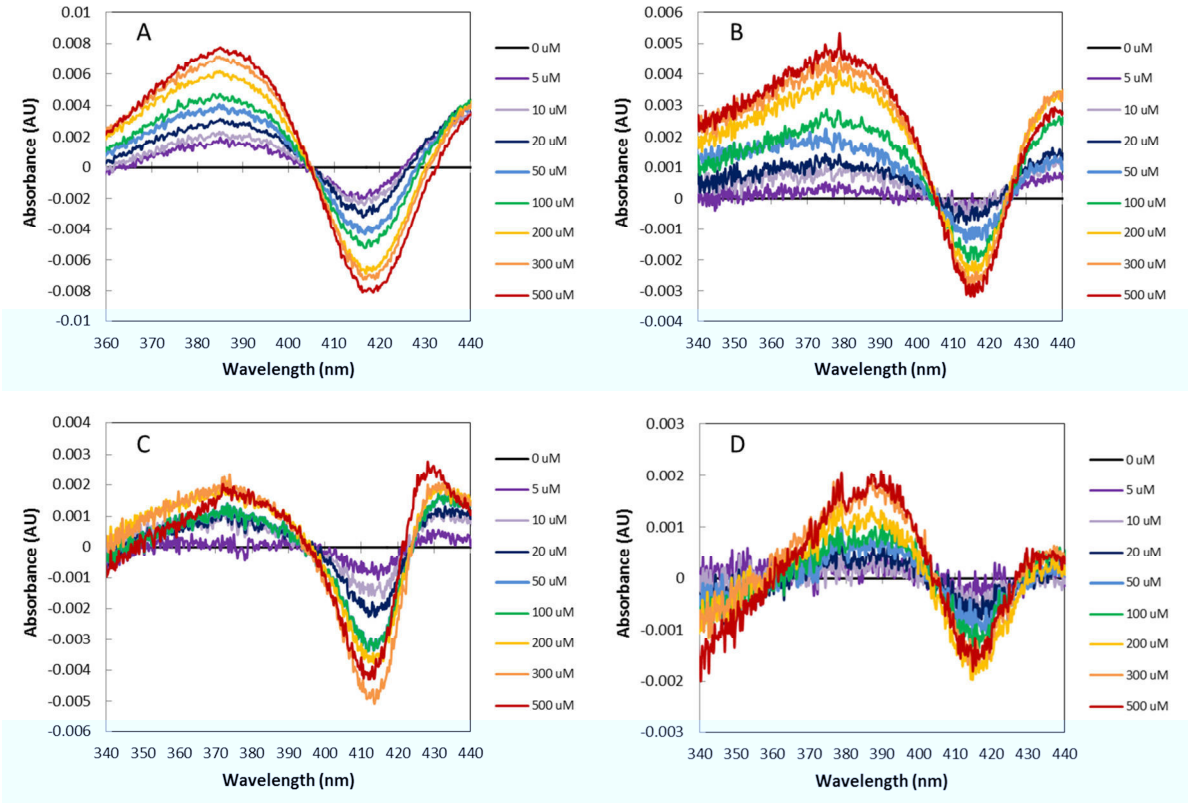

Figure 2.13 Substrate Binding Difference Spectra of wt 2C9, R125C, R132C, and K432C. Substrate binding difference spectra of (A) wt 2C9, (B) R125C, (C) R132C, and (D) K432C were taken in the presence of increasing (0, 5, 10, 20, 50, 100, 200, 300, and 500 μM) concentrations of tolbutamide. Difference spectra were taken by subtracting the absorption spectrum of 2C9 with a vehicular blank from the absorption spectrum of 2C9 in the presence of tolbutamide.

Dissociation constants for tolbutamide binding to wt 2C9 and the mutants R125C, R132C, and K432C were obtained by fitting the change in absorbance between HS and LS heme seen at increasing tolbutamide concentrations to a simple 1:1 binding model with saturation. Figure 2.14 shows the raw data and best fit for saturation binding of tolbutamide to wt 2C9 and

the single mutants R125C, R132C, and K432C. The fitted K_D values are included within each plot. The mutants R125C and K432C both have a higher dissociation constant for tolbutamide (101.8 and 75.3 μM, respectively) than wt 2C9 (52.8 μM), suggesting that the mutations R125C and K432C adversely affect substrate binding of tolbutamide. It is possible that the mutations residues R125C and K432C alter the structure of 2C9 such that the conformation of the binding pocket changes. Interestingly, this change is more dramatic in the R125C mutant than the K432C one, even though results from the peroxide-supported activity assay with Vivid® BOMCC suggested that the K432C mutation is more detrimental for catalysis. It is possible that the decrease in substrate affinity seen with the R125C mutant is tolbutamide-specific and thus is not manifested in catalysis with Vivid® BOMCC. An increase in the K_M for tolbutamide was seen with the naturally occurring 2C9 mutant R125H, which provides some evidence that residue R125 may be involved in substrate binding[38]. The mutant R132C has a more than two-fold lower dissociation constant for tolbutamide (21.9 μM) than wt 2C9, suggesting that residue R132 plays a role in substrate binding. Because R132 is a surface residue it is likely that mutations at this residue affect substrate binding via interactions with interior residues close to the substrate binding pocket. If the mechanism behind the increased affinity for tolbutamide of the R132C mutant is universal to all substrates, then it is possible that the increased activity seen in the peroxide-supported activity assay with R132C and Vivid® BOMCC may be due in part to tighter binding of the substrate.

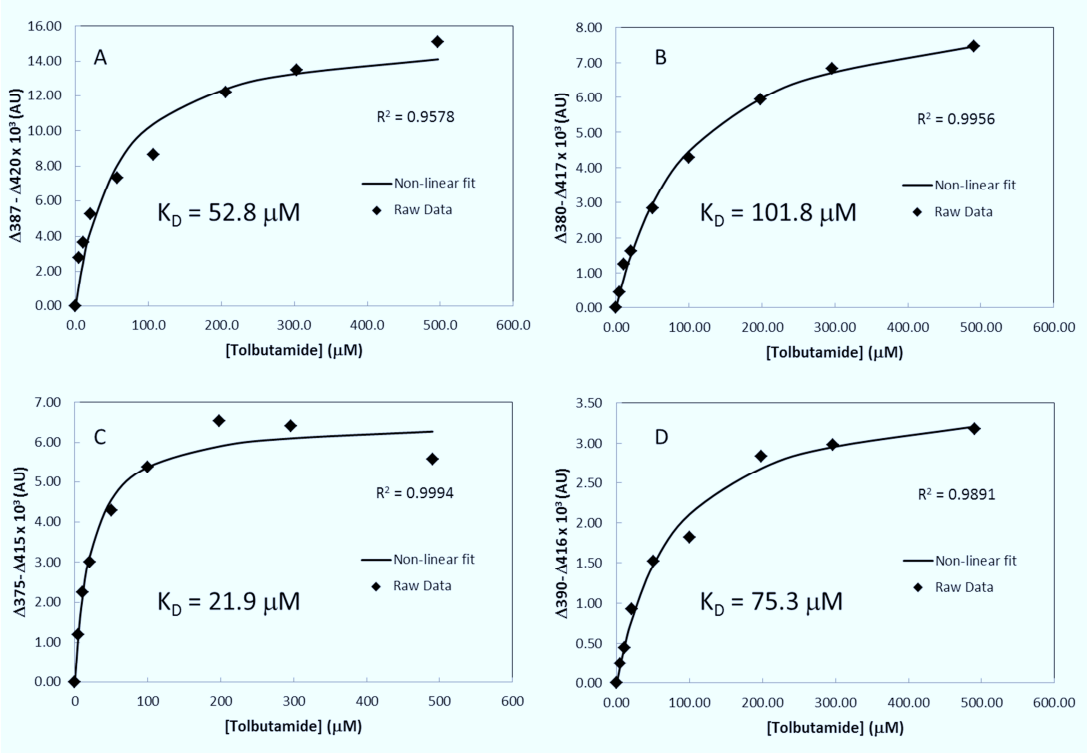

Figure 2.14 Raw Data and Best Fit Lines for Saturation Binding of Tolbutamide to wt 2C9, R125C, R132C, and K432C. Raw data are the absorbance differences (in AU) between HS and LS heme as a function of tolbutamide concentration (in μM) for (A) wt 2C9, (B) R125C, (C) R132C, and (D) K432C. The obtained K_D values are from a best fit of the raw data to a 1:1 saturation binding model using non-linear least-squares regression analysis.

2.3.4 Kinetic Activity Assays with Tolbutamide

To further characterize wt 2C9 and the mutants R125C, R132C, and K432C, peroxide-supported kinetic activity assays were performed with tolbutamide. Initial reaction rates were determined by measuring the amount of the product 4-hydroxytolbutamide produced over time via HPLC. Cumene hydroperoxide was used in lieu of CPR and NADPH because the low reaction rates seen with R125C, R132C, and K432C in the reconstitution assay with Vivid® BOMCC suggested that product formation rates with these mutants would be very slow with P450 reductase and NADPH. Initial rates were measured with 20, 50, 100, 200, 300, 500, and 800 μM tolbutamide, and initial rates taken from three separate experiments performed on three separate days were averaged to get an average initial rate for each tolbutamide concentration. Figure 2.15 shows the raw data and best fit lines to the Michaelis-Menten equation for plots of the initial rate of 4-hydroxytolbutamide formation as a function of tolbutamide concentration for wt 2C9, R125C, R132C, and K432C. As seen in Figure 2.15, the data fit nicely to the Michaelis-Menten equation with correlation coefficients greater than or equal to 0.97. This is expected, as tolbutamide hydroxylation has been reported in the literature to follow simple Michaelis-Menten kinetics[40]. Fitted values for the turnover rate (k_{cat}) and apparent Michaelis-Menten constant (K_M^{app}) for wt 2C9, R125C, R132C, and K432C are shown in Table 2.1 along with the respective tolbutamide dissociation constant as a reference. These values should be interpreted with care however, as the P450 catalytic mechanism is still poorly understood and it is unclear whether or not the Michaelis-Menten equation is an accurate model for CYP catalysis[41].

The k_{cat} values for peroxide-supported tolbutamide hydroxylation with wt 2C9 and the single 2C9 mutants are all very low (ranging from 0.4 to 0.8 min^{-1}). This is somewhat expected, as 2C9 has been reported in the literature to have a very slow turnover rate with tolbutamide[40]. However, the k_{cat} values obtained in the present study are an order of magnitude lower than values reported in the literature; a recent study by Traylor et al. reported a k_{cat} value of 6 ± 1 min^{-1} for tolbutamide hydroxylation by 2C9 baculosomes[42]. Most of the k_{cat} values reported in the literature though are for reactions with P450 reductase and NADPH and not CuOOH-supported ones. Peroxide-supported CYP reactions are notoriously slower than NADPH-supported ones. The k_{cat} for CuOOH-supported testosterone 6β-hydroxylation by recombinant CYP3A4 was found to be 0.81 min^{-1} whereas a k_{cat} of 22.1 min^{-1} was found for the same reaction with P450 reductase and NADPH[31]. In a similar study, the k_{cat} value for the CuOOH-supported reaction of 2C9 with a laser active dye was found to be nearly 17 times lower than that of the NADPH-supported reaction[43]. In light of these previous studies, the k_{cat} values obtained in the present study for wt 2C9, R125C, R132C, and K432C seem reasonable. Both R125C and K432C each exhibit k_{cat} values for tolbutamide hydroxylation that are nearly twice that of wt 2C9 while R132C, at 0.5 min^{-1}, has a k_{cat} value that is closest to that of wt 2C9. Based on the k_{cat} values alone, it appears that the mutations R125C and K432C have a positive effect on the turnover of tolbutamide while the mutation R132C has a neutral effect. This effect on turnover appears to be substrate-specific, as the same trend was not observed for specific activity of the mutants R125C, R132C, and K432C in a CuOOH-supported reaction with Vivid® BOMCC.

The apparent K_M value for wt 2C9 with tolbutamide (218.4 ± 43.9 μM) agrees well with values reported in the literature for 2C9 in human liver microsomes (62 to 371 μM)[44-48] and baculosomes (366 μM)[42]. The mutants R125C, R132C, and K432C all have larger apparent K_M values than wt 2C9, ranging from 368.7 ± 47.9 μM for R132C to 633.8 ± 149.1 μM for K432C.

The apparent K_M value for R132C and tolbutamide is close to that of wt 2C9 while R125C and K432C exhibit apparent K_M values for tolbutamide that are approximately two and three times larger, respectively, than that of wt 2C9. It is tempting to say from this analysis that the mutations R125C and K432C adversely affect substrate binding of tolbutamide but this is not necessarily the case. A comparison between the apparent K_M and dissociation constant (K_D) values for tolbutamide and wt 2C9, R125C, R132C, and K432C reveals a marked discrepancy between the two values. This discrepancy has been found for other 2C9 substrates such as flurbiprofen[49] and suggests that the apparent Michealis-Menten constant K_M for CYP enzymes reflects more than just substrate binding. Clearly, the apparent Michaelis-Menten constant K_M does not equate to the dissociation constant K_D in CYP reactions and thus cannot be used as a stand-alone value to evaluate the effects of the mutations R125C, R132C, and K432C on substrate binding of tolbutamide.

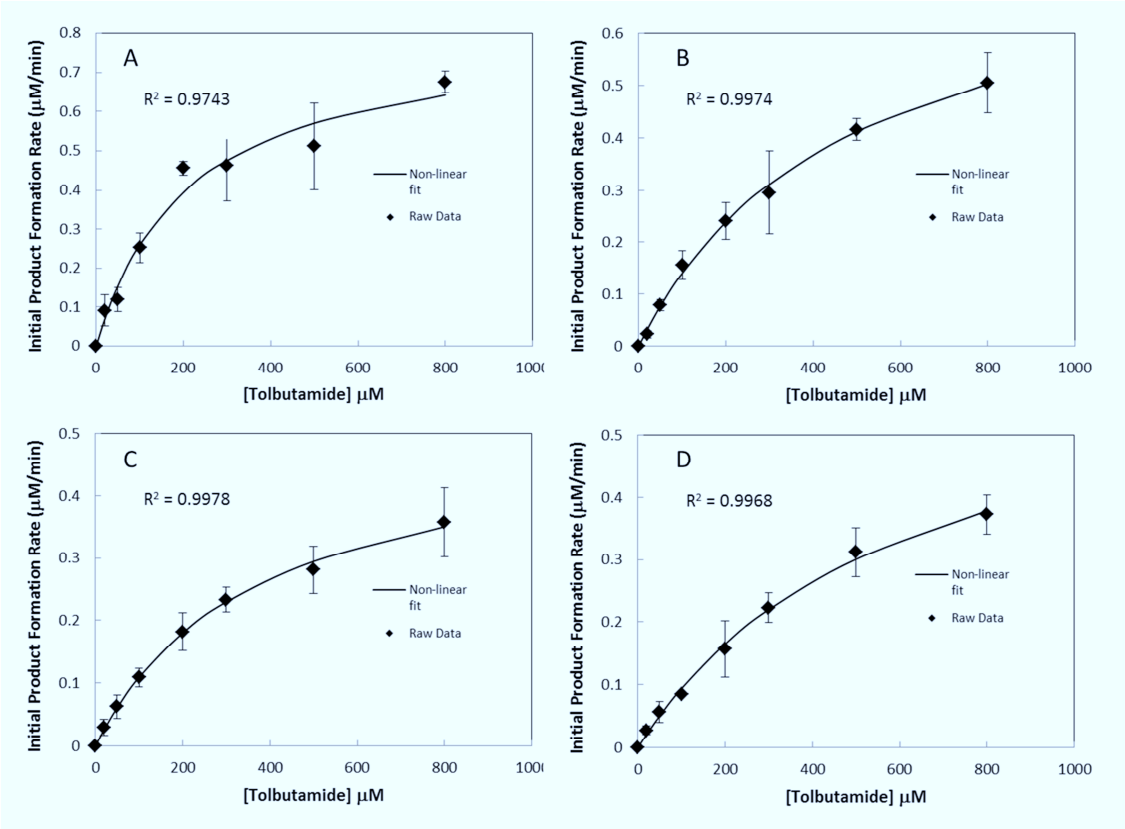

Figure 2.15 Raw Data and Best Fit Lines to the Michaelis-Menten Equation for Plots of Initial Product Formation Rate as a Function of Tolbutamide Concentration for wt 2C9, R125C, R132C, and K432C. Raw data are the initial rates of formation of the product 4-hydroxytolbutamide as a function of tolbutamide concentration for (A) wt 2C9, (B) R125C, (C) R132C, and (D) K432C. An individual data point is the average value for three different experiments performed on three separate days. Best fit lines were obtained by fitting the raw data to the Michaelis-Menten equation using non-linear least-squares regression analysis. A CYP concentration of 1 μM was used to obtain the wt 2C9 data, and a CYP concentration of 2 μM was used to obtain the R125C, R132C, and K432C data.

Enzyme	K_M^{app} (μM)	k_{cat} (min^{-1})	k_{cat}/K_M ($min^{-1}\mu M^{-1}$)	K_D (μM)
wt 2C9	218.4 ± 43.9	0.4 ± 0.05	1.8×10^{-3}	53.8
R125C	471.6 ± 56.4	0.8 ± 0.04	1.7×10^{-3}	101.8
R132C	368.7 ± 47.9	0.5 ± 0.09	1.4×10^{-3}	21.9
K432C	633.8 ± 149.1	0.7 ± 0.09	1.1×10^{-3}	75.3

Table 2.1 Fitted values for the Apparent Michaelis-Menten Constant (K_M^{app}) and Turnover Rate (k_{cat}) for CuOOH-Supported Catalysis of Tolbutamide with wt 2C9, R125C, R132C, and K432C, along with the Tolbutamide Dissociation Constants (K_D) as Reference. The reported values for k_{cat} and K_M^{app} were calculated as the average k_{cat} and K_M^{app} values found from three different experiments on three separate days. Reported errors are the standard deviations.

2.3.5 Conjugation with Texas Red® C2 Maleimide

To investigate whether or not wt 2C9 and the mutants R125C, R132C, and K432C could be site-specifically attached to a maleimide-coated gold electrode, wt 2C9 and the single 2C9 mutants were reacted with the maleimide-containing fluorophore Texas Red® C2 maleimide, which absorbs at 595 nm (Figure 2.16). Wild-type 2C9 and the single mutants R125C, R132C, and K432C were reacted with Texas Red® C2 maleimide for two hours at room temperature and protein-bound dye was separated from free dye using a size-exclusion column. Conjugated protein was evaluated qualitatively for the presence of Texas Red by visible absorption spectroscopy and SDS-PAGE. As shown in Figure 2.17, wt 2C9, R125C, R132C, and K432C all bound to Texas Red® C2 maleimide, evidenced by the presence of absorption peaks for LS ferric (Fe^{3+}) heme and Texas Red at 418 and 595 nm, respectively. This was confirmed by fluorescence imaging of an SDS-PAGE gel (Figure 2.18) of wt 2C9, R125C, R132C, and K432C bound to Texas Red® C2 maleimide. These results suggest that the Cys residues on wt 2C9 and the single 2C9 mutants R125C, R132C, and K432C are maleimide reactive and will covalently link to a maleimide-functionalized SAM on gold. However, it is unclear from the visible absorption spectra and the SDS-PAGE gel exactly how many Texas Red molecules are attached to each protein. Therefore, electrospray ionization mass spectrometry (ESI-MS) was used to quantify the number of Texas Red molecules per 2C9 enzyme and thus the number of reactive Cys residues. This is important to know because the two native surface Cys residues (C338 and C372) on the single 2C9 mutants can potentially react with a maleimide-coated gold electrode in addition to the engineered Cys residues on the proximal side, causing 2C9 to be immobilized in multiple places. ESI mass spectra were taken of wt 2C9, R125C, R132C, and K432C alone and conjugated with Texas Red® C2 maleimide; however, a mass spectrum for wt 2C9 conjugated to Texas Red® C2 maleimide was not obtained due to issues with sample stability. Thus, the number of reactive Cys residues on 2C9 was not determined but can be assumed to be either one or two because there are only two native surface Cys residues on wt 2C9.

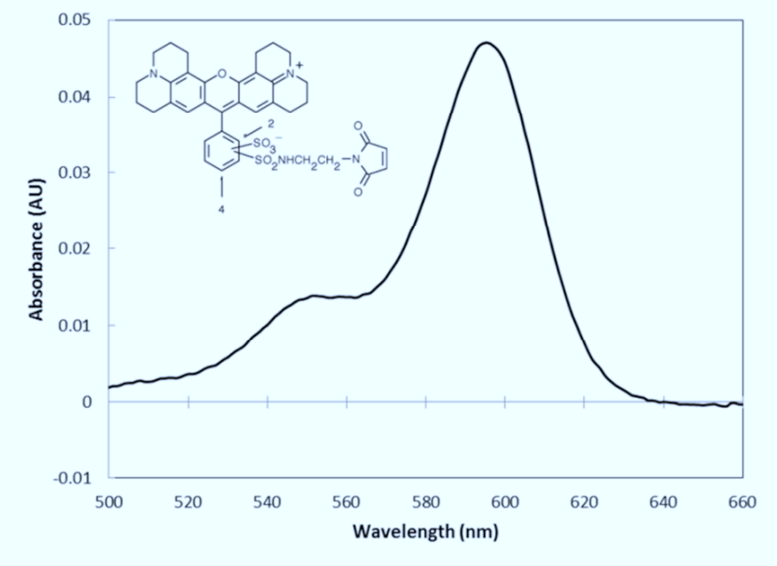

Figure 2.16 Absorption Spectrum of Texas Red® C2 Maleimide. Texas Red® C2 maleimide (structure shown in inset) absorbs strongly at 595 nm and has a molecular weight of 728.8 g/mole.

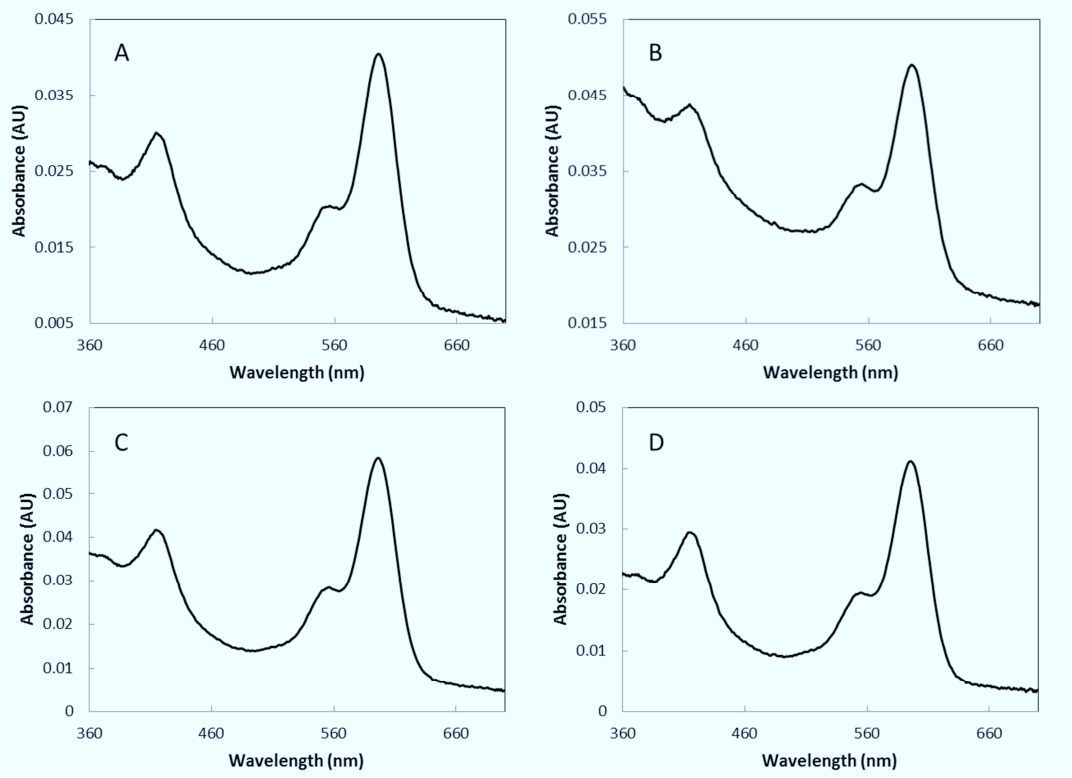

Figure 2.17 Absorption Spectra of wt 2C9, R125C, R132C, and K432C Conjugated to Texas Red® C2 Maleimide. Absorption spectra of (A) wt 2C9, (B) R125C, (C) R132C, and (D) K432C conjugated to Texas Red® C2 maleimide show absorption peaks at approximately 418 and 595 nm for LS ferric (Fe^{3+}) heme and Texas Red, respectively.

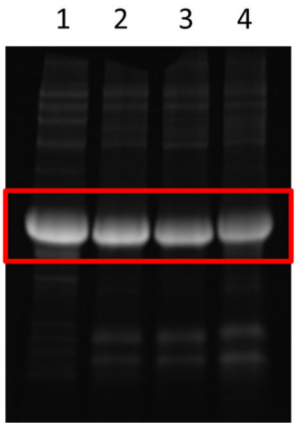

Figure 2.18 Fluorescent Scan of an SDS-PAGE Gel of wt 2C9, R125C, R132C, and K432C Conjugated to Texas Red® C2 Maleimide. Lanes 1 thru 4 are wt 2C9, R125C, R132C, and K432C, respectively. Bands at the appropriate molecular weight for 2C9 (approximately 55 kDa) are highlighted with a red box.

Figure 2.19 shows the deconvoluted ESI mass spectra for unmodified wt 2C9, R125C, R132C, and K432C. Included in each plot are the predicted and measured mass values for each protein in Daltons (Da). There is good agreement between the predicted and measured mass values for R125C, R132C, and K432C, and a difference of 18 Da between the predicted and measured mass values for wt 2C9 likely indicates there is a water molecule present. Figure 2.20 shows the deconvoluted ESI mass spectra of R125C, R132C, and K432C conjugated to Texas Red® C2 maleimide. The results show that all three 2C9 mutants conjugated to Texas Red® C2 maleimide, albeit to different degrees. The mass spectrum of conjugated R125C exhibits two peaks for conjugated protein: one high abundance peak at 57,235 Da corresponds to 3.8 Texas Red molecules per protein and a second, low abundance, peak at 55,973 Da corresponds to 2.0 Texas Red molecules per protein. Because there are only three surface Cys residues on R125C it is physically impossible to have more than three molecules of Texas Red covalently linked to the protein; thus, the high abundance peak seen at 57,235 Da is either an anomaly or represents R125C conjugated to three Texas Red molecules. A similar pattern can be seen in the mass spectrum for conjugated R132C: a high abundance peak at 57,232 Da corresponds to 3.8 Texas Red molecules per protein and a low abundance peak at 55,830 corresponds to 1.8 Texas Red molecules per protein. Again, the high abundance peak at 57,232 Da is either an anomaly—it has almost exactly the same mass as the high abundance peak seen with conjugated R132C—or represents R132C conjugated to three Texas Red molecules. The low abundance peak seen at 57,232 Da most likely represents R132C conjugated to one Texas Red molecule as it is impossible that eight-tenths of a Texas Red molecule could be conjugated to R132C. The mass spectrum for conjugated K432C has a high abundance peak at 54,527 Da that corresponds to unmodified protein and a very low abundance peak at 55,255 Da that corresponds to 1.0 Texas Red molecule per protein. Thus, it appears that out of all the single 2C9 mutants, only K432C has only one reactive Cys residue and will immobilize to a maleimide-coated gold electrode in a single orientation. This reactive Cys residue on K432C is most likely the engineered Cys at residue 432 as the native surface Cys residues have a low surface exposure. However, the presence of a significant peak for unmodified protein and the very low abundance of the Texas-Red conjugate in the mass spectrum for conjugated K432C suggest that the yield for the maleimide/thiol coupling reaction is low with K432C. Based on these results, it appears that the

2C9 mutants R125C and R132C readily couple with maleimide at all three surface Cys residues (the engineered cysteine and C338/C372).

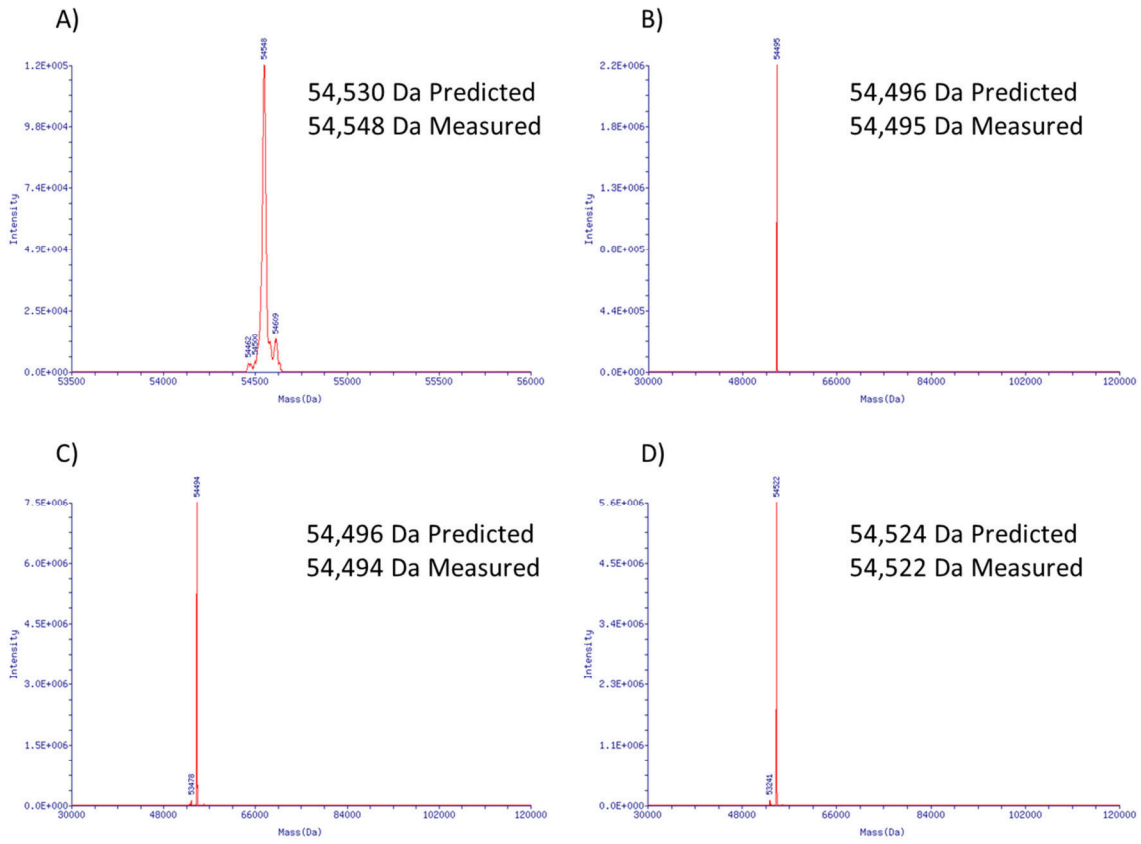

Figure 2.19 Deconvoluted ESI Mass Spectra of Unmodified wt 2C9, R125C, R132C, and K432C. Mass spectra of (A) wt 2C9, (B) R125C, (C) R132C, and (D) K432C show good agreement between the predicted and measured mass values (in Daltons).

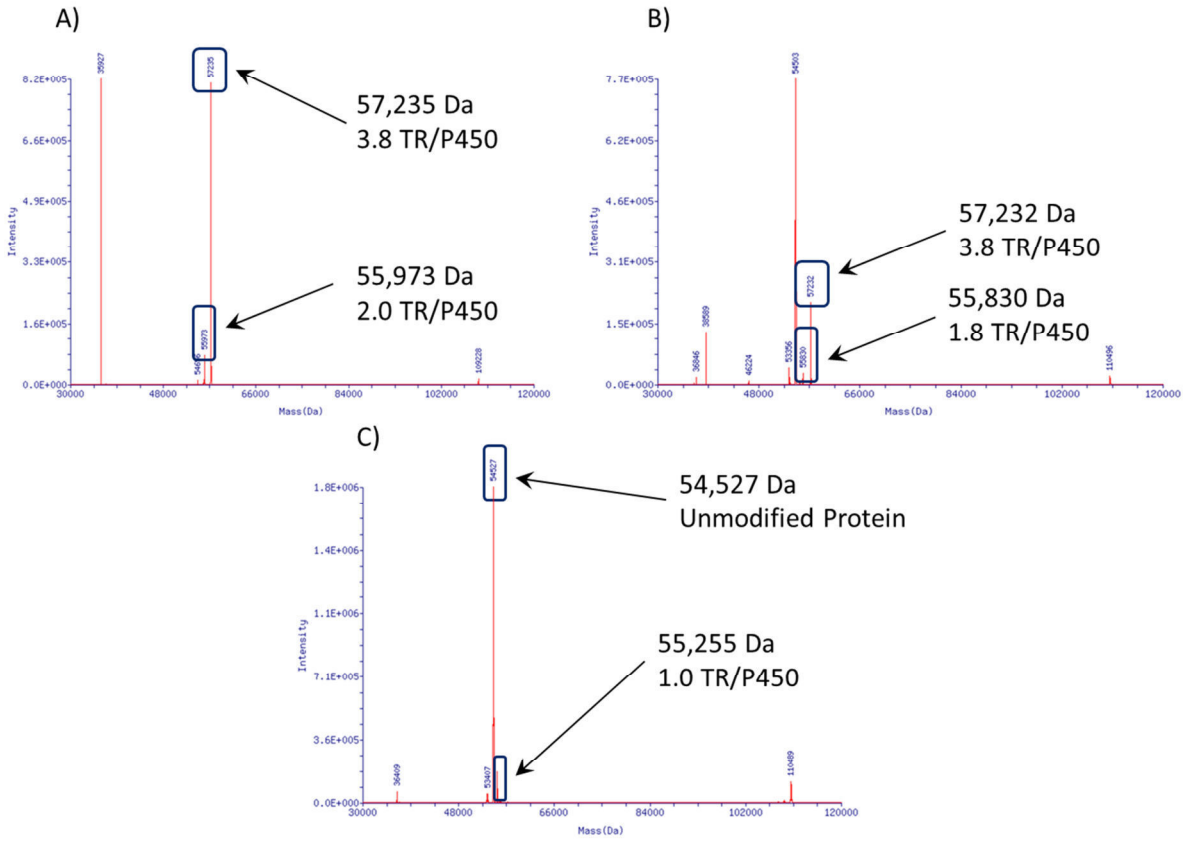

Figure 2.20 Deconvoluted ESI Mass Spectra of R125C, R132C, and K432C Conjugated to Texas Red® C2 Maleimide. Mass Spectra of (A) R125C, (B) R132C, and (C) K432C conjugated to Texas Red® C2 maleimide (TR). The relevant peaks are outlined in blue and labeled with their respective mass values (in Daltons) and the calculated number of conjugated Texas Red molecules per protein.

2.4 Conclusion

Wild-type CYP2C9 and several 2C9 mutants were successfully expressed, purified, and characterized for site-specific attachment at surface Cys residues to a maleimide-functionalized SAM on a gold electrode. Residues R125, R132, and K432 on the proximal side of the iron heme were found to be involved in binding of the electron transfer partner enzymes P450 reductase and/or cytochrome b_5; thus, engineered Cys residues were introduced at positions 125, 132, and 432 via site-directed mutagenesis in the hope that site-specific attachment at these residues would orient the enzyme for electron transfer on a maleimide-coated gold electrode. Two native Cys residues, C338 and C372, exist on the surface of 2C9 on the proximal side of the heme and therefore additional mutants were developed by mutating residues R125, R132, and K432 individually to cysteines and mutating both C338 and C372 to serines. These triple 2C9 mutants, designated SCF-R125C, SCF-R132C, and SCF-K432C are the single surface Cys versions of the single 2C9 mutants R125C, R132C, and K432C, respectively and site-specific attachment of these triple mutants on a maleimide-coated gold electrode would be expected to result in uniform proximal-side orientation of 2C9 on an electrode. The single 2C9 mutants R125C, R132C, and K432C expressed well in *E. coli* and were able to be purified; however, only SCF-R125C and SCF-K432C were able to be purified even though all three of the triple 2C9 mutants expressed in *E. coli.* Peroxide-supported activity assays with the fluorogenic substrate

Vivid® BOMCC showed that all three of the single 2C9 mutants R125C, R132C, and K432C were active and that R132C, in particular, exhibited a marked increase in specific activity (37%) over wt 2C9. Although the triple 2C9 mutants SCF-R125C and SCF-K432C purified successfully, results from absorption spectroscopy and peroxide-supported reactions with Vivid® BOMCC suggested that they were unstable and had low activity, making them unsuitable for further study and inclusion in a 2C9 electrode system.

The substrate binding of the 2C9 substrate tolbutamide and kinetics of peroxide-supported tolbutamide hydroxylation with wt 2C9 and the single 2C9 mutants was studied using substrate binding difference spectroscopy and HPLC analysis of the product 4-hydroxytolbutamide. Results showed that the mutant R132C had a more than two-fold greater affinity for tolbutamide than wt 2C9 and exhibited kinetic constants (k_{cat} and K_M^{app}) that were similar to those of wt 2C9. R125C and K432C however, both exhibited a decrease in affinity for tolbutamide when compared to wt 2C9 and had markedly different kinetics for tolbutamide (increased K_M^{app} and increased k_{cat}) than wt 2C9. Taken together, these results suggest that the R132C mutation least affects the wild-type kinetics of tolbutamide and may actually result in increased activity (at least with certain substrates such as Vivid® BOMCC). All three of the single 2C9 mutants R125C, R132C, and K432C are reactive with maleimide, as evidenced by the successful conjugation of Texas Red® C2 maleimide to all three proteins. However, the abundance for Texas-Red conjugated K432C was very low and suggests that K432C does not react as readily with maleimide as R125C or R132C. Mass spectra of Texas Red-conjugated R125C and R132C revealed that a maximum of three Texas Red molecules can react with each protein, suggesting that all three of the surface Cys residues on R125C and R132C are reactive. The mass spectra for R132C additionally contained a peak corresponding to only one Texas Red molecule per protein however, and it is likely that this Texas Red molecule is conjugated at residue 132 due to the large surface exposure of this residue compared to C338 and C372. In conclusion, the single 2C9 mutants R125C, R132C, and K432C are active against a fluorogenic marker substrate (Vivid® BOMCC) and a native 2C9 substrate (tolbutamide) and should immobilize easily to a maleimide-functionalized electrode to create a CYP2C9 biosensor. However, because there are three reactive Cys residues on these mutants, 2C9 may not be uniformly oriented on the electrode at the reductase binding site but its orientation will be more controlled (three possible orientations) than the random orientation that results from amine coupling to more than 20 surface exposed amines (lysine residues). In addition, both C338 and C372 are on the proximal side of the heme so site-specific attachment at these residues will still orient 2C9 for electron transfer. Thus, the development of the 2C9 mutants R125C, R132C, and K432C represents a significant step towards the oriented attachment of CYP2C9 to a maleimide-functionalized gold electrode as a biosensor design.

2.5 References

1. Kazlauskaite, J., Westlake, A.C.G., Wong, L., Hill, H.A.O. Direct electrochemistry of cytochrome P450cam. *Chem. Commun.* (1996) 18:2189-2190.
2. Fantuzzi, A., Fairhead, M., Gilardi, G. Direct electrochemistry of immobilized human cytochrome P450 2E1. *JACS* (2004) 126:5040-5041.
3. Wester, M.R., Yano, J.K., Schoch, G.A., Yang, C., Griffin, K.J., Stout, C.D., Johnson, E.F. The structure of human cytochrome P450 2C9 complexed with flurbiprofen at 2.0-Å resolution. *J. Biol. Chem.* (2004) 279:35630-35637.
4. Kazlauskaite, J., Westlake, A.C.G., Wong, L., Hill, H.A.O. Direct electrochemistry of cytochrome P450cam. *Chem. Commun.* (1996) 18:2189-2190.
5. Kam-Wing Lo, K., Wong, L., Hill, A.O. Surface-modified mutants of cytochrome $P450_{cam}$: enzymatic properties and electrochemistry. *FEBS Letters* (1999) 451:342-346.
6. Stayton, P.S., Sligar, S.G. The cytochrome P-450cam binding surface as defined by site-directed mutagenesis and electrostatic modeling. *Biochemistry* (1990) 29:7381-7386.
7. Ferroro, V.E.V., Andolfi, L., Di Nardo, G., Sadeghi, S.J., Fantuzzi, A., Cannistraro, S., Gilardi, G. Protein and electrode engineering for the covalent immobilization of P450 BMP on gold. *Anal. Chem.* (2008) 80:8438-8446.
8. Panicco, P., Dodhia, V.R., Fantuzzi, A., Gilardi, G. Enzyme-based amperometric platform to determine the polymorphic response in drug metabolism by cytochromes P450. *Anal. Chem.* (2011) 83:2179-2186.
9. Mak, L.H., Sadeghi, S.J., Fantuzzi, A., Gilardi, G. Control of human cytochrome P450 2E1 electrocatalytic response as a result of unique orientation on gold electrodes. *Anal. Chem.* (2010) 82:5357-5362.
10. Dodhia, V.R., Sassone, C., Fantuzzi, A., Di Nardo, G., Sadeghi, S.J., Gilardi, G. Modulating the coupling efficiency of human cytochrome P450 CYP3A4 at electrode surfaces through protein engineering. *Electrochem. Commun.* (2008) 10:1744-1747.
11. Williams, J.A., Hyland, R., Jones, B.C., Smith, D.A., Hurst, S., Goosen, T.C., Peterkin, V., Koup, J.R., Ball, S.E. Drug-drug interactions for UDP-glucuronosyltransferase substrates: a pharmacokinetic explanation for typically observed low exposure (AUC_i/AUC) ratios. *Drug Metab. Dispos.* (2004) 32:1201-1208.
12. Miners, J.O., Birkett, D.J. Cytochrome P4502C9: an enzyme of major importance in human drug metabolism. Br. J. Clin. Pharmacol. (1998) 45:525-538.
13. Shukla, A., Gillam, E.M., Mitchell, D.J., Bernhardt, P.V. Direct electrochemistry of enzymes from the cytochrome P450 2C family. *Electrochem. Commun.* (2005) 7:437-442.
14. Johnson, D.L., Lewis, B.C., Elliot, D.J., Miners, J.O., Martin, L.L. Electrochemical characterization of the human cytochrome P450 CYP2C9. *Biochem. Pharmacol.* (2005) 69:1533-1541.
15. Ying, M., Kabulski, J.L., Wollenberg, L. Chen, X., Subramanian, M., Tracy, T.S., Lederman, D., Gannett, P.M., Wu, N. Electrocatalytic drug metabolism by CYP2C9 bonded to a self-assembled monolayer-modified electrode. *Drug Metab. Disp.* (2009) 37:892-899.

16. Bridges, A., Gruenke, L., Chang, Y., Vakser, I.A., Loew, G., Waskell, L. Identification of the binding site on Cytochrome P450 2B4 for Cytochrome b5 and Cytochrome P450 Reductase. *J. Biol. Chem.* (1998) 273: 17036-17049.
17. Im, S., Waskell, L. The interaction of microsomal cytochrome P450 2B4 with its redox partners cytochrome P450 reductase and b5. *Arch. Biochem. Biophys.* (2011) 507:144-153.
18. Sandhu, P., Baba, T., Guengerich, F.P. Expression of modified cytochrome P450 2C10 (2C9) in *Escherichia coli*, purification, and reconstitution of catalytic activity. *Arch. Biochem. Biophys.* (1993) 306:443-450.
19. Omura, T., Sato, R. The carbon monoxide-binding pigment of liver microsomes. *J. Biol. Chem.* (1964) 239:2370-2378.
20. Yamazaki, H., Gillam, E.M.J., Dong, M., Johnson, W.W., Guengerich, F.P., Shimada, T. Reconstitution of recombinant cytochrome P450 2C10(2C9) and comparison with cytochrome P450 3A4 and other forms: effects of cytochrome P450-P450 and cytochrome P450-b_5 interactions. *Arch. Biochem. Biophys.* (1997) 342:329-337.
21. Hlavica, P., Schulze, J., Lewis, D.F.V. Functional interaction of cytochrome P450 with its redox partners: a critical assessment and update of the topology of predicted contact regions. *J. Inorgan. Biochem.* (2003) 96:279-297.
22. Lewis, D.F.V., Hlavica, P. Interactions between redox partners in various cytochrome P450 systems: functional and structural aspects. *Biochim. Biophys. Acta* (2000) 1460:353-374.
23. Perera, R., Sono, M., Sigman, J.A., Pfister, T.D., Lu, Y., Dawson, J.H. Neutral thiol as a proximal ligand to ferrous heme iron: implications for heme proteins that lose cysteine thiolate ligation on reduction. *PNAS* (2003) 100:3641-3646.
24. Mouro, C., Jung, C., Bondon, A., Simonneaux, G. Comparative fourier transform infrared studies of the secondary structure and the CO heme ligand environment in cytochrome P-450cam and cytochrome P-20cam. *Biochemistry* (1997) 36:8125-8134.
25. Hui Bon Hoa, G., Di Primo, C., Dondaire, I., Sligar, S., Gunsalus, I.C., Douzou, P. Conformational changes of cytochromes P-450cam and P-450lin induced by high pressure. *Biochemistry* (1989) 28:651-656.
26. Imai, Y., Sato, R. Conversion of P-450 to P-420 by neutral salts and some other reagents. *Eur. J. Biochem.* (1967) 1:419-426.
27. Yu, C.A., Gunsalus, I.C. Cytochrome P-450_{cam}: II. Interconversion with P-420. *J. Biol. Chem.* (1974) 249:102-106.
28. O'Keefe, D.H., Ebel, R.E., Peterson, J.A., Maxwell, J.C., Caughey, W.S. An infrared spectroscopic study of carbon monoxide binding to ferrous cytochrome P-450. *Biochemistry* (1978) 17:5845-5852.
29. Williams, P.A., Cosme, J., Ward, A., Angove, H.C., Vinković, D.M., Jhoti, H. Crystal structure of human cytochrome P450 2C9 with bound warfarin. *Nature* (2003) 424:464-468.
30. Joo, H., Lin, Z., Arnold, F. H. Laboratory evolution of peroxide-mediated cytochrome P450 hydroxylation. *Nature* (1999) 399:670-673.
31. Kumar, S., Liu, H., Halpert, J.R. Engineering of cytochrome P450 3A4 for enhanced peroxide-mediated substrate oxidation using directed evolution and site-directed mutagenesis. *Drug Metab. Disp.* (2006) 34:1958-1965.

32. Cirino, P.C., Arnold, F.H. A self-sufficient peroxide-driven hydroxylation biocatalyst. *Angew. Chem., Int. Ed.* (2003) 42:3299-3301.
33. Cirino, P.C., Arnold, F.H. Regoselectivity and activity of cytochrome P450 mB-3 and mutant F87A in reactions driven by hydrogen peroxide. *Adv. Synth. Catal.* (2002) 344:932-937.
34. Chefson, A., Zhao, J., Auclair, K. Replacement of the natural cofactors by selected hydrogen peroxide donors or organic peroxides results in improved activity for CYP3A4 and CYP2D6. ChemBioChem (2006) 7:916-919.
35. Crespi, C.L., Miller, V.P. The R144C change in the CYP2C9*2 allele alters interaction of the cytochrome P450 with NADPH:cytochrome P450 oxidoreductase. *Pharmacogenetics* (1997) 7:203-210.
36. Yin, T., Maekawa, K., Kamide, K., Saito, Y., Hanada, H., Miyashita, K., Kokubo, Y., Akaiwa, Y., Otsubo, R., Nagatsuka, K., Otsuki, T., Horio, T., Takiuchi, S., Kawano, Y., Minematsu, K., Naritomi, H., Tomoike, H., Sawada, H., Miyata, T. Genetic variations of CYP2C9 in 724 Japanese individuals and their impact on the antihypertensive effects of losartan. *Hypertens. Res.* (2008) 31:1549-1557.
37. Mo, S., Zhou, A., Yang, L., Wei, M.Q., Zhou, S. New insights into structural features and functional relevance of human cytochrome P450 2C9. Part II. *Curr. Drug Metab.* (2009) 10:1127-1150.
38. DeLozier, T.C., Lee, S.C., Coulter, S.J., Goh, B.C., Goldstein, J.A. Functional characterization of novel allelic variants of CYP2C9 recently discovered in southeast Asians. *J. Pharmacol. Exp. Ther.* (2005) 315:1085-1090.
39. Denisov, I.G., Makris, T.M., Sligar, S.G., Schlichting, I. Structure and chemistry of cytochrome P450. *Chem. Rev.* (2005) 105:2253-2277.
40. Yuan, R., Madani, S., Wei, X., Reynolds, K., Huan, S. Evaluation of cytochrome P450 probe substrates commonly used by the pharmaceutical industry to study in vitro drug interactions. *Drug Metab. Disp* (2002) 30:1311-1319.
41. Guengerich, F.P. Cytochrome P450s: What have we learned and what are the future issues? *Drug Metab. Rev.* (2004) 36:159-197.
42. Traylor, M.J., Ryan, J.D., Arnon, E.S., Dordick, J.S., Clark, D.S. Rapid and quantitative measurement of metabolic stability without chromatography or mass spectrometry. *JACS* (2011) 133:14476-14479.
43. Kumar, S. Identification of a novel laser dye substrate of mammalian cytochromes P450: Application in rapid kinetic analysis, inhibitor screening, and directed evolution. *J. Biomol. Screen.* (2007) 12:677-682.
44. Miners, J.O., Birkett, D.J. Use of tolbutamide as a substrate probe for human hepatic cytochrome P450 2C9. *Methods Enzymol.* (1996) 272:139-145.
45. Miners, J.O., Smith, K.J., Robson, R.A., McManus, M.E., Veronese, M.E., Birkett, D.J. Tolbutamide hydroxylation by human liver microsomes. Kinetic characterization and relationship to other cytochrome P-450 dependent xenobiotic oxidations. *Biochem. Pharmacol.* (1988) 37:1137-1144.
46. Back, D.J., Tjia, J.F., Karbwang, J., Colbert, J. In vitro inhibition studies of tolbutamide hydroxylase activity of human liver microsomes by azoles, sulphonamides and quinolines. *Br. J. Clin. Pharmacol.* (1988) 26:23-29.

47. Doecke, C.J., Veronese, M.E., Pond, S.M., Miners, J.O., Birkett, D.J., Sansom, L.N., McManus, M.E. Relationship between phenytoin and tolbutamide hydroxylations in human liver microsomes. *Br. J. Clin. Pharmacol.* (1991) 31:125-130.
48. Bourríe, M., Meunier, V., Berger, Y., Fabre, G. Cytochrome P450 isoform inhibitors as a tool for the investigation of metabolic reactions catalyzed by human liver microsomes. *J. Pharmacol. Exp. Ther.* (1996) 277:321-332.
49. Hutzler, J.M., Wienkers, L.C., Wahlstrom, J.L., Carlson, T.J., Tracy, T.S. Activation of cytochrome P450 2C9-mediated metabolism: mechanistic evidence in support of kinetic observations. *Arch. Biochem. Biophys.* (2003) 410:16-24.

Chapter 3. Surface Characterization and Electrochemical Analysis of Cytochrome P450 2C9 Immobilized to a Self-Assembled Monolayer on a Gold Electrode

3.1 Introduction

There are only two studies in the literature on the direct electrochemistry of cytochrome P450 2C9 (CYP2C9) covalently attached to an electrode[1,2], and both of these studies involve amine coupling of the enzyme via EDC/NHS to a carboxy-terminated self-assembled monolayer (SAM) on gold. In 2009, Yang et al. fabricated a 2C9 electrode by amine coupling the enzyme to a mixed SAM of octanethiol (OT) and 11-mercaptoundecanoic acid (MUA) on gold, and the immobilized 2C9 was electroactive and behaved as a biosensor for the detection of the 2C9 substrate warfarin[1]. HPLC detection of the warfarin metabolite 7-hydroxywarfarin in the electrolyte after electrolysis with the 2C9 electrode and warfarin confirmed that the immobilized 2C9 was capable of electrochemically-driven catalysis. In the more recent study, Panicco et al. also used amine coupling to immobilize the polymorphic 2C9 variants 2C9*1 (wild-type), 2C9*2 (R144C), and 2C9*3 (I359L) on gold electrodes modified with a mixed SAM of 6-hexanethiol and 7-mercaptoheptanoic acid. The authors used the resulting 2C9 electrodes as biosensors to screen for reactivity with warfarin and were able to tell the polymorphic variants apart based on their electrochemically-derived K_M^{app} and k_{cat} values with warfarin[2].

Both of these studies resulted in electroactive enzyme on an electrode and creation of functional 2C9 biosensors despite the fact that both research groups used long chain alkanethiol SAMs that notoriously block electron transfer[3]. However, because amine coupling is an inherently random attachment method that occurs at amine (lysine residues) groups on the surface of the enzyme, the orientation of 2C9 on the electrode in these studies was most likely random and certainly not uniformly oriented in an electroactive orientation. Previous studies have shown that electron transfer to CYPs via the electron transfer partner enzyme P450 reductase (CPR) occurs on the proximal side of the enzyme where the heme cofactor is closest to the surface; basic residues on the proximal side of CYP interact electrostatically with acidic residues on CPR[4,5]. Thus, it makes sense that site-specific attachment of CYP to an electrode at amino acid residues on the proximal side would uniformly orient the enzyme on its electroactive face and ensure that electron transfer occurs on the electrode the same way it occurs *in vivo* with CPR. Ideally, site-specific attachment at residues involved in binding of CPR would allow the electrode to interact with CYP in the same location that CPR does. This approach has been tentatively explored in the literature with the bacterial P450s $P450_{CAM}$ and BM-3[6-8] but surprisingly has not been attempted much for mammalian CYPs[9,10] and in fact, to our knowledge, has never been attempted for 2C9.

One way to site-specifically attach CYP to an electrode is through maleimide/thiol coupling; a thiol group (cysteine residue, Cys) engineered at the binding site for CPR will react specifically with maleimide groups on an electrode and immobilize the enzyme in an electroactive orientation. The Gilardi group at the University of Turin in Italy has explored this technique for attachment of the human drug-metabolizing CYP 2E1 to a SAM on a gold electrode modified with maleimide groups[9,10]. However, in both of their studies they used the *native* surface Cys residues C261 and C268 to control the orientation of 2E1 on the electrode. These residues coincidentally resided on the proximal side of the enzyme but were not located at the P450 reductase binding site. Our laboratory has developed and characterized several 2C9

mutants that contained single Cys mutations engineered specifically on the proximal side of the heme at the P450 reductase binding site. Attachment of these mutants, designated R125C, R132C, and K432C to a maleimide-coated SAM on a gold electrode is expected to orient the enzyme on the proximal side such that electron transfer occurs on the electrode as it does *in vivo* with CPR. There are two native surface Cys residues (C338 and C372) on the surface of 2C9 that could react with maleimide groups on a gold electrode. However, C338 and C372 are also located on the proximal side of the enzyme and therefore attachment at these residues would also orient 2C9 on the proximal side, albeit not at the P450 reductase binding site.

In the present study, recombinant, his-tagged wild-type (wt) 2C9 and the single Cys mutants R125C, R132C, and K432C were covalently attached to SAM-modified gold electrodes via one of three different attachment methods. The resulting electrodes were characterized via cyclic voltammetry (CV) with and without the 2C9 substrate tolbutamide to compare the effect, if any, that orientation has on the direct electrochemistry of 2C9 on a gold electrode and to evaluate whether or not these different attachment methods lead to a viable 2C9 biosensor. The attachment methods studied include random attachment via amine coupling, oriented attachment via Ni-NTA/His-tag coupling, and oriented attachment via maleimide/thiol coupling. As shown in Figure 3.1, all three attachment methods begin with formation of either a mercaptopropionic acid (MPA) or cystamine (CYSAM) SAM on gold. Random attachment via amine coupling employs the classic reagents EDC (1-ethyl-3-[3-dimethylaminopropyl] carbodiimide hydrochloride) and NHS (N-hydroxysuccinimide) to activate the carboxyls for immobilization while oriented attachment via maleimide/thiol coupling uses an amine reactive maleimide compound to functionalize the CYSAM with maleimide groups. Oriented attachment via Ni-NTA/His-tag coupling makes use of a 6x His-tag on the C-terminus of recombinantly expressed 2C9 to orient the enzyme on the electrode uniformly on its C-terminus, and the compound NH_2-NTA (amino-nitrilotriacetic acid) is used to functionalize the MPA SAM with NTA. Various techniques such as AFM, CV, QCM-D (quartz-crystal microbalance with dissipation), and FT-IR were used to characterize the gold electrode and SAMs, and an enzymatic activity assay of the 2C9 electrodes with a fluorogenic substrate was used to evaluate the immobilization of wt and mutant 2C9. Indirect electrochemistry of the 2C9 mutant R132C immobilized via maleimide/thiol coupling was also explored with the mediator compound phenosafranine.

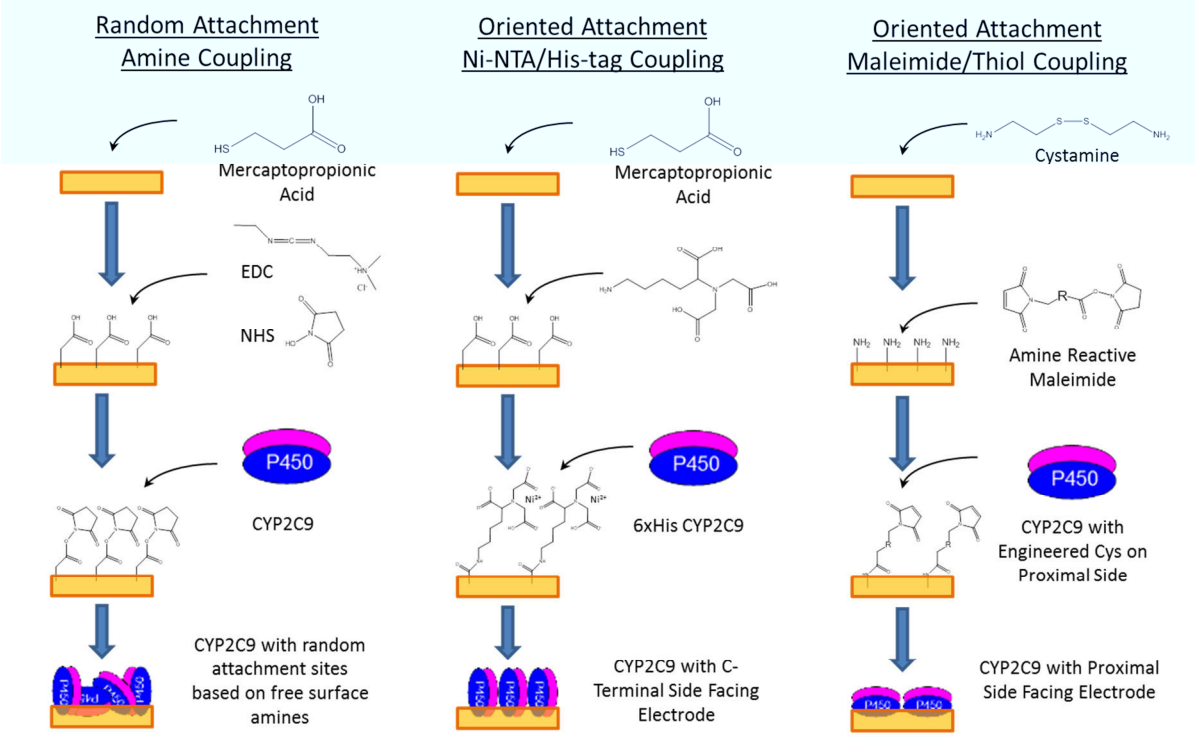

Figure 3.1 Schematic of Three Different Attachment Methods Used to Immobilize CYP2C9 on a Gold Electrode. All three attachment methods require formation of either an MPA or cystamine SAM on the gold electrode as a first surface modification step. Random attachment via amine coupling uses the reagents EDC and NHS to activate the carboxyl groups for immobilization of 2C9 and the enzyme is oriented randomly based on surface-exposed amines (lysine residues). Oriented attachment via Ni-NTA/His-tag coupling makes use of a C-terminal 6x His-tag on the recombinantly expressed 2C9 to immobilize 2C9 on its C-terminus, and the compound NH_2-NTA is used to functionalize the MPA SAM with NTA. Oriented attachment via maleimide/thiol coupling uses an amine-reactive maleimide compound to functionalize the cystamine SAM with maleimide groups, and 2C9 with an engineered Cys residue on the proximal side is oriented with the proximal side facing the electrode.

3.2 Materials and Methods

3.2.1 Materials

Vivid® BOMCC, TCEP (tris-(2-carboxyethyl)phosphine, hydrochloride), and BODIPY® FL-L-cystine were purchased from Invitrogen (Life Technologies, Carlsbad, CA). MPA (mercaptopropionic acid), cystamine dihydrochloride, EDC (1-ethyl-3-[3-dimethylaminopropyl] carbodiimide hydrochloride), NHS (N-hydroxysuccinimide), tolbutamide, diclofenac sodium salt, sodium cholate, sodium dithionite, CuOOH (cumene hydroperoxide), phenosafranine, ferrocenecarboxylic acid, HATU (*O*-(7-Azabenzotriazol-1-yl)-*N,N,N′,N′*-tetramethyluronium hexafluorophosphate), DIPEA (diisopropylethanolamine), PS (L-α-phosphatidyl-L-serine from *Glycine Max* (soybean)), and Catalase (from bovine liver) were all purchased from Sigma-Aldrich (St. Louis, MO). Aminoferrocene and N-succinimidyl-3-maleimidopropionate were from TCI America (Portland, OR), and Sulfo-SMCC (sulfosuccinimidyl-4-(*N*-maleimidomethyl) cyclohexane-1-carboxylate) was from Pierce Protein Research Products (Thermo Fisher Scientific, Rockford, IL). NH_2-NTA (Amino-nitrilotriacetic acid) was purchased from United States Biological (Swampscott, MA). DLPC (1,2-dilauroyl-*sn*-glycero-3-phosphocholine) and DOPC (1,2-dioleoyl-*sn*-glycero-3-phospho choline) lipids were purchased from Avanti Polar Lipids Inc. (Alabaster, AL). The silane 4-aminobutyltriethoxysilane was purchased from Gelest

Inc. (Morrisville, PA). All other chemicals or reagents used were of the highest available quality and were from Sigma-Aldrich or Fisher Scientific unless stated otherwise.

3.2.2 Methods

Electrochemical Measurements

Electrochemical measurements were made using a homemade electrochemical cell made from a machined polypropylene block (Figure 3.2). Gold-coated glass slides (1" x 3" in size; 1000 Å evaporated gold layer on top of a 50 Å evaporated titanium adhesion layer) were used as working electrodes and were purchased from EMF Corporation (Ithaca, NY). A rubber O-ring (1.3 cm in diameter) served as a seal on top of a gold-coated glass slide and defined a working electrode area of approximately 1.3 cm^2. A platinum (Pt) mesh spot-welded to a Pt (Alfa Aesar, Ward Hill, MA) wire was inserted into the homemade electrochemical cell and served as the counter electrode, and the reference electrode was made of Ag/AgCl (3 M NaCl) (BASi Inc., West Lafayette, IN). Ports on opposite sides of the electrochemical cell allow for circulation of electrolyte with a peristaltic pump. Cyclic voltammetry (CV) and chronoamperometry (CA) experiments were performed using a Gamry PCI-4/300 potentiostat (Gamry Instruments, Warminster, PA) connected to a PC. Copper tape from Ted Pella Inc. (Redding, CA) was used to connect the gold-coated glass slide working electrode to the potentiostat leads. All potentials are referenced to Ag/AgCl (3 M NaCl) unless stated otherwise, and all electrochemical measurements were performed at room temperature.

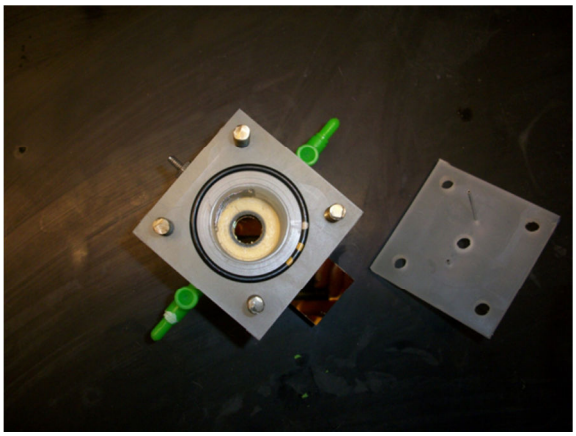

Figure 3.2 Custom-Machined Electrochemical Cell. A polypropylene block served as a body for the custom-machined electrochemical cell. A gold-coated glass slide, Pt mesh/Pt wire, and Ag/AgCl (3 M NaCl) electrode served as the working, counter, and reference electrodes, respectively, and an O-ring of approximately 1.3 cm in diameter defined a working electrode area of 1.3 cm^2. Ports on the sides of the cell allow for electrolyte circulation with a peristaltic pump.

Surface Characterization of Gold Electrodes

The surface roughness of gold electrodes was measured using electrochemical potential cycling. The gold electrode was electrochemically oxidized and reduced by cycling the potential between -0.2 and 1.6 V at a scan rate of 50 mV/s in 0.1 M H_2SO_4, and the charge density passed during reduction of the gold oxide layer was calculated. This calculated charge density (in $\mu C/cm^2$) was divided by the theoretical charge density of 420 $\mu C/cm^2$ for reduction of a gold oxide monolayer on a perfectly flat gold electrode[11], leading to a roughness factor, R_f, for the

gold electrode that represents the ratio between the actual and geometric surface areas. The surface roughness of the gold electrode was also characterized qualitatively via AFM. AFM imaging was done using a Pico SPM instrument (Molecular Imaging) and regular silicon tips (MikroMasch, San Jose, CA) in contact mode, and scans were done on a 2 μm x 2 μm area. The surface coverage of MPA and cystamine SAMs on gold electrodes was measured via electrochemical reductive desorption. The potential of a SAM-coated gold electrode was cycled between 0.0 and -1.4 V at a scan rate of 50 mV/s in 0.5 M NaOH, and the charge passed upon reductive desorption of the SAM was calculated. Faraday's law of electrolysis was then used to calculate the surface coverage (Γ_m, in moles/cm^2) of the SAM on the gold electrode from the surface charge passed upon reductive desorption.

Reaction of Sulfo-SMCC and N-Succinimidyl-3-maleimidopropionate with BODIPY® FL-L-cystine on Glass Slides

Glass slides were cleaned with soap and water followed by sonication sequentially in DI water and isopropanol for 10 minutes each. These slides were further cleaned by oxygen plasma treatment for five minutes before silane treatment with 4-aminobutyltriethoxysilane. Glass slides were functionalized with 4-aminobutyltriethoxysilane via chemical vapor deposition; slides were left under vacuum for one hour in a dessicator with a hot heat block containing an aliquot of 4-aminobutyltriethoxysilane. Amine-functionalized glass slides were then incubated in either a 25 mM solution of N-succinimidyl-3-maleimido propionate in DMF for 40 minutes at room temperature (treatment A) or a 2 mg/ml solution of Sulfo-SMCC in coupling buffer (50 mM KPi, 150 mM NaCl, 10 mM EDTA, pH 7.2) for one hour at room temperature (treatment B). Slides were then washed either three times each in DMF and then DI water (for slides treated with treatment A) or three times with coupling buffer (for slides treated with treatment B). Following functionalization with maleimide groups, the glass slides were then treated with the fluorophore BODIPY® FL-L-cystine by incubation for two hours at room temperature in a solution of 1 mM BODIPY® FL-L-cystine and 18 mM TCEP in 50 mM KPi, pH 7.4. The amount of BODIPY® FL bound to maleimide-coated glass slides treated with either Sulfo-SMCC or N-succinimidyl-3-maleimidopropionate was assessed by measuring the absorbance of the bound BODIPY® FL fluorophore from 400 to 600 nm in a spectrophotometer (Lambda 650 UV/Vis spectrophotometer, PerkinElmer, Waltham, MA).

Immobilization of Wild-type CYP2C9 and Mutants to Gold Electrodes

Wild-type CYP2C9 and the mutants R125C, R132C, and K432C were separately immobilized to gold-coated glass slides using one of three methods: random attachment via amine coupling, oriented attachment via Ni-NTA/His coupling, and oriented attachment via maleimide/thiol coupling. Gold-coated glass slides were cleaned prior to surface modification by immersion in a hot (~75°C) piranha solution and electrochemical potential cycling. Briefly, the gold-coated glass slide was cleaned for 5 minutes in hot piranha (a 4:1 mixture by volume of H_2SO_4 and H_2O_2). CAUTION: Piranha solution is very corrosive and heats up quickly and should be handled with proper safety precautions. After cleaning in piranha, the gold electrodes were rinsed with DI water and dried with a nitrogen stream. The newly cleaned gold electrodes were electrochemically oxidized and reduced by cycling the potential three times from -0.2 to 1.6 V in 0.1 M H_2SO_4 at a scan rate of 50 mV/s to remove any residual adsorbed species and activate the gold electrode for surface treatment.

For random attachment via amine coupling, a freshly cleaned gold-coated glass slide was first immersed in a 20 mM solution of MPA in water overnight at room temperature to form a carboxy-functionalized SAM. After overnight SAM formation, the gold electrode was washed three times with DI water to remove residual MPA and then incubated for two hours at room temperature in a 50 mM KPi (pH 5.8) buffer containing 2 mM EDC and 5 mM NHS to activate the carboxy-SAM for amine coupling. The gold electrode was washed three times in 50 mM KPi (pH 5.8) to remove unreacted EDC/NHS and then incubated for 30 minutes at room temperature with a 10 μM solution of 2C9 (either wild-type or one of the mutants R125C, R132C, and K432C) in pH 7.4 buffer containing 50 mM KPi, 10% glycerol, and 0.3% sodium cholate. The resulting 2C9 electrode was washed copiously three times in 50 mM KPi (pH 7.4) buffer to remove unbound CYP protein and then stored at 4°C until further use.

For oriented attachment via Ni-NTA/His coupling, a freshly cleaned gold-coated glass slide was first immersed in a 20 mM solution of MPA in water overnight at room temperature to form a carboxy-functionalized SAM. After overnight SAM formation, the gold electrode was washed three times with DI water to remove residual MPA and then incubated for 30 minutes at room temperature in a 50 mM KPi (pH 5.8) buffer containing 10 mM EDC and 10 mM NHS to activate the carboxy-SAM for amine coupling. The gold electrode was then washed three times in 50 mM KPi (pH 5.8) to remove unreacted EDC/NHS and then incubated overnight at room temperature in a 3 mg/ml solution of NH_2-NTA in pH 8.0 50 mM KPi buffer. Following functionalization with NTA, the gold electrode was washed three times in 50 mM KPi (pH 8.0) and incubated sequentially in 1 mM NaOH and 200 mM $NiCl_2$ for 30 minutes and one hour, respectively, at room temperature to charge the NTA with Ni^{2+} ions. After charging with Ni^{2+} ions, the Ni-NTA functionalized gold electrode was equilibrated by washing three times with 50 mM KPi (pH 7.4) and then incubated overnight at 4°C in a 10 μM solution of 2C9 (either wild-type or one R125C, R132C, and K432C) in pH 7.4 buffer containing 50 mM KPi, 10% glycerol, and 0.3% sodium cholate. The resulting 2C9 electrode was washed copiously three times in 50 mM KPi (pH 7.4) buffer to remove unbound CYP protein and then stored at 4°C until further use.

For oriented attachment via maleimide/thiol coupling, a freshly cleaned gold-coated glass slide was first immersed in a 50 mM solution of cystamine dihydrochloride in water overnight at room temperature to form an amine-functionalized SAM (CYSAM). After overnight SAM formation, the gold electrode was washed three times in DI water to remove residual cystamine and then incubated for 40 minutes at room temperature in a 25 mM solution of N-succinimidyl-3-maleimidopropionate in DMF to functionalize the CYSAM with maleimide groups. The gold electrode was then washed three times each with DMF and then DI water to remove any unreacted N-succinimidyl-3-maleimidopropionate. The maleimide-functionalized gold electrode was then incubated for two hours at 4°C in a solution of 10 μM 2C9 (either wild-type or R125C, R132C, and K432C) and 200 μM TCEP in 50 mM KPi, 10% glycerol, 0.3% sodium cholate, pH 7.4. The resulting 2C9 electrode was washed copiously three times in 50 mM KPi (pH 7.4) to remove unbound CYP protein and then stored at 4°C until further use.

Enzyme Activity of 2C9 Electrodes with Vivid® BOMCC

The activities of wt 2C9 and the mutants R125C, R132C, and K432C immobilized on a gold electrode via the three different attachment methods were measured in a CuOOH-supported

activity assay with the fluorogenic substrate Vivid® BOMCC. 2C9 electrodes were incubated in a 300 µl reaction mixture of 100 µM Vivid BOMCC, 500 µM sodium cholate, 20 µg/ml of a lipid mix (a 1:1:1 mixture of DLPC:DOPC:PS), and 50 mM KPi (pH 7.4), and the reaction was initiated by the addition of 500 µM CuOOH. The fluorescence at 460 nm of the Vivid® Blue product (excitation 409 nm, emission 460 nm) in a 100 µl aliquot of the reaction mix was measured every 10 minutes in SpectraMAX M2 plate reader (Molecular Devices LLC, Sunnyvale, CA), and the progress of the reaction was monitored for two hours. The activities of the 2C9 electrodes were normalized for the amount of immobilized enzyme by dividing the fluorescent intensities at each timepoint by the amount of 2C9 (in µM) incubated on the surface of the electrode during immobilization.

FT-IR Characterization

FT-IR measurements were carried out on a Bruker IFS 66v/s FT-IR spectrometer (Bruker Optics, Billerica, MA) on Beamline 1.4.2 of the Advanced Light Source at the Lawrence Berkeley National Laboratory in Berkeley, CA. Spectra were collected using p-polarized light at a grazing angle incidence of 80° from the surface normal using a Harrick Seagull™ variable angle reflection accessory (Harrick Scientific, Pleasantville, NY). The detector and beamsplitter were made of mercury-cadmium-telluride (MCT) and KBr, respectively. A resolution of approximately 1 cm^{-1} was used, and a total of 512 scans were collected overnight in a nitrogen-purged chamber to improve the signal-to-noise ratio and eliminate signal from atmospheric water.

Quartz-Crystal Microbalance with Dissipation (QCM-D) Studies

QCM-D experiments were performed to calculate the surface coverage of the MPA and cystamine SAMs. All surface modification steps were done at room temperature and at a flow rate of 125 µl/min unless stated otherwise, and frequency values from either the 3rd (fundamental frequency = 15 MHz), 5th (fundamental frequency = 25 MHz), or 7th (fundamental frequency = 35 MHz) overtones were used to calculate the surface coverage using the Sauerbrey equation. Viscoelasticity was not accounted for as the dissipation values were very low ($\Delta D < 10$). Briefly, gold sensor crystals from qSense (Biolin Scientific, Inc., Linthicum Heights, MD) were cleaned prior to QCM experiments by immersion in a hot (~75°C) solution of 5:1:1 (by volume) H_2O:H_2O_2:NH_4OH for 10 minutes followed by oxygen plasma treatment for 10 minutes. After cleaning, the sensor crystals were loaded into a qSense E-4 QCM instrument (Biolin Scientific, Inc., Linthicum Heights, MD), and a baseline signal was collected in water for approximately 10 minutes. For measurement of MPA SAM surface coverage, a 20 mM MPA solution in water was flowed over the sensor crystals for 10 minutes, and the sensor crystals were then incubated overnight in the MPA solution. The following day, unbound MPA was removed from the sensor crystals by flowing water for approximately 10 minutes. For measurement of cystamine surface coverage, a 50 mM cystamine dihydrochloride solution in water was flowed over the sensor crystals for 10 minutes, and the sensor crystals were then incubated overnight in the cystamine solution. The following day, unbound cystamine was removed by flowing water for approximately 10 minutes.

Cyclic Voltammetry of Ferrocene on MPA and Cystamine SAMs on Gold Electrodes

For attachment of aminoferrocene to the MPA SAM on a gold electrode, the MPA SAM was first formed by incubating a freshly-cleaned gold electrode in a solution of 20 mM MPA in water overnight at room temperature. The following day, unbound MPA was removed by washing the gold electrode three times in DI water. The carboxy-functionalized gold electrode was then incubated for one hour at room temperature in a solution of 20 mM aminoferrocene, 40 mM HATU, and 40 mM DIPEA in DMF. Unreacted aminoferrocene was removed by washing the electrode three times each in DMF and then DI water before drying in a stream of nitrogen. For attachment of ferrocenecarboxylic acid to a cystamine SAM (CYSAM) on a gold electrode, the CYSAM was first formed by incubating a freshly-cleaned gold electrode in a solution of 50 mM cystamine dihydrochloride in water overnight at room temperature. The following day, unbound cystamine was removed by washing the gold electrode three times in DI water. The amine-functionalized gold electrode was then incubated for one hour at room temperature in a solution of 50 mM ferrocenecarboxylic acid, 100 mM HATU, and 100 mM DIPEA. Unreacted ferrocenecarboxylic acid was removed by washing the electrode three times each in DMF and then DI water before drying in a stream of nitrogen. Cyclic voltammetry of the ferrocene electrodes was performed in 0.1 M $HClO_4$ at scan rates of 20, 50, 100, 200, 400, 600, 800, 100, 1200, 1400, and 1600 mV/s.

Cyclic Voltammetry of 2C9 Electrodes

Cyclic voltammetry of 2C9 electrodes was performed in either anaerobic or aerobic conditions in a pH 7.4 electrolyte containing 50 mM KPi and 0.1 M KCl. For anaerobic CV, the electrolyte was purged with high-purity Argon for at least one hour before the experiment and the electrochemical cell was kept in an anaerobic chamber during the experiment. Anaerobic CV scans of the 2C9 electrode were collected from 0.00 to -0.75 V for three cycles at scan rates of 10, 20, 40, 60, 80, 100, 200, 400, 800, 1000, and 1200 mV/s. For aerobic CV, electrolyte exposed to the atmosphere was used in the electrochemical cell and the experiment was performed on the bench-top. Aerobic CV scans of the 2C9 electrode were collected from 0.00 to -0.75 V for three cycles at scan rates of 10, 20, 40, 60, 80, 100, 200, 400, 800, 1000, and 1200 mV/s. Aerobic CV scans were also taken in the presence of increasing concentrations (20, 50, 100, 200, 300, 500, and 800 μM) of tolbutamide. For aerobic CV experiments with tolbutamide, 100 μl of a 100x solution of tolbutamide dissolved in DMSO was added to 10 ml of electrolyte and allowed to interact with the 2C9 electrode for 10 minutes. After this 10 minute incubation in tolbutamide, aerobic CV scans of the 2C9 electrode were collected from 0.00 to -0.75 V for three cycles at scan rates of 10, 60, 200, and 1200 mV/s.

Chronoamperometry with the Mediator Phenosafranine

The compound phenosafranine (PS) was tested as a mediator for electron transfer to the 2C9 mutant R132C immobilized to a gold electrode via maleimide/thiol coupling. Chronoamperometry experiments were performed with either R132C or maleimide-coated electrodes at a potential of -0.75 V in an unstirred pH 7.4 electrolyte containing 50 mM KPi, 0.1 M KCl, 1500 U/ml catalase, and 1.2 mM PS mediator. Aliquots of 25 mM tolbutamide dissolved in DMSO were added separately to the electrolyte in increments, and the electrolyte was then mixed to create solutions of approximately 10, 20, 50, 100, 200, 300, and 500 μM tolbutamide. The current was measured for 10 minutes after each addition of tolbutamide, and

curves of current versus time for each tolbutamide concentration were overlaid to create one single plot.

HPLC Analysis

HPLC was used to monitor the amount of tolbutamide present in the electrolyte during chronoamperometry with the mediator PS and either R132C (immobilized via maleimide/thiol coupling) or maleimide-coated electrodes. Chronoamperometry was carried out at as described above (with 1500 U/ml catalase and 1.2 mM PS) for two hours in the presence of 200 μM tolbutamide. Aliquots of 200 μl of electrolyte were extracted after 0, 10, 20, 40, 60, 80, 100, and 120 minutes of electrolysis and mixed 1:1 with an internal standard (500 μM diclofenac dissolved in methanol). A tolbutamide calibration curve was prepared by diluting 5, 10, 20, and 50 μM 4-hydroxytolbutamide (in electrolyte with 1.2 mM PS and 1500 U/ml catalase) 1:1 with the internal standard (500 μM diclofenac dissolved in methanol). Twenty microliters of the calibration curve and timepoint samples were injected separately at a flow rate of 0.4 ml/min onto a C18 HPLC column (Prevail C18 3u, 150 mm x 3.0 mm, Grace Discovery Sciences, Deerfield, IL) connected to an Agilent 1200 series liquid chromatograph (LC) system with a UV/Vis detector, and the eluate was monitored at 236 nm. Solvent A was 95% H_2O and 5% MeOH with 0.05% formic acid and Solvent B was 100% MeOH with 0.05% formic acid. The following linear gradient was used: 0-8 mins: 50% Solvent B, 8-15 mins: 90% Solvent B, 16 -25 mins: 50% Solvent B. The area of the tolbutamide peak relative to that of the internal standard peak (the relative response) was calculated for each timepoint sample and compared to the calibration curve to calculate the concentration of tolbutamide in each timepoint sample.

3.3 Results and Discussion

3.3.1 Surface Characterization of Gold Electrodes

Gold-coated glass slides made by EMF Corporation were used as gold working electrodes. The gold coating (1000 Å thick) is evaporated onto a titanium (50 Å thick) adhesion layer on glass and thus the surface morphology of the gold electrode is expected to be that of polycrystalline gold—a "rolling-hills" morphology characterized by a number of crystalline grains at different orientations[12]. AFM imaging of bare gold electrodes (Fig 3.3) confirmed that the gold-coated glass slides were predominantly polycrystalline gold. As seen in Fig 3.3, the gold surface exhibits multiple sized grains in different orientations and is therefore very rough. The rough surface of the gold electrodes precluded AFM imaging of 2C9 molecules on electrodes as it was difficult to distinguish individual crystallites from enzyme molecules. In addition, the rough surface morphology of the polycrystalline gold means that the effective surface area of the gold electrodes is larger than the geometric area, which may actually be advantageous for improving electrical contact with 2C9. There is precedent in the literature for using roughened gold electrodes for making CYP biosensors. Komatsu and co-workers found that a CYP3A4 electrode made from a rough gold electrode (made via sputter-coating) exhibited enhanced electron transfer when compared to flat gold electrodes[13], and in a recent follow-up study the same research group described the creation of gold 'nanodome arrays' that enhanced the electroactivity of immobilized CYP[14].

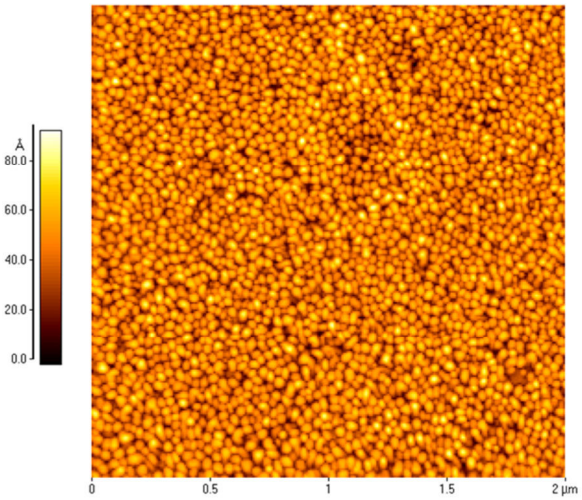

Figure 3.3 AFM Image of Gold-Coated Glass Slide Used as a Gold Working Electrode. The surface of a gold-coated glass slide exhibits a number of crystalline grains of different sizes and heights that is characteristic of polycrystalline gold. The image is 2 µm x 2 µm and the height difference from dark to light is 80.0 Å.

The surface roughness of the gold was also evaluated electrochemically. A gold electrode made from a gold-coated glass was subjected to electrochemical potential cycling from -0.2 to 1.6 V in 0.1 M H_2SO_4 at a scan rate of 50 mV/s to observe the oxidation and reduction of the gold layer. Figure 3.4 shows a CV scan obtained from electrochemical potential cycling of the gold electrode. The CV scan is very similar to voltammograms published in the literature for the oxidation and reduction of polycrystalline gold electrodes[11], and contains several peaks at approximately 1.0, 1.1, and 1.3 V for formation of a gold oxide monolayer and one single peak at approximately 0.9 V for reduction of the gold oxide monolayer. The roughness factor, R_f, of the gold electrode, or the ratio between the actual area and geometric area, can be calculated by comparing the charge density passed upon reduction of the gold oxide monolayer to the theoretical value (420 µC/cm^2) for a perfectly flat gold oxide monolayer. After subtracting the baseline current, integration of the reduction peak in Figure 3.4 gives a charge density of 881 µC/cm^2. Dividing this by 420 µC/cm^2 gives an R_f value of 2.0, meaning the actual surface area of the gold working electrode is twice that of the geometric surface area (1.3 cm^2). This is a reasonable number considering the rough morphology of the gold electrode seen via AFM imaging.

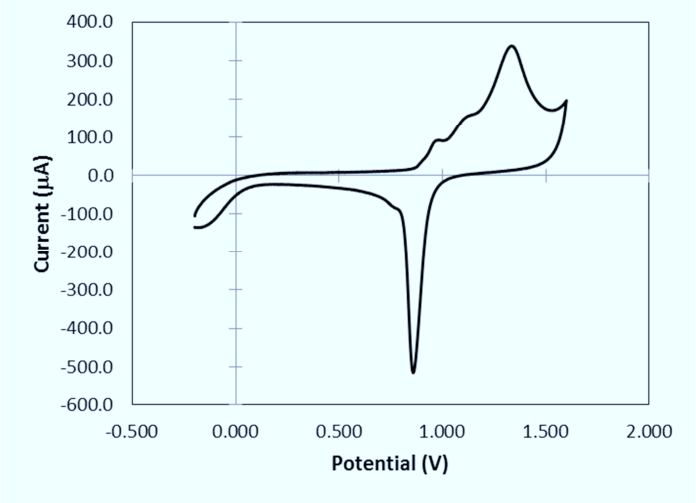

Figure 3.4 CV Scan of a Polycrystalline Gold Electrode in 0.1 M H_2SO_4 at a Scan Rate of 50 mV/s. The CV scan of a polycrystalline gold electrode made from a gold-coated glass slide exhibits characteristic anodic peaks at approximately 1.0, 1.1, and 1.3 V for formation of a gold oxide monolayer and one single cathodic peak at approximately 0.9 V for reduction of the gold oxide monolayer.

3.3.2 Surface Characterization of MPA and Cystamine SAMs on Gold

SAMs formed from MPA and cystamine on gold electrodes were characterized via reductive desorption and a QCM-D. First a QCM-D was used to monitor the adsorption of MPA and cystamine on gold sensor crystals. The gold sensor crystals are made via sputtering; thus, they are polycrystalline gold and essentially serve as a model surface for the gold-coated glass slides used as working electrodes. The QCM-D technique has been described elsewhere[15] but essentially a QCM-D monitors the change in mass at the surface of a quartz crystal (the sensor crystal) by measuring the changes in its resonant frequency. Additions of mass to the surface of the sensor crystal causes a decrease in the resonant frequency, and these events are related via the Sauerbrey equation[16], which describes the change in mass at the sensor crystal as a function of the change in resonant frequency and the physical properties of the crystal. Figure 3.5 shows the plots of surface concentration versus time obtained via the QCM-D for the overnight adsorption of MPA (Fig. 3.5A) and cystamine (Fig. 3.5B) on gold. Based on this QCM-D data, one can see that the MPA and cystamine SAMs do indeed form on the gold electrode, and the surface coverage for each is 2.7×10^{-9} and 1.6×10^{-8} moles/cm^2, respectively. It has been reported[17] in the literature that the surface coverage of an ideal, densely packed alkanethiol SAM on gold is 7.6×10^{-10} moles/cm^2. Therefore, based on the QCM-D measurements, it appears that there is approximately 3.2 and 20.8 times as much MPA and cystamine SAM, respectively, on the gold electrode, than there would be if they each formed an ideal, densely packed monolayer. Even if we assume that the roughness factor of the gold sensor crystals used in the QCM-D is approximately the same ($R_f = 2.0$) as that of the gold-coated glass slide electrode and calculate the surface coverages of the MPA and cystamine SAM based on the actual surface area (1.3×10^{-9} and 7.9×10^{-9} moles/cm^2, respectively), these values still exceed that of an ideal, densely packed monolayer. The ideal surface coverage value of 7.6×10^{-10} moles/cm^2 comes from the theoretical packing density of alkanethiols on a Au(111) crystal face[18]. The gold sensor crystals and the gold-coated glass slide electrodes however are not Au(111) but polycrystalline gold, which is a mixture of Au(111), Au(110), and Au(100); thus, the theoretical packing density of alkanethiols on the gold sensor crystals and gold electrode may be different than the ideal value

of 7.6 x 10^{-10} moles/cm^2. However, the fact that the QCM-D data shows what appears to be a single adsorption event for both the MPA and cystamine SAM and that both surface coverage values are very close to the ideal value suggests that the MPA and cystamine SAM forms a complete monolayer on the gold sensor crystals and therefore the gold electrode surface.

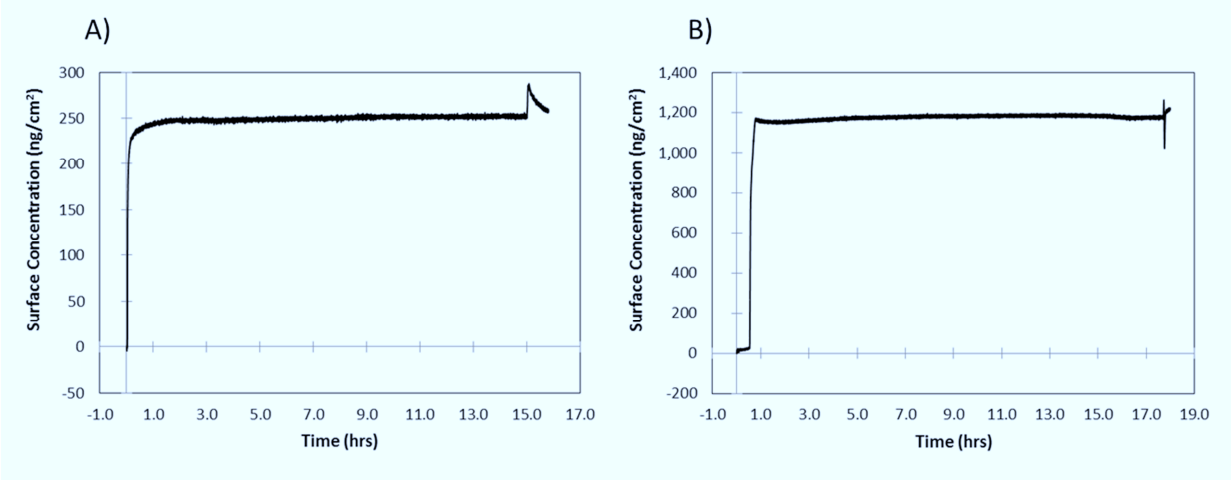

Figure 3.5 QCM-D Measurement of the Surface Coverage of MPA and Cystamine SAMs on Gold. A QCM-D was used to monitor the overnight adsorption of (A) MPA and (B) cystamine on gold to form SAMs. The calculated surface coverages of the MPA and cystamine SAMs are 2.7 x 10^{-9} and 1.6 x 10^{-8} moles/cm^2, respectively.

Reductive desorption of the MPA and cystamine SAMs was also used to confirm SAM adsorption on the gold electrode and measure the SAM surface coverage. Electrodes modified with MPA or cystamine SAM were cycled three times in 0.5 NaOH from 0.0 to -1.4 V at 50 mV/s to reductively desorb the SAM from the gold surface. Reductive desorption of a SAM on gold occurs in alkaline conditions via reduction of the gold bound sulfur atom and 'lifting-off' of the alkanethiolate[19-22], and can be described by the following equation:

$$AuS(CH_2)_nR + e^- \rightarrow Au + {}^-S(CH_2)_nR \qquad (1)$$

where *n* is the number of hydrocarbons in the alkanethiol and *R* is the terminal functional group on the SAM. In general, the ease of reductive desorption of the SAM is dependent on the stability of the monolayer; stable and ordered SAMs exhibit more negative reductive potentials than diffuse and disordered SAMs. Figure 3.6 shows CV scans for the reductive desorption of an MPA (Fig. 3.6A) and cystamine (Fig. 3.6B) SAM on a gold electrode. The first scan of the MPA SAM on gold exhibits a broad cathodic peak at approximately -1.1 V and a sharp cathodic peak at approximately -0.8 V. The cathodic peak at -1.1 V correlates with the cathodic peak for reductive desorption of a similar SAM, 3-mercaptopropylsulfonate (MPS) seen in a previous study[17], and most likely represents reductive desorption. It is unclear what reductive process is causing the sharp cathodic peak at -0.8 V and it is not present in subsequent scans. The first scan of the cystamine SAM on gold exhibits several broad cathodic peaks from -0.8 to -1.2 V, suggesting that the cystamine SAM adsorbs at different binding sites with varying degrees of stability. This is not surprising, given the heterogeneous nature of the polycrystalline gold surface. Subsequent scans of both the MPA and cystamine SAMs on gold show a progressive decline in the reduction peak currents which is a consequence of diffusion in solution of reductively desorbed MPA and cystamine[17]. After the baseline currents were subtracted, integration of the cathodic peaks for reductive desorption resulted in a charge of -197.5 and -575

μC for desorption of MPA and cystamine, respectively. The surface coverage, Γ_m, of the MPA and cystamine SAMs were calculated using Faraday's law of electrolysis:

$$\Gamma_m = \frac{Q_m}{nFA} \quad (2)$$

where Q_m is the charge passed upon reduction of the SAM, n is the number of moles of electrons transferred per mole of reactant (in this case one), F is Faraday's constant (96485.3 C/mole e^-), and A is the electrode area (in this case 2.6 cm^2 for the geometric surface area multiplied by the roughness factor 2.0). Using Eq. (2), the calculated surface coverage for the MPA and cystamine SAMs are 7.9 x 10^{-10} and 2.3 x 10^{-9} moles/cm^2, respectively. These values are very close to the ideal SAM surface coverage value of 7.6 x 10^{-10} moles/cm^2 and agree well with the surface coverage values obtained for the MPA and cystamine SAMs with the QCM-D.

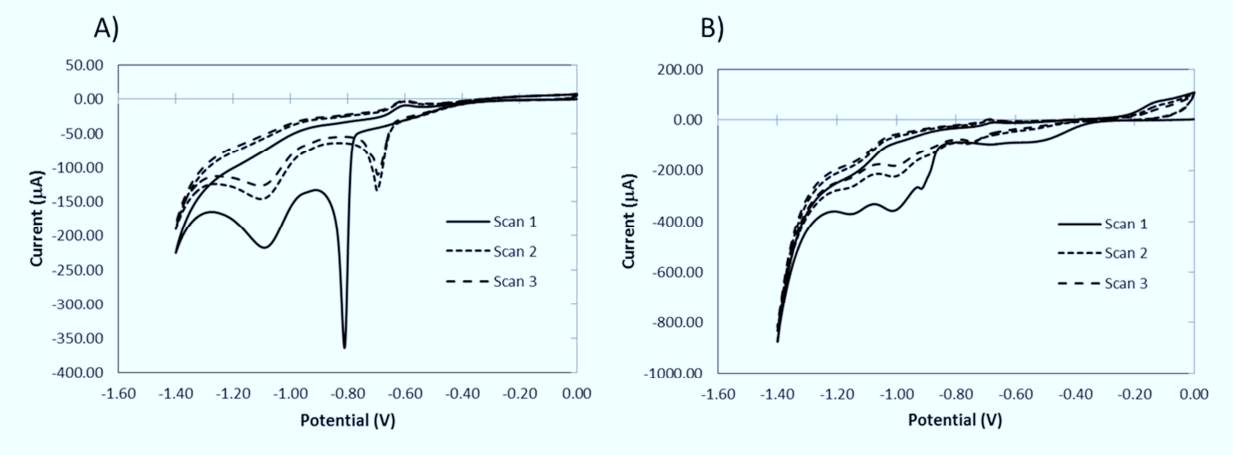

Figure 3.6 Reductive Desorption of MPA and Cystamine SAMs on Gold Electrodes. MPA (A) and cystamine (B) SAMs were reductively desorbed from gold electrodes in 0.5 M NaOH by scanning the potential three times from 0.0 to -1.4 V at 50 mV/s.

3.3.3 Reaction of Sulfo-SMCC and N-Succinimidyl-3-maleimidopropionate with BODIPY® FL-L-cystine

Sulfo-SMCC and N-succinimidyl-3-maleimidopropionate (Figure 3.7) were tested as the amine-reactive maleimide reagent for oriented attachment of 2C9 to a gold electrode via maleimide/thiol coupling. The compounds differ in the type of linker between the amine reactive NHS and the maleimide. To test the reactivity of these compounds against thiols, the disulfide-containing dye BODIPY® FL-L-cystine was reacted with amine-functionalized glass slides modified with either Sulfo-SMCC or N-succinimidyl-3-maleimidopropionate. BODIPY® FL-L-cystine, seen in Figure 3.8 is virtually non-fluorescent in its native disulfide state but absorbs strongly at approximately 500 nm and becomes fluorescent when it is reduced via the reducing agent TCEP to two separate thiol-linked fluorophores. Reduced BODIPY® FL-L-cystine therefore, contains a thiol group and will react to maleimide groups and can act as a fluorescent surrogate for 2C9. Thus, the extent of absorbance of BODIPY® FL on maleimide-glass slides functionalized via either Sulfo-SMCC or N-succinimidyl-3-maleimidopropionate was used to evaluate the reactivity of these two compounds. Glass slides were functionalized sequentially with 4-aminobutyltriethoxysilane and either Sulfo-SMCC or N-succinimidyl-3-maleimidopropionate prior to reaction with reduced BODIPY® FL-L-cystine

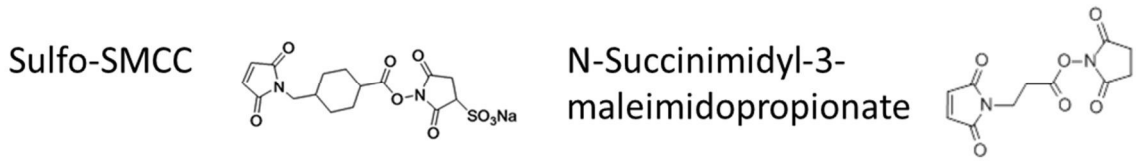

Figure 3.7 The Amine-Reactive Maleimide Compounds Sulfo-SMCC and N-Succinimidyl-3-maleimidopropionate.

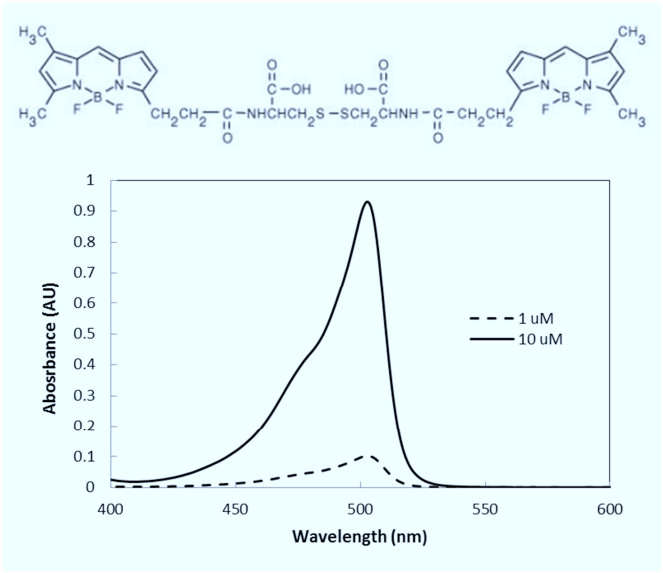

Figure 3.8 Absorption Spectrum of BODIPY® FL-L-cystine in the Presence of the Reducing Agent TCEP and 50 mM KPi (pH 7.4). BODIPY® FL-L-cystine is virtually non-fluorescent as a disulfide (top) but absorbs strongly at approximately 500 nm and becomes fluorescent in the presence of a reducing agent such as TCEP that reduces the disulfides to thiols.

Absorption spectra of BODIPY® FL-conjugated glass slides functionalized via either Sulfo-SMCC or N-succinimidyl-3-maleimidopropionate are shown in Figure 3.9. Peaks at approximately 500 and 518 nm for absorption of the BODIPY® FL fluorophore are present in the spectra for amine-functionalized glass slides modified with Sulfo-SMCC and N-succinimidyl-3-maleimidopropionate. These results suggest that BODIPY® FL reacted with both types of maleimide-containing compounds on the surface of the glass slide; however, the absorption peak for BODIPY® FL is clearly much larger for the sample modified with N-succinimidyl-3-maleimidopropionate. Thus, it appears that the amine-reactive compound N-succinimidyl-3-maleimidopropionate is more reactive to thiols than Sulfo-SMCC and was used to functionalize maleimide groups on gold for the oriented attachment of 2C9 via maleimide/thiol coupling. There is a slight shift in the BODIPY® FL absorption wavelength for the glass slide modified with N-succinimidyl-3-maleimidopropionate (518 nm versus 500 nm); the absorbance properties of the BODIPY® FL fluorophore may be altered slightly when it is conjugated to N-succinimidyl-maleimidopropionate on glass.

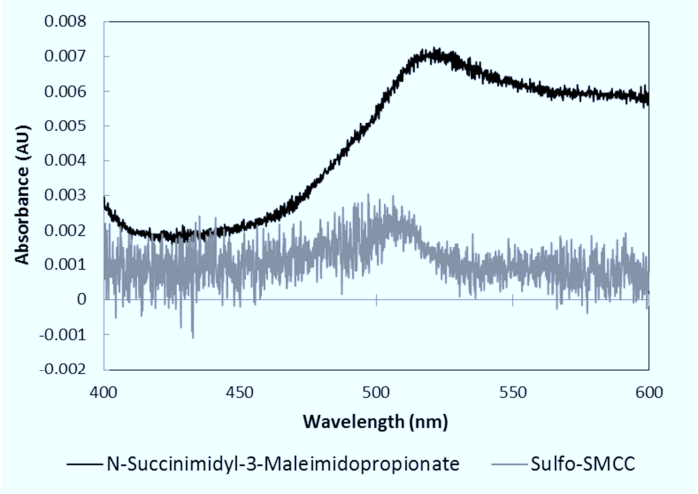

Figure 3.9 Absorption Spectra of the Fluorophore BODIPY® FL Conjugated to Maleimide Glass Slides Functionalized via Sulfo-SMCC or N-Succinimidyl-3-maleimidopropionate. BODIPY® FL-L-cystine was reacted in the presence of TCEP to amine-functionalized glass slides that had been modified with maleimides either by Sulfo-SMCC (grey line) or N-succinimidyl-3-maleimidopropionate (black line).

3.3.4 Enzyme Activity of 2C9 Electrodes with Vivid® BOMCC

To confirm immobilization and attachment of wt 2C9 and the single Cys mutants R125C, R132C, and K432C on gold electrodes, peroxide-supported activity assays with the fluorogenic substrate Vivid® BOMCC were performed. Both wt 2C9 and the single Cys mutants R125C, R132C, and K432C were previously found to be active in a peroxide-supported activity assay with Vivid® BOMCC in solution; thus, they would be expected to have activity with Vivid® BOMCC on an electrode if they are active after immobilization. To this end, 2C9 electrodes made using the three different attachment methods and either wild-type enzyme or the single Cys mutants were tested for activity with Vivid® BOMCC. A reaction solution containing cumene hydroperoxide, sodium cholate, lipids, and Vivid® BOMCC was incubated directly on the surface of the 2C9 electrode for two hours, and the fluorescence of the Vivid® Blue product (excitation 409 nm, emission 460 nm) was measured every 10 minutes. Figure 3.10 shows the results from activity assays with the 2C9 electrodes and Vivid® BOMCC for all three attachment methods. The fluorescent intensities were normalized based on the amount of CYP protein (in μM) that was incubated on the electrode during the enzyme immobilization. Based on the results, we can conclude that wt 2C9 and the single Cys mutants R125C, R132C, and K432C were successfully coupled to the gold electrode via all three attachment methods because activity with Vivid® BOMCC was measured for all cases. Activity assays with Vivid® BOMCC were also performed for an MPA-only surface, a Ni-NTA-only surface, and a maleimide-only surface, and no activity was detected without the presence of enzyme (data not shown). The mutant R132C had the highest activity with Vivid® BOMCC amongst wt 2C9 and the single Cys mutants, agreeing with results obtained earlier from the peroxide-supported activity assay in solution with Vivid® BOMCC where R132C had the highest specific activity. R132C has an especially high relative activity when it is immobilized using oriented attachment via maleimide/thiol coupling. Thus, it can be used as a model to represent the behavior and activity of 2C9 immobilized to an electrode via an engineered cysteine and maleimide/thiol coupling. Notably, different attachment methods result in different degrees of enzyme activity. Immobilization via oriented attachment with a Ni-NTA/His-tag results in the most active enzyme

for all the 2C9 variants, most likely because immobilization at the C-terminus is less constraining than attachment via amine coupling or maleimide/thiol coupling. Surprisingly, wt 2C9 is the least active enzyme amongst all the 2C9 variants tested for all attachment methods and maintains nearly the same activity with each attachment method. The single Cys mutants R125C, R132C, and K432C all perform better than wt 2C9 when they are immobilized via Ni-NTA/His-tag coupling but only R132C and K432C are consistently more active than wt 2C9 for the other two attachment methods (random attachment and oriented attachment via maleimide/thiol coupling). The fact that different attachment chemistries lead to different enzyme activities provides further proof that the 2C9 enzymes are covalently attached to the gold electrodes; one would expect the same enzyme activities for all attachment methods if 2C9 were merely physically adsorbed on the surface of the electrode.

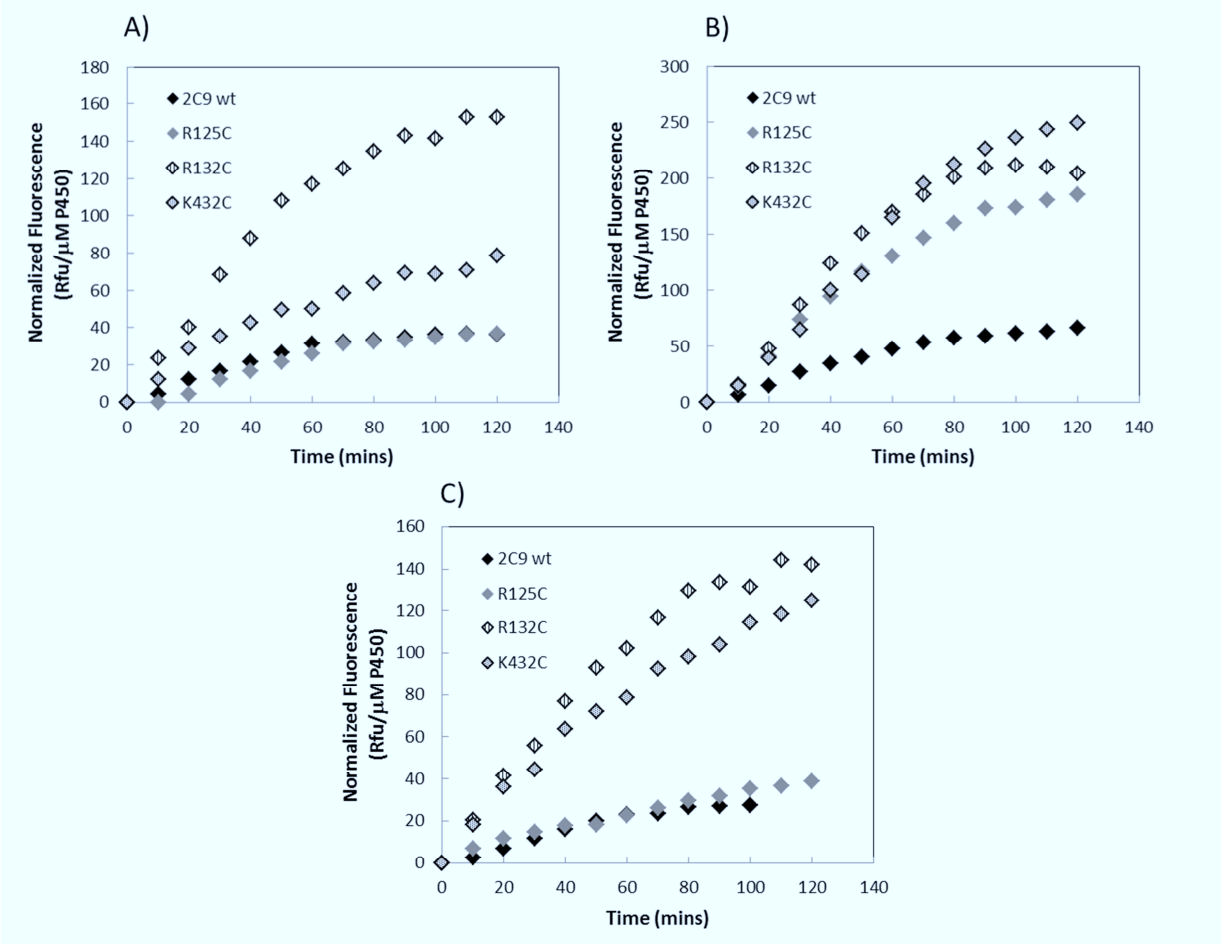

Figure 3.10 Activity Assays with Vivid® BOMCC of 2C9 Electrodes Made with Three Different Attachment Methods. Plots of the fluorescence of the Vivid® Blue product (excitation 409 nm, emission 460 nm) over time for 2C9 electrodes made using (A) random attachment via amine coupling, (B) oriented attachment via Ni-NTA/His-tag coupling, and (C) oriented attachment via maleimide/thiol coupling. Fluorescent intensity measurements were normalized to the amount of CYP protein (in µM) incubated on the electrode during the immobilization.

3.3.5 FT-IR Characterization

Before enzymatic activity assays with Vivid BOMCC were used to confirm immobilization of wt 2C9 and the single Cys mutants on the gold electrodes, FT-IR spectroscopy

was used to characterize the surface chemistry of a single 2C9 electrode: R132C immobilized with oriented attachment via maleimide/thiol coupling. Grazing angle incidence FT-IR was performed as an initial test for the presence of enzyme and the correct surface chemistry on the gold electrode. Scans at an angle of 80° to the surface normal were collected for bare gold, maleimide, and R132C electrodes. As seen in Figure 3.11, the FT-IR scans confirmed the presence of amide-linked maleimide and enzyme (R132C) on the gold electrodes. Peak assignments for the maleimide electrode and the R132C electrode were based on values in the literature[23] and a previous study on the oriented attachment of the drug-metabolizing CYP 2E1 to a maleimide-SAM on gold[9]. The spectrum for bare gold electrode exhibited a single peak for stretching of atmospheric CO_2 at approximately 2300 cm^{-1} while the spectrum for the maleimide electrode exhibited peaks for the asymmetric/symmetric stretching of CH_2, asymmetric/symmetric stretching of the imide of maleimide, C-N stretching of maleimide, and stretching of the amide bond linking the maleimide to the MPA SAM. There is a great deal of noise surrounding the peaks for the maleimide group in the spectra for the maleimide electrode, and these were attributed to atmospheric water that was not purged from the FT-IR chamber during the scans. The spectrum for the R132C electrode exhibits characteristic amide peaks associated with the different conformations of amide bonds in protein, namely the Amide I (1659 cm^{-1}), Amide II (1536 cm-1), and Amide III (1244 cm^{-1}) peaks. The peak heights for asymmetric/symmetric hydrocarbon (CH_2) stretching increased, which is to be expected since proteins contain a great deal of CH_2 groups. Taken together, these FT-IR results confirm modification of the electrode surface with maleimide groups and covalent attachment of 2C9 enzyme (the mutant R132C) to the gold electrode. Further FT-IR experiments with the other attachment methods and 2C9 variants (wild-type, R125C, and K432C) were deemed unnecessary after the activity data discussed in the previous section (3.3.4) was obtained that confirmed immobilization of all the enzymes via all three attachment methods.

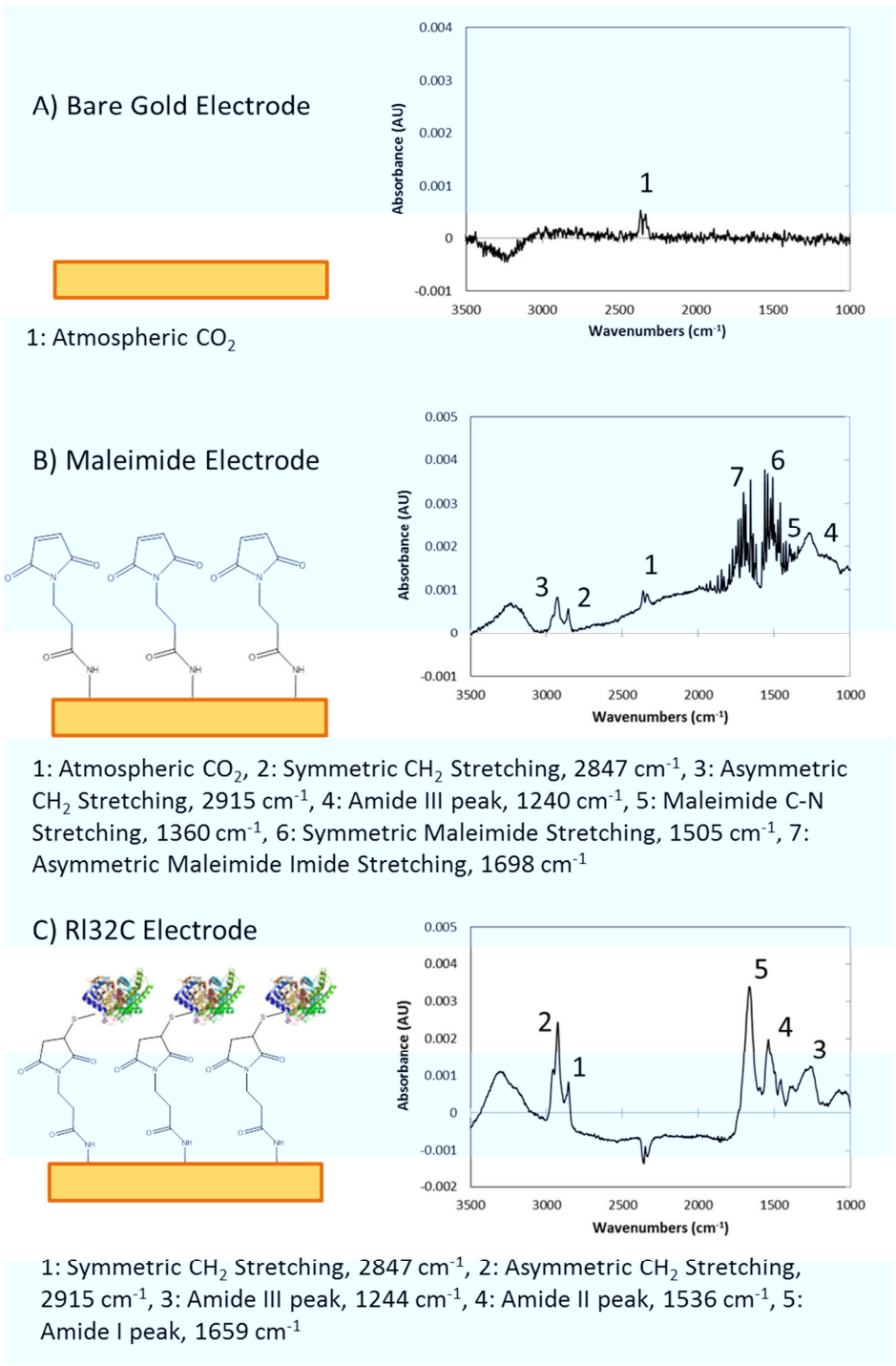

Figure 3.11 Grazing Angle Incidence FT-IR Spectra Collected for Bare Gold, Maleimide, and R132C Electrodes. Spectra were collected at an angle of 80° to the surface normal in a nitrogen-purged chamber to improve the signal-to-noise ratio and eliminate signals from atmospheric water. (A) FT-IR spectrum for a bare gold electrode. (B) FT-IR spectrum for a maleimide-functionalized electrode. (C) FT-IR spectrum for R132C immobilized on a maleimide-functionalized electrode. Peak assignments are noted underneath each plot.

3.3.6 Cyclic Voltammetry of Ferrocene on MPA and Cystamine SAMs on Gold Electrodes

As shown in Figure 3.12, the small molecule redox compounds aminoferrocene and ferrocenecarboxylic acid were attached to the MPA and cystamine SAMs, respectively to assess whether or not electron transfer though the MPA and cystamine SAMs was possible. Ferrocene is a readily-available metal complex frequently used as a model redox compound in electrochemistry studies[24] and therefore serves as a good redox model for our electrode system. Aminoferrocene and ferrocenecarboxylic acid were coupled via amine coupling to an MPA and cystamine SAM on gold, respectively, using the coupling reagent HATU and the base DIPEA. Cyclic voltammetry of the ferrocene electrodes was performed in 1 M HClO4 at scan rates ranging from 20 to 1600 mV/s. Evidence of a reversible pair of redox peaks in the CV scans would prove that electron transfer is possible through the MPA and cystamine SAMs on gold, and a linear relationship between the anodic and cathodic peak current (i_p) and the scan rate (υ) would further prove that the ferrocene is covalently attached to the SAMs as such a relationship is indicative of a surface redox species[24]. Figure 3.13 shows the CV scans taken with ferrocene electrodes made from MPA and cystamine SAMs on gold. Included are plots of the peak anodic and cathodic currents versus the scan rate for each CV.

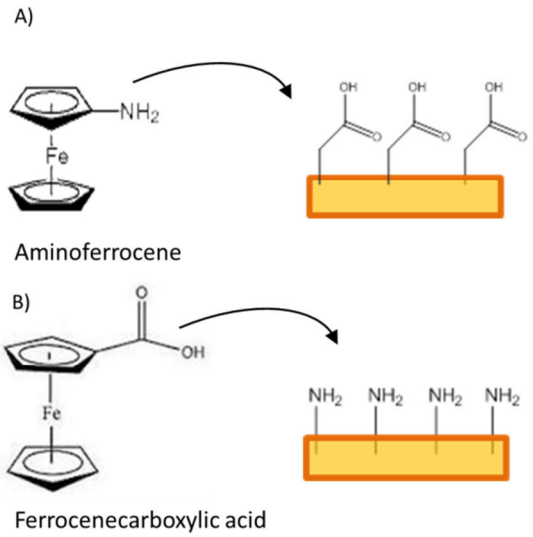

Figure 3.12 Covalent Attachment of Aminoferrocene and Ferrocenecarboxylic acid to (A) an MPA SAM and (B) a Cystamine SAM on Gold Electrodes.

As seen in Figure 3.13, a pair of reversible redox peaks are seen in the CV scans for aminoferrocene and ferrocenecarboxylic acid coupled to an MPA and cystamine SAM, respectively, suggesting that the covalently-coupled ferrocene is redox active and electron transfer is possible through the MPA and cystamine SAMs on gold. Plots of the peak anodic and cathodic currents versus scan rate are linear for the oxidation and reduction of ferrocene on both MPA and cystamine SAMs; therefore, the redox response seen in the CV scans is from a surface confined species, confirming that the ferrocene is covalently coupled to the electrode. The amount of redox active species immobilized on the electrode can be calculated by the following equation[24] relating the peak current to the scan rate:

$$i_p = \frac{n^2F^2}{4RT} \upsilon A \Gamma_m \quad (3)$$

where i_p is the anodic or cathodic peak current, n is the number of moles of electrons transferred per mole of the electroactive species (in this case one), F is Faraday's constant (96485.3 C/mole e^-), R is the universal gas constant, T is the temperature (in Kelvin), υ is the scan rate, A is the actual surface area of the electrode, and Γ_m is the surface coverage of the electroactive species. The slopes for the anodic current vs. scan rate plots and Eq. (3) were used to calculate surface coverage; the surface coverage values for electroactive ferrocene on MPA and cystamine SAMs were calculated to be 1.8×10^{-11} and 8.2×10^{-12} moles/cm^2, respectively. These values are reasonable, considering that the surface coverage values for the MPA and cystamine SAMs were found via reductive desorption to be 7.9×10^{-10} and 2.3×10^{-9} moles/cm^2, respectively, but suggest that only 2.3 and 0.4% of the MPA and cystamine SAMs, respectively, are covered with electroactive ferrocene. If all reactive groups on the MPA and cystamine SAMs react with ferrocene (i.e., the yield for the coupling reaction is 100%) then the low values obtained for the amount of electroactive ferrocene mean that only 2.3 and 0.4% of the coupled ferrocene is electroactive. However, it is unlikely that all the reactive groups on the MPA and cystamine SAMs reacted. If we assume that all coupled ferrocene molecules are electroactive, then the low values obtained for the amount of electroactive ferrocene mean that only 2.3 and 0.4% of the reactive groups on the MPA and cystamine SAMs are reacting. It is likely that the actual situation is a combination of these two extremes: not all of the reactive groups on the MPA and cystamine SAMs react and not all of the attached ferrocene is electroactive. In any case, the results from this study with ferrocene tell us that (1) electron transfer is possible through the MPA and cystamine SAMs and should be for the case of 2C9 electrodes and (2) it is likely that very few carboxyls and amines on the MPA and cystamine SAMs, respectively, react with ferrocene. It is unclear how this low reactivity affects attachment of 2C9; wt 2C9 and the singly Cys mutants R125C, R132C, and K432C clearly can be immobilized onto electrodes modified by MPA and cystamine SAMs but it is unclear what the surface coverages of these enzymes are on these SAM-modified electrodes and what percentage of the total amount of SAM on the surface couples with enzyme.

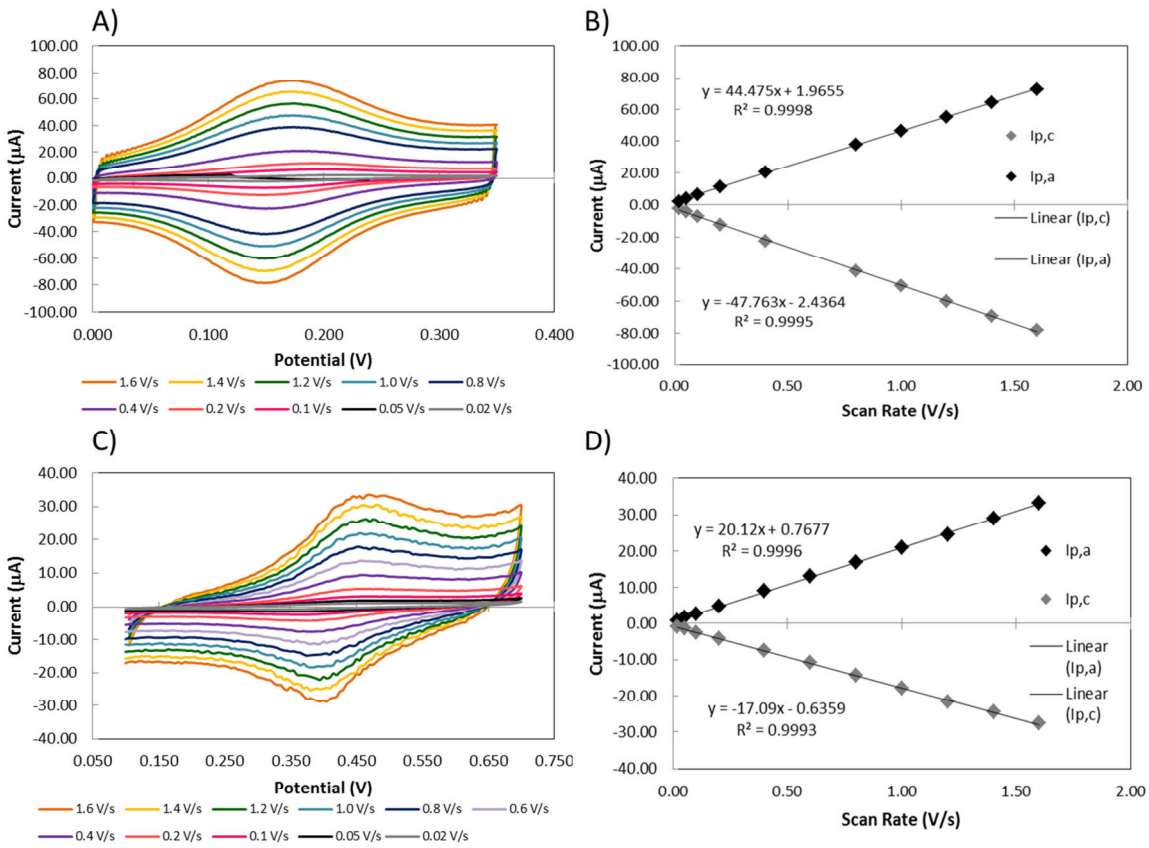

Figure 3.13 CV Scans and Plots of Peak Current versus Scan Rate for Ferrocene Covalently Coupled to an MPA and Cystamine SAM on Gold Electrodes. (A) CV scan of aminoferrocene coupled to MPA SAM on gold. (B) Plot of peak current versus scan rate for CV shown in (A). (C) CV scan of ferrocenecarboxylic acid coupled to a cystamine SAM on gold. (D) Plot of peak current versus scan rate for CV shown in (C). CV scans were taken in 1 M $HClO_4$

3.3.7 Cyclic Voltammetry of 2C9 Electrodes

Anaerobic and aerobic cyclic voltammetry in 50 mM KPi, 0.1 M KCl (pH 7.4) was performed with 2C9 electrodes made via all three attachment methods to assess whether or not direct electron transfer was occurring from the electrode to the immobilized 2C9 and driving catalysis with the 2C9 substrate tolbutamide. The anaerobic CVs were taken in argon-purged electrolyte in an anaerobic chamber and the aerobic CVs were taken in the atmosphere on the bench-top. Aerobic CVs were also taken of the 2C9 electrodes with 500 µM tolbutamide in the electrolyte. Anaerobic CVs (Figure 3.14) of CYP electrodes have traditionally been used to detect reduction and oxidation of the iron heme; without oxygen the immobilized CYP can be reversibly reduced and oxidized without entering the catalytic cycle[25,26]. Typical aerobic CVs of electroactive CYPs (Figure 3.15) exhibit increased reduction peaks and diminished oxidation peaks because the reduced heme binds oxygen which triggers a second electron transfer. In the presence of oxygen, the oxidized heme is regenerated non-electrochemically by a peroxide-shunt pathway that releases oxygen radicals and/or peroxide; hence the oxidation peak in an aerobic CV of an electroactive CYP is diminished. Aerobic CVs taken in the presence of a CYP substrate show an even larger reduction peak as the enzyme catalyzes substrate and consumes even more electrons. Thus, CVs of 2C9 electrodes were evaluated with these features in mind.

Figure 3.16 shows anerobic CVs taken at a scan rate of 60 mV/s of the 2C9 and R132C electrodes immobilized by random attachment via amine coupling (Fig. 3.16A and B), oriented attachment via Ni-NTA/His-tag coupling (Fig. 3.16C and D), and oriented attachment via maleimide/thiol coupling (Fig. 3.16E and F). CVs for the respective no-enzyme control electrodes functionalized with MPA SAM, Ni-NTA, and maleimide are included in each set of plots as a comparison. Although CVs were collected for wt 2C9 and all the single Cys mutants R125C, R132C, and K432C, data from wt 2C9 and only one single Cys mutant, R132C, are shown for clarity as a similar response was seen with the mutants R125C and K432C.

As seen in Fig. 3.16, a clear cathodic peak (at approximately -0.5 V) is visible in the CVs for wt 2C9 and R132C immobilized by random attachment via amine coupling and oriented attachment via maleimide/thiol coupling. However, no discernible peaks are visible in the CVs of wt 2C9 and R132C immobilized by oriented attachment via Ni-NTA/His-tag coupling, suggesting that direct electrochemistry to 2C9 immobilized on a gold electrode is not possible using this attachment chemistry. Very faint anodic peaks (at approximately -0.45 V) are visible in the CVs of wt 2C9 and R132C immobilized to the electrode by random attachment via amine coupling and oriented attachment via maleimide/thiol coupling. The redox peaks exhibited in the CVs of wt 2C9 and R132C for random attachment and oriented attachment via maleimide/thiol coupling are consistent with those found by Yang et al. for 2C9 amine coupled to a long-chain SAM on gold (Figure 3.14)[1]. Therefore, at first glance, it appears that wt 2C9 and R132C may be electroactive when immobilized to a gold electrode via amine coupling and oriented attachment via maleimide/thiol coupling. However, the anaerobic CVs for the corresponding no-enzyme electrodes (MPA SAM and maleimide on gold) either also exhibit reduction and oxidation peaks at nearly the same potential values (for the case of the MPA SAM) or overlay on top of the CVs of the wt 2C9 and R132C electrodes (for the case of the maleimide electrode). In fact, upon further inspection, the CVs of wt 2C9 and R132C immobilized by amine coupling to the MPA SAM appear to be diminished versions of the redox peaks observed in the no-enzyme electrode modified with MPA SAM. In summary, a redox process does appear to be occurring on the wt 2C9 and R132C electrodes made by random attachment and oriented attachment via maleimide/thiol coupling but it does not appear to be enzyme-related and instead is related to the underlying monolayer. Therefore, we can make no conclusions regarding the effectiveness of oriented attachment in promoting the direct electrochemistry of 2C9 on a gold electrode, at least with these particular attachment chemistries.

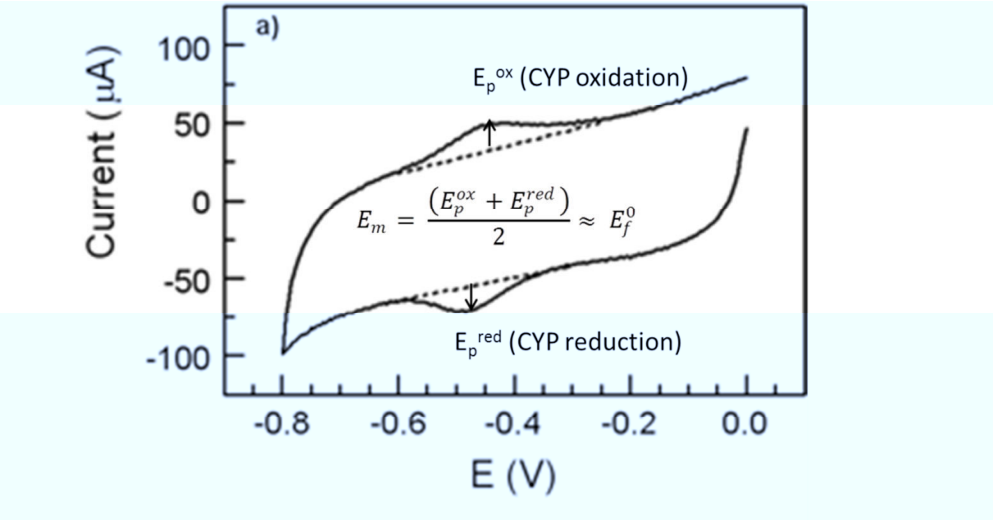

Figure 3.14 Representative Anaerobic CV of CYP2C9 Immobilized to an Electrode via Amine Coupling to a Long-Chain SAM on Gold. The anaerobic CV scan of an electroactive CYP enzyme on an electrode modified with a mixed SAM of octanethiol (OT) and 11-mercaptoundecanoic acid (MUA) consists of a pair of reversible redox peaks for reduction and oxidation of the iron heme. The formal potential (E_f^0) for reduction and oxidation of the enzyme is calculated as the midpoint potential (E_m) between the reduction (E_p^{red}) and oxidation (E_p^{ox}) peak potentials. Potentials are referenced to a Ag/AgCl (3 M KCl) reference electrode and the scan rate is 1.6 V/s. Figure reproduced and adapted with permission from (1).

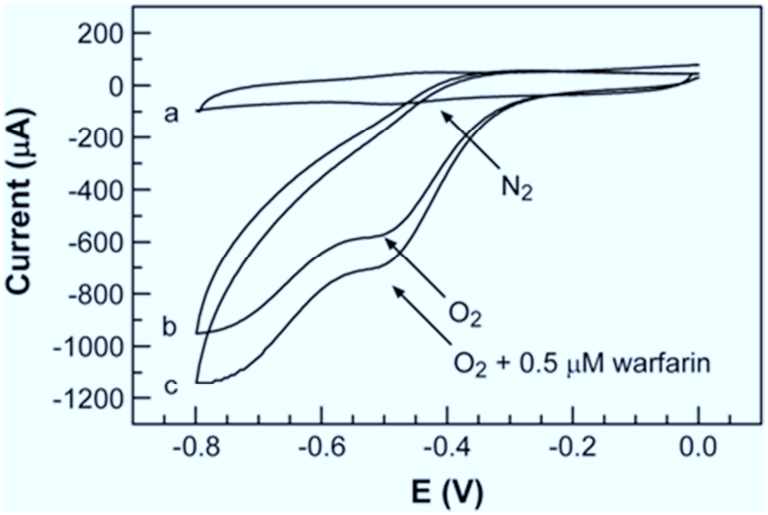

Figure 3.15 Representative Anaeraboic and Aerobic CVs of CYP2C9 Immobilized to an Electrode via Amine Coupling to a Long-Chain SAM on Gold. The aerobic CV scan of an electroactive CYP on an electrode modified with a mixed SAM of octanethiol (OT) and 11-mercaptoundecanoic acid (MUA) shows an increased reduction peak caused by the additional transfer of electrons to the reduced and oxygen-bound iron heme. An aerobic CV scan of the 2C9 electrode in the presence of the 2C9 substrate warfarin exhibits an even greater reduction peak as the enzyme uses more electrons to catalyze the substrate. Potentials are referenced to a Ag/AgCl (3 M KCl) electrode and the scan rate is 1.6 V/s. Figure reproduced with permission from (1).

Aerobic CV scans of the wt 2C9 and R132C electrodes with and without the substrate tolbutamide were also taken to confirm whether the redox peaks seen in the anaerobic CVs are monolayer related or enzyme-related. It could be that the redox peaks seen in the anaerobic CVs of wt 2C9 and R132C electrodes are enzyme-related and coincidentally correspond with redox peaks seen on the corresponding no-enzyme electrodes. If this is the case, CVs taken in aerobic buffer of the wt 2C9 and R132C electrodes should exhibit increased cathodic peak areas (much like the representative CV seen in Figure 3.15) while the CVs of the corresponding no-enzyme

electrodes should remain the same. In addition, aerobic CVs taken of the wt 2C9 and R132C electrodes in the presence of the substrate tolbutamide should exhibit even larger cathodic peak areas indicative of catalysis if the immobilized enzymes are in fact electroactive. Figures 3.17, 3.18, and 3.19 include CVs of wt 2C9, R132C, and no-enzyme electrodes collected in anaerobic buffer, aerobic buffer, and aerobic buffer containing 500 μM of the 2C9 substrate tolbutamide. Figure 3.17 shows CVs for electrodes made by random attachment via amine coupling, Figure 3.18 shows CVs for electrodes made by oriented attachment via Ni-NTA/His-tag coupling, and Figure 3.19 shows CVs for electrodes made by oriented attachment via maleimide/thiol coupling. At first glance, the data appear to show that wt 2C9 and R132C are indeed electroactive and capable of electrochemically-driven catalysis of tolbutamide. A larger cathodic peak area can be seen in the aerobic CVs for both wt 2C9 and R132C electrodes made by all three attachment methods, although the cathodic peaks seen in the CVs of 2C9 electrodes made by Ni-NTA/His-tag coupling are quite faint. Aerobic CVs of wt 2C9 and R132C electrodes in the presence of 500 μM of tolbutamide exhibit even larger cathodic peak areas, suggesting that the immobilized enzymes are capable of electrochemically-driven catalysis. All in all, the data look suspiciously similar to the set of CVs shown in Figure 3.15 from the Yang et al. paper[1], especially the CV data set shown in Figure 3.18B for R132C immobilized to the gold electrode by oriented attachment via maleimide/thiol coupling. However, in looking at the CV data for the MPA SAM, Ni-NTA, and maleimide electrodes shown in Figs. 3.17C, 3.18C, and 3.19C, respectively, we can see that once again the same pattern of electrochemical behavior is present in the no-enzyme electrodes. This is especially true for the CV data of the maleimide electrode depicted in Figure 3.19C. The fact that we see the same pattern of larger cathodic peak areas for CV scans of the no-enzyme electrodes as we do with the wt 2C9 and R132C electrodes makes it very hard to conclude that these enzymes are electroactive on the gold electrode for any of the three attachment methods. It is especially surprising to see an even larger cathodic peak for CV scans of the no-enzyme electrodes taken in 500 μM tolbutamide, as the only difference between these CV scans and those in aerobic buffer is the presence of tolbutamide. We would expect to see a difference in the cathodic peak areas of aerobic CVs taken with and without tolbutamide for an electrode containing electroactive 2C9 but not for an electrode made of the underlying monolayer that would not be expected to interact with tolbutamide. Taken together, the results from these aerobic CVs with and without tolbutamide further suggest that wt 2C9 and R132C are not electroactive on the gold electrode and the redox response seen in the CV scans is merely monolayer related. It is also possible that tolbutamide itself may be redox active—the structure of tolbutamide contains a sulfur dioxide (SO_2) group, which is known to be a reducing agent.

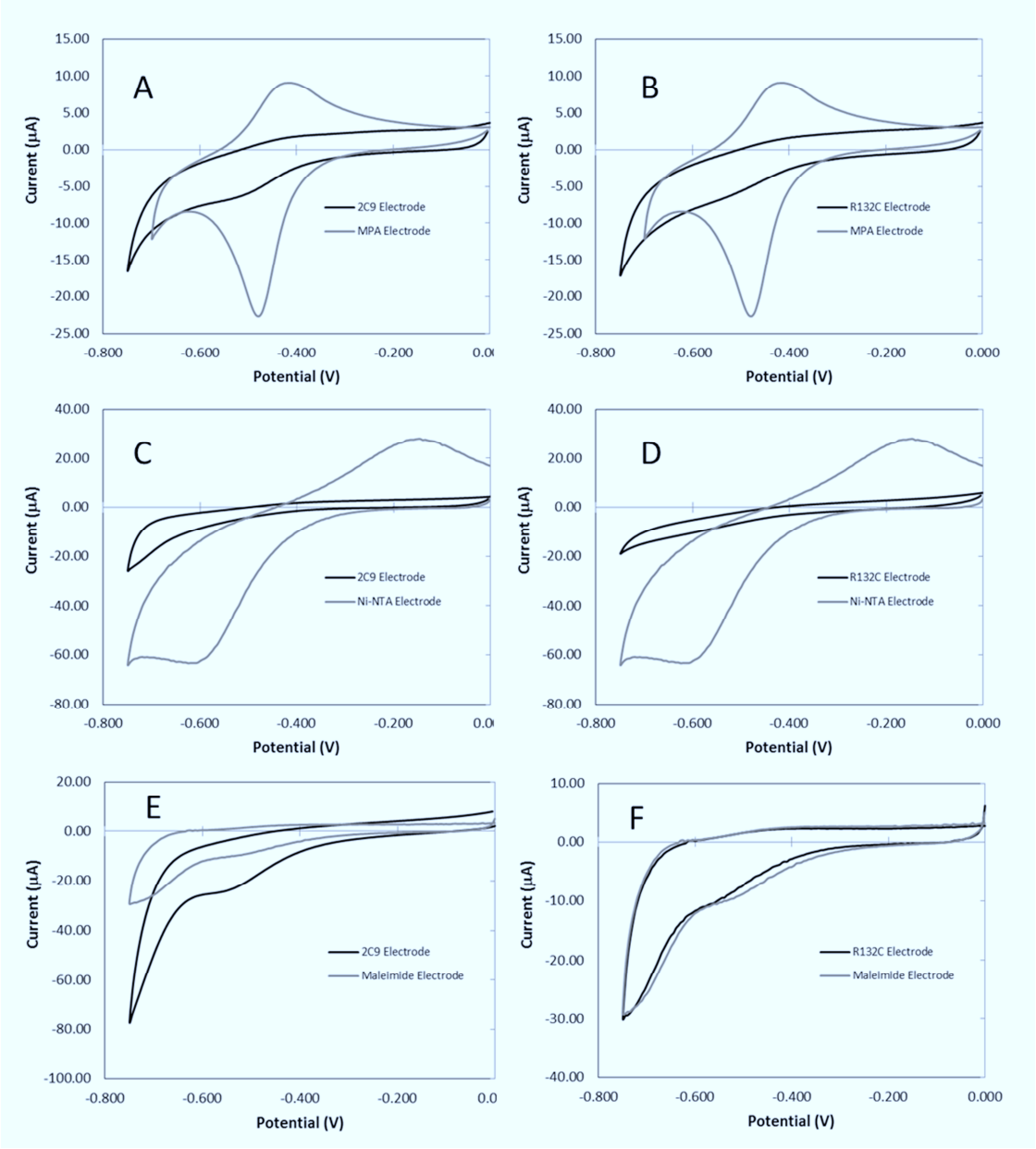

Figure 3.16 Anaerobic CVs of wt 2C9 and R132C Electrodes Made Using Random Attachment via Amine Coupling, Oriented Attachment via Ni-NTA/His-tag Coupling, and Oriented Attachment via Maleimide/Thiol Coupling, along with Anaerobic CVs of MPA SAM, Ni-NTA, and Maleimide Electrodes as No-Enzyme Controls. Anaerobic CVs of wt 2C9 (A,C,E) and R132C (B,D,F) electrodes made using random attachment via amine coupling (top panels), oriented attachment via Ni-NTA/His-tag coupling (middle panels), and oriented attachment via maleimide/thiol coupling. Anaerobic CVs of no-enzyme electrodes (MPA SAM, Ni-NTA, and maleimide only) are included for reference. CV scans were taken at a scan rate of 60 mV/s.

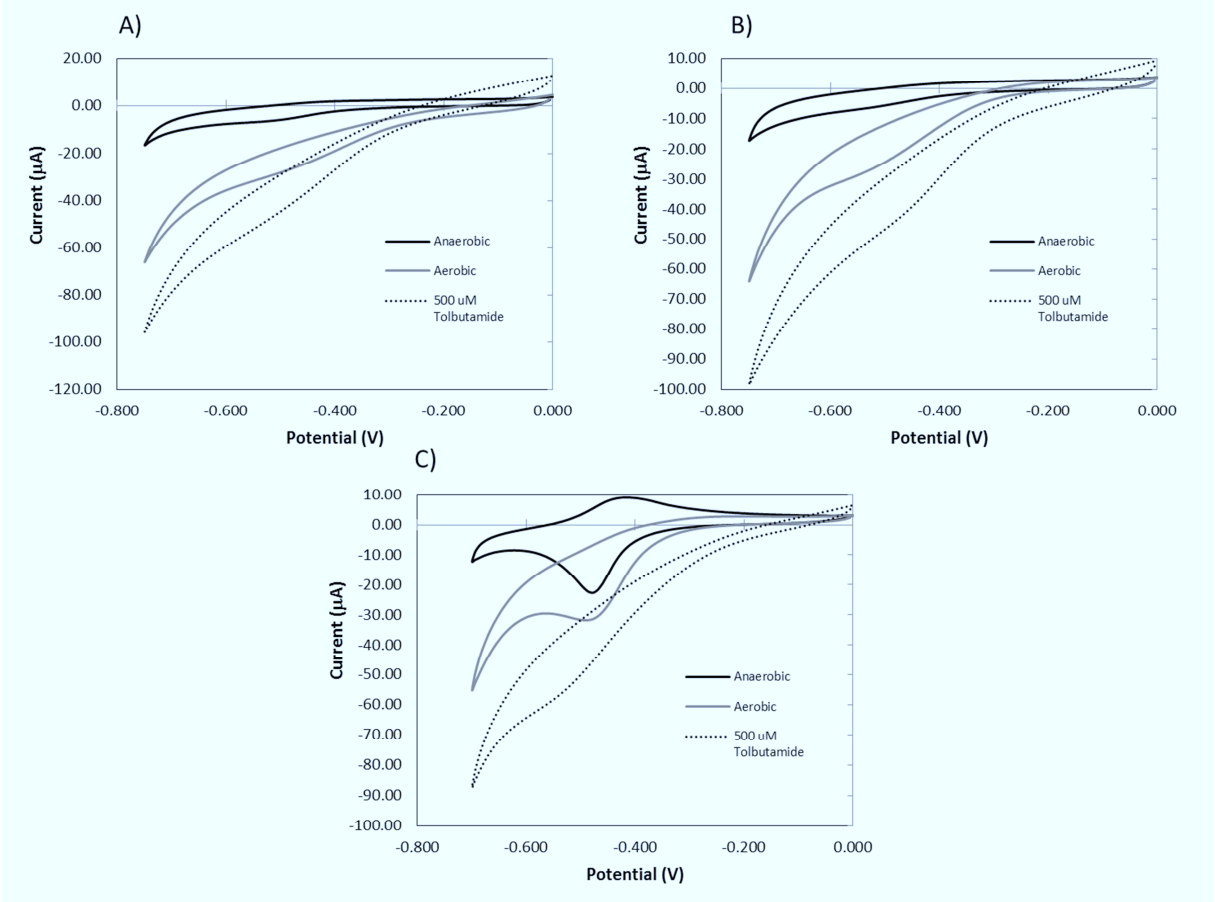

Figure 3.17 CV Scans of an MPA SAM Electrode and 2C9 and R132C Electrodes Immobilized by Random Attachment via Amine Coupling Taken in Anaerobic Buffer, Aerobic Buffer, and Aerobic Buffer containing 500 µM Tolbutamide. CV scans of (A) wt 2C9 electrode, (B) R132C electrode, and (C) MPA SAM electrode. CV scans were taken at a scan rate of 60 mV/s.

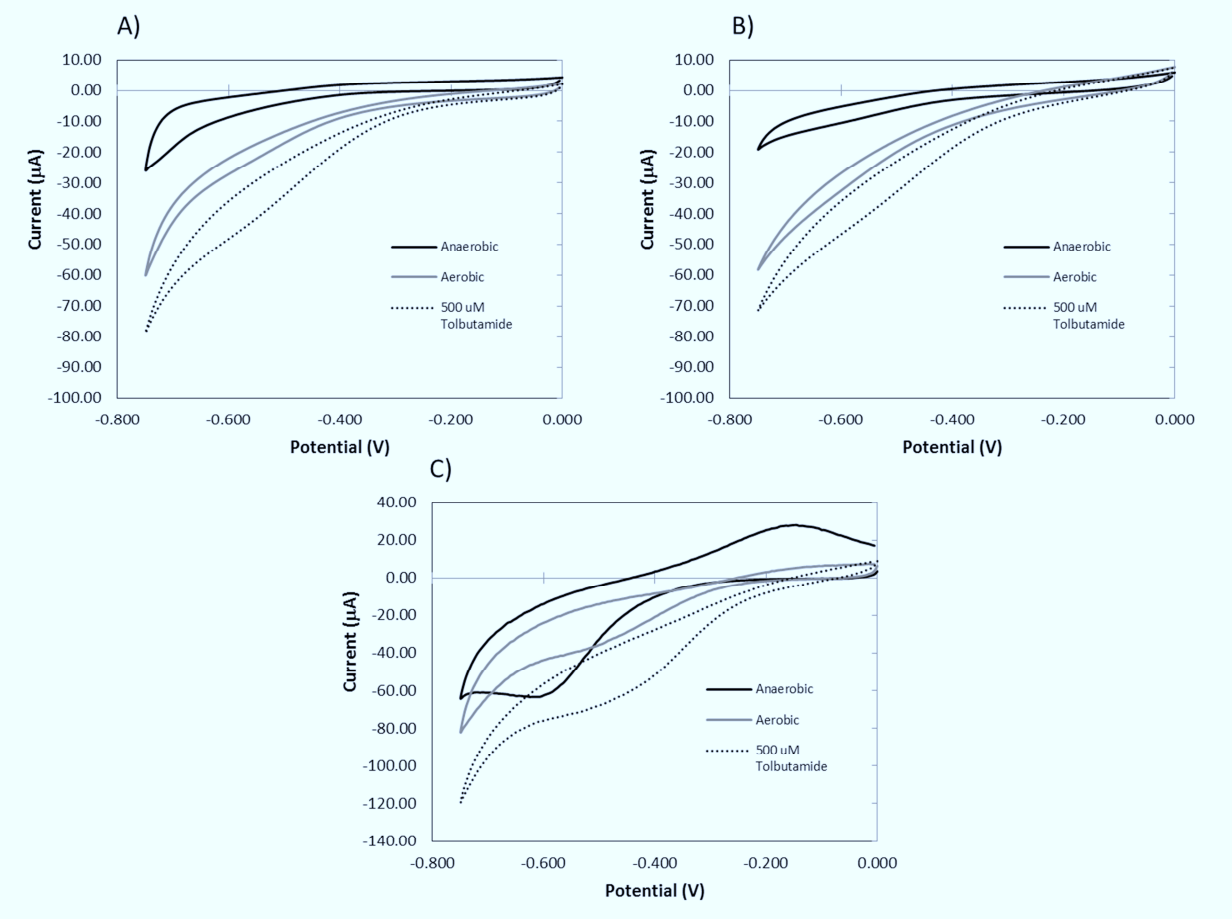

Figure 3.18 CV Scans of a Ni-NTA Electrode and 2C9 and R132C Electrodes Immobilized by Oriented Attachment via Ni-NTA/His-tag Coupling Taken in Anaerobic Buffer, Aerobic Buffer, and Aerobic Buffer containing 500 µM Tolbutamide. CV scans of (A) wt 2C9 electrode, (B) R132C electrode, and (C) Ni-NTA electrode. CV scans were taken at a scan rate of 60 mV/s.

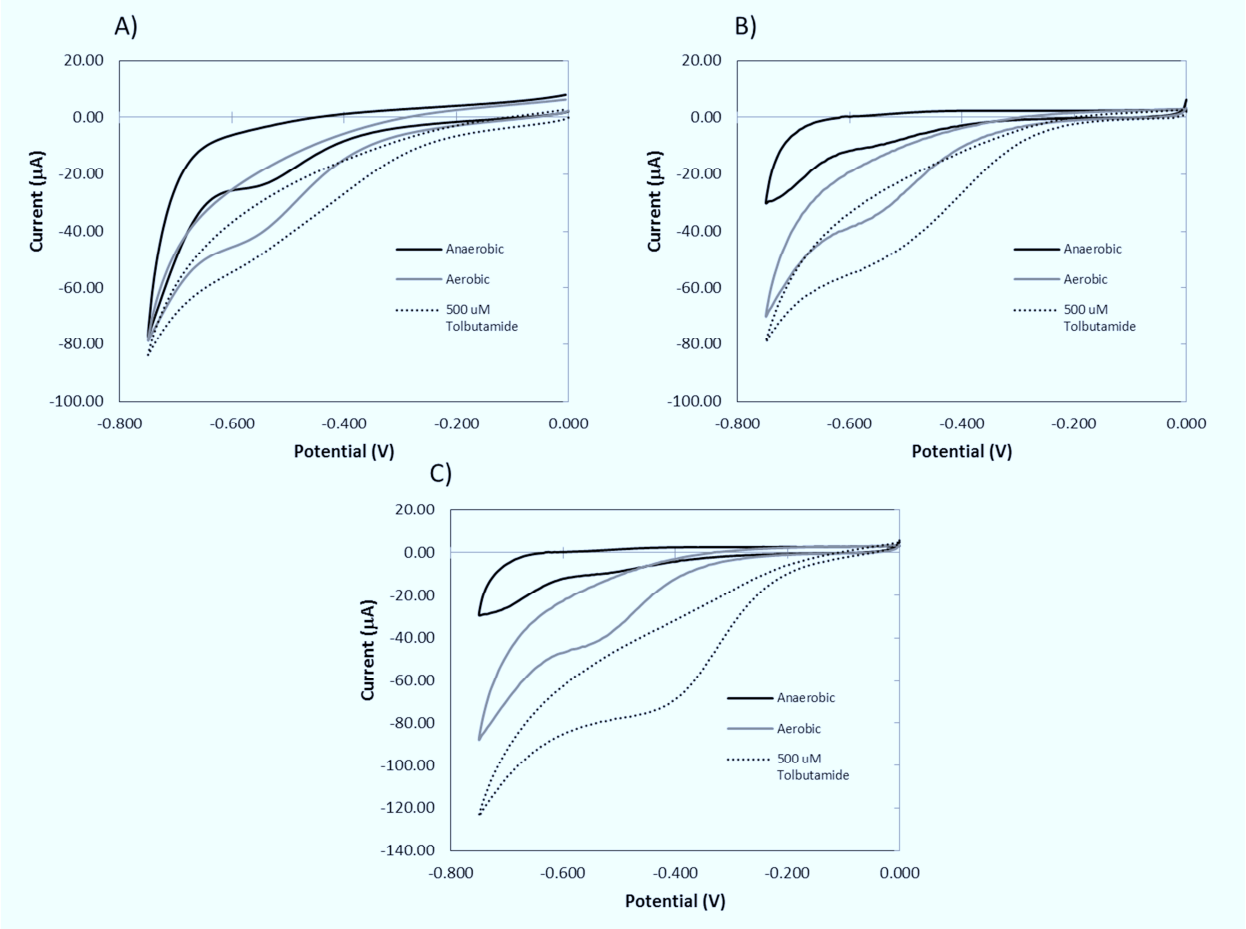

Figure 3.19 CV Scans of a Maleimide Electrode and 2C9 and R132C Electrodes Made with Oriented Attachment via Maleimide/Thiol Coupling Taken in Anaerobic Buffer, Aerobic Buffer, and Aerobic Buffer with 500 µM Tolbutamide. CV scans of (A) wt 2C9 electrode, (B) R132C electrode, and (C) Ni-NTA electrode. CV scans were taken at a scan rate of 60 mV/s.

To test these two theories, two sets of experiments were conducted. In the first set of experiments, anaerobic CV scans were taken of the no-enzyme MPA SAM, Ni-NTA, and maleimide electrodes at scan rates ranging from 10 to 1200 mV/s to observe the redox processes associated with the underlying monolayers. In the second set of experiments, aerobic CV scans were taken of a bare gold electrode with and without 800 µM tolbutamide to observe the redox process, if any, occurring with tolbutamide in aerobic buffer. Figure 3.20 shows CVs taken in aerobic buffer of the no-enzyme MPA SAM, Ni-NTA, and maleimide electrodes, along with plots of the peak current versus scan rate for each. As seen in the figure, there is a surface redox process occurring on all three electrode surfaces because the plots of peak current versus scan rate are linear. Thus, a chemical functional group on the modified electrodes or even the underlying SAM itself appears to be electroactive. In all cases, the cathodic peak is always larger than the anodic peak, suggesting that the redox process occurring on the surfaces of these electrodes may not be reversible or that there are two separate redox processes occurring that are not linked (i.e., reduction of one type of species and oxidation of another). By using Eq. (3) described in section 3.3.6 we can calculate the surface concentration of electroactive species on these electrodes. Because the reduction and oxidation processes occurring on these no-enzyme electrodes appear to be different, a surface concentration can be calculated for the anodic and

cathodic processes on each electrode. Table 3.1 shows the calculated surface concentrations of electroactive species on gold electrodes functionalized with MPA SAM, Ni-NTA, and maleimide.

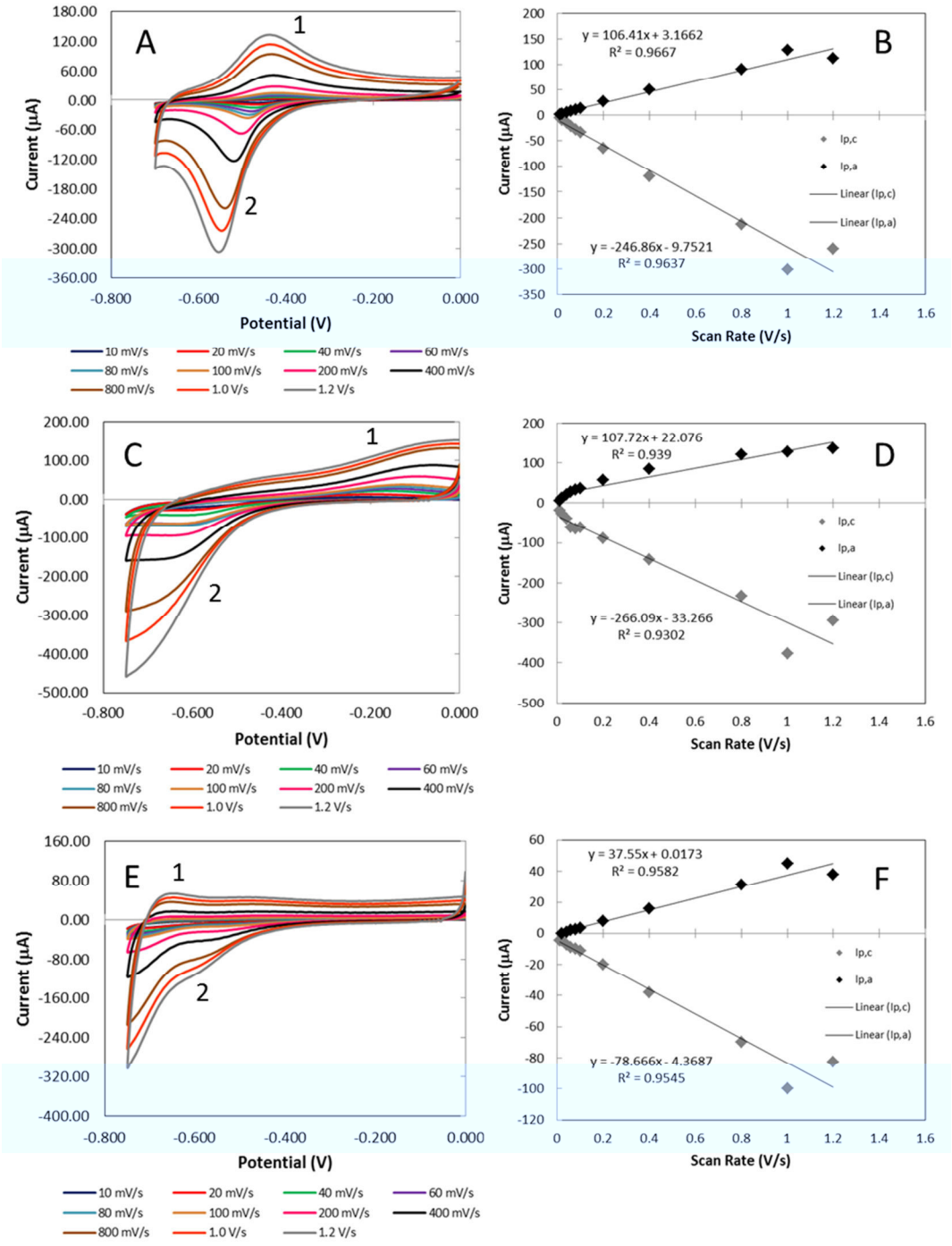

Figure 3.20 Aerobic CV Scans and Plots of Peak Current versus Scan Rate for Gold Electrodes Modified with MPA SAM, Ni-NTA, and Maleimide. (A) CV scan of MPA SAM on gold. (B) Plot of peak current versus scan rate for CV shown in (A). (C) CV scan of Ni-NTA on gold. (D) Plot of peak current versus scan rate for CV shown in (C). (E) CV scan of maleimide on gold. (F) Plot of peak current versus scan rate for CV shown in (E). The anodic and cathodic peaks in each CV scan are marked with a 1 or 2, respectively.

Electrode Surface	Electroactive Surface Concentration (moles/cm^2)	
	Reduction	Oxidation
MPA SAM	1.0×10^{-10}	4.4×10^{-11}
Ni-NTA	1.1×10^{-10}	4.4×10^{-11}
Maleimide	3.2×10^{-11}	1.5×10^{-11}

Table 3.1 Electroactive Surface Concentrations of Species Undergoing Reduction and Oxidation on Gold Electrodes Modified with MPA SAM, Ni-NTA, and Maleimide.

Three conclusions can be made based on the data in Table 3.1. One, there are more species being reduced on all three electrodes than species being oxidized, which was evident from the CV scans. Second, the calculated surface concentrations of electroactive species on these electrodes are all smaller than the surface coverage values for the MPA and cystamine SAMs found via reductive desorption (7.9×10^{-10} and 2.3×10^{-9} moles/cm^2, respectively), which makes sense if the electroactive species are located on the surface (i.e., it would be unexpected to have more electroactive species per area than there are reactive groups per area for the underlying SAMs). Finally, a comparison between the electroactive surface concentrations for the MPA SAM and Ni-NTA electrodes reveals that the values are surprisingly similar. Recall that the Ni-NTA electrode is made by first forming a MPA SAM on the gold electrode; thus, the underlying surface of the Ni-NTA electrode is an MPA SAM and as such has similar chemical properties to the unmodified MPA SAM electrode. It is possible then that the same surface redox process is occurring on the MPA SAM and Ni-NTA electrodes. Aerobic CV scans of both electrodes are markedly different but perhaps the addition of Ni-NTA to the MPA SAM affects the formal potentials and reversibility of this surface redox process, leading to a peak separation and different reduction and oxidation potentials in the CV of the Ni-NTA electrode.

Based on the aforementioned data, the redox processes seen in the CVs of the wt 2C9 and R132C electrodes are most likely monolayer-related but they could also be caused by reduction and oxidation of tolbutamide itself. Figure 3.21 shows CVs of a freshly-cleaned bare gold electrode in aerobic buffer and aerobic buffer containing 800 μM of tolbutamide.

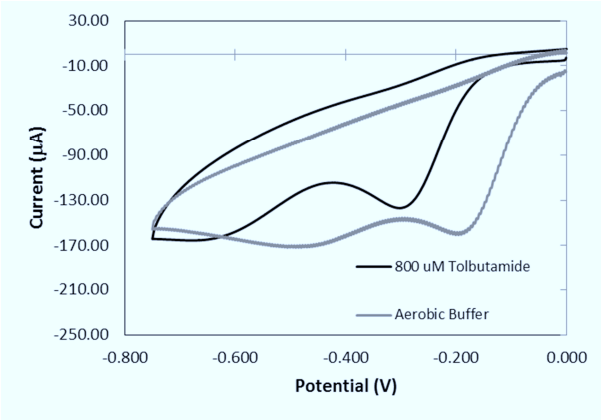

Figure 3.21 CVs of a Bare Gold Electrode in Aerobic Buffer with and without 800 μM Tolbutamide. The scan rate is 50 mV/s.

As seen in the figure, there is a reduction peak in the CV scan for a bare gold electrode in aerobic buffer with 800 μM tolbutamide; however, the same reduction peak is present in the CV scan for a bare gold electrode in aerobic buffer without tolbutamide, suggesting that tolbutamide is not the electroactive species being reduced. These results also suggest that tolbutamide is not the electroactive species being reduced in the aerobic CV scans of the wt 2C9, R132C, and no-enzyme electrodes in tolbutamide. This leaves the underlying monolayer as the source of the redox process seen in the CV scans of wt 2C9 and R132C electrodes. It is unclear exactly what redox process is occurring on the surface of the MPA SAM, Ni-NTA, and maleimide electrodes but it is certainly possible that the underlying MPA and cystamine SAMs are being electrochemically desorbed from the gold electrode during CV experiments. However, as seen previously in section 3.3.2, reductive desorption of the MPA and cystamine SAMs in 0.5 M NaOH occurs at more negative potentials (-1.0 V or less) than the cathodic potentials seen in CV scans of the no-enzyme MPA SAM, Ni-NTA, and maleimide electrodes. Therefore, reductive desorption seems unlikely, unless it occurs at pH 7.4 (the pH of the aerobic buffer) at a less negative potential than it does at a basic pH in 0.5 M NaOH. This is possible though, as more protons are available at a less basic pH and thus formation of negatively charged thiolates via reductive desorption would occur more readily because of the higher probability of charge neutralization by protons in solution.

3.3.8 Chronoamperometry with the Mediator Phenosafranine

In a final attempt to electrochemically activate 2C9 on an electrode and effect electrochemical turnover of the substrate tolbutamide, the compound phenosafranine (PS, structure seen in Figure 3.22) was tested as a mediator to shuttle electrons from the electrode to immobilized 2C9. To shuttle electrons between the electrode and immobilized 2C9, a mediator compound must have a redox potential that is more negative than 2C9. Phenosafranine's redox potential is -449 mV and is more negative than the previously published redox potential of -41 mV for 2C9 on a graphite electrode[28] and is nearly the same as the redox potential of -450 mV found for 2C9 in the Yang et al. study[1]. Most mammalian CYPs have been found to have a moderately negative redox potential; therefore PS should be a good choice for an electrochemical mediator for CYP reactions. In a previous electrochemical study with the bacterial CYP P450cin, PS was found to be the best mediator out of safranin T, FAD, FMN, ethyl viologen, and methyl viologen in terms of the amount of product produced during electrolysis[29] and therefore was chosen for use with 2C9. As an initial attempt, the single Cys mutant R132C immobilized by oriented attachment via maleimide/thiol coupling was used in a chronoamperometry experiment with PS. Aerobic buffer containing 1.2 mM PS and 1500 U/ml catalase was incubated with the R132C electrode, and the potential was set at -0.750 V. Catalase, an enzyme that converts hydrogen peroxide to water and oxygen, was added to destroy any hydrogen peroxide generated by the electrode and/or 2C9 that could denature the enzyme. Increasing concentrations of tolbutamide were added to the electrolyte solution every 10 minutes by mixing aliquots of 25 mM tolbutamide (dissolved in DMSO) with the electrolyte, and the current was measured over time. If a mediator experiment works properly, the reduction current measured at the electrode is rate-limited by the enzymatic reaction occurring with substrate as freshly oxidized mediator is only available at the surface once the enzyme completes a catalytic cycle and the reduced mediator passes electrons onto it (Figure 3.23). Thus, a plot of current versus time for a chronoamperometry experiment performed with a mediator should show stepwise increases in the steady-state current as the substrate concentration increases. Looking at

the plot in Figure 3.24 however, we can see that this is not the case. After every addition of tolbutamide, the current simply decays exponentially over time to the same value and does not undergo a stepwise increase with increasing concentrations of tolbutamide. This current decay is a well-described behavior in electrochemistry that is indicative of chronoamperometry of a redox species in an unstirred solution[30]. Thus, it appears that PS is not acting as a mediator to shuttle electrons from the electrode to immobilized R132C and is instead simply acting as a redox species in solution that is unaffected by the presence of enzyme. It is also possible though that PS *is* mediating electron transfer to immobilized R132C but the rate of diffusion of PS to the surface of the electrode is faster than the rate at which R132C reacts, meaning that the current measured for the reduction of PS is not reflecting the rate of reaction of R132C with tolbutamide. If the latter is occurring, we should be able to detect the tolbutamide metabolite 4-hydroxytolbutamide in the electrolyte solution via HPLC.

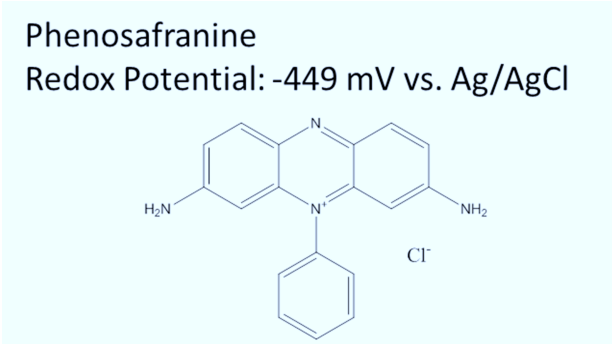

Figure 3.22 The Structure and Redox Potential of the Mediator Compound Phenosafranine.

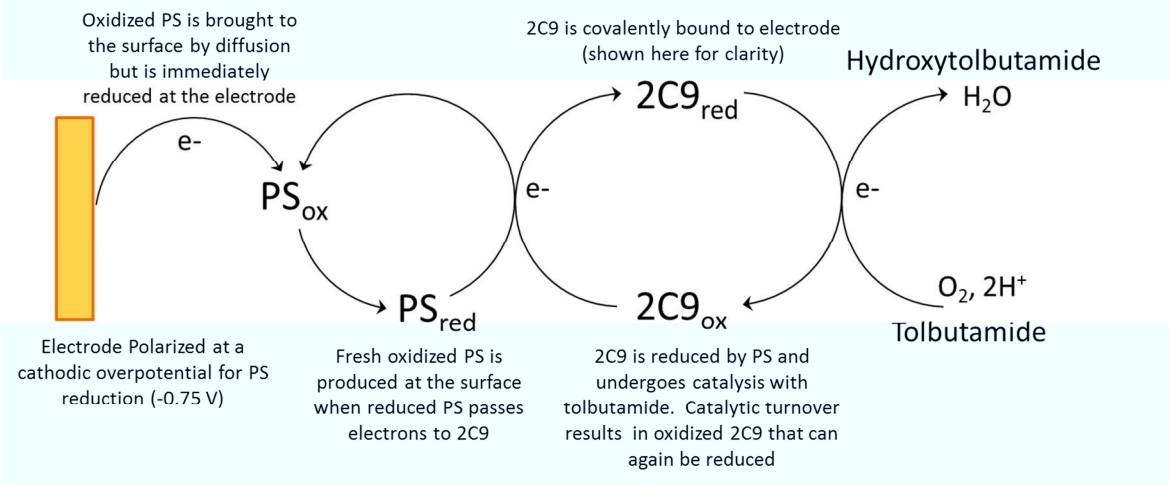

Figure 3.23 Schematic of Indirect Electrochemical Catalysis of Tolbutamide by CYP2C9 and the Mediator Phenosafranine. The electrode is polarized at a large cathodic overpotential for PS reduction (-0.75 V) such that PS is reduced as soon as it diffuses to the electrode surface. Once reduced, PS then passes electrons to immobilized 2C9 (it is shown away from the electrode in this figure for clarity) in the oxidized ferric (Fe^{3+}) state, reducing it to the ferrous (Fe^{2+}) state so that it can bind oxygen and initiate catalysis with tolbutamide. Freshly oxidized PS is only produced at the electrode surface by diffusion from the bulk or by electron transfer with immobilized 2C9. If the rate of catalysis of 2C9 with tolbutamide is faster than the rate at which diffusion brings new oxidized PS to the surface, then the reduction of PS at the electrode surface is rate-limited by the enzymatic reaction and the current measured at the electrode reflects the rate of catalysis with tolbutamide.

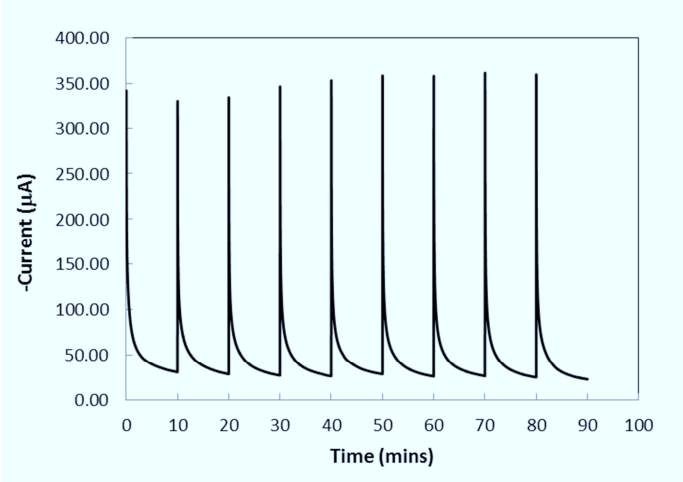

Figure 3.24 Chronoamperometry of the R132C Electrode in 1.2 mM Phenosafranine with Increasing Concentrations of Tolbutamide. Chronoamperometry was conducted at a potential of -0.75 V in the presence of 1.2 mM phenosafranine and 1500 U/ml catalase. Aliquots of 25 mM tolbutamide were added to the electrolyte (and the electrolyte was mixed) every 10 minutes in increasing concentrations from approximately 1 to 500 μM.

3.3.9 HPLC Analysis of Phenosafranine Mediator Experiment

To confirm whether or not the aforementioned PS mediator experiment was working, an electrolysis experiment with the R132C electrode (made with oriented attachment via maleimide/thiol coupling) and PS mediator was conducted in aerobic buffer with 200 μM tolbutamide for two hours. Every 10 to 20 minutes, a sample of the electrolyte was extracted for HPLC analysis and the concentration of tolbutamide was thus followed during the course of the experiment. The electrolyte solution was not stirred therefore HPLC samples were removed from as close to the electrode surface as possible. In addition to tolbutamide, the HPLC chromatograms were analyzed for the presence of the tolbutamide metabolite 4-hydroxytolbutamide as evidence of PS-mediated 2C9 catalysis. The results were somewhat surprising. Figure 3.25 shows a plot of tolbutamide concentration versus time obtained for electrolysis with PS and the R132C and no-enzyme maleimide electrodes. The concentration of tolbutamide sharply decreases from approximately 200 to 160 μM after the first 10 minutes of electrolysis for both the R132C and maleimide electrodes before leveling off and remaining nearly constant for the remainder of the experiment. It is unclear what is happening—an analysis of HPLC chromatograms did not indicate the presence of any 4-hydroxytolbutamide in the electrolyte. Whatever *is* occurring to tolbutamide during the first 10 minutes of electrolysis does not seem to be specific to 2C9 as it occurs on both the R132C and no-enzyme maleimide electrodes. This could indicate that tolbutamide is being destroyed or altered via an electrochemical process as suggested previously in section 3.3.7 on the cyclic voltammetry of 2C9 electrodes. What is certain however, is that the mediator experiment with PS and the R132C electrode is not working; if the sharp decrease in tolbutamide concentration is due to enzymatic catalysis there would be evidence of the product 4-hydroxytolbutamide in the electrolyte but this is not the case. Although this experiment serves as further proof that PS is not acting as a mediator, it raises interesting questions about the electrochemistry of tolbutamide that may be answered in future studies.

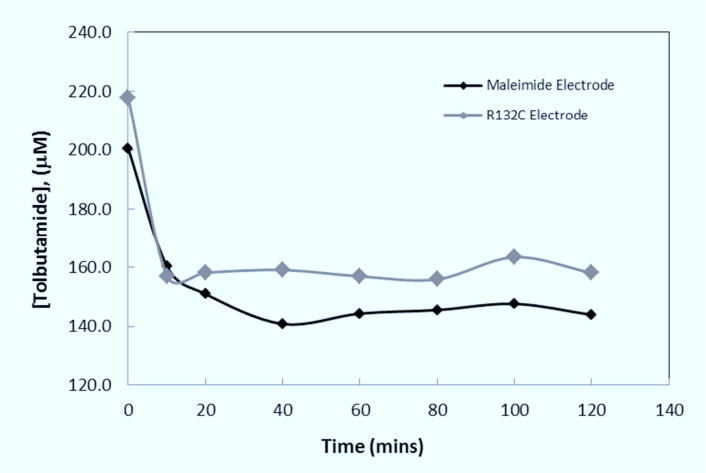

Figure 3.25 Concentration of Tolbutamide in the Electrolyte versus Time for Electrolysis with the R132C and Maleimide Electrodes and the Mediator Phenosafraine. Electrolysis was carried out at a potential of -0.75 V and with 1.2 mM PS and 1500 U/ml catalase in the electrolyte.

3.4 Conclusion

Wild-type 2C9 and the single Cys mutants R125C, R132C, and K432C were successfully immobilized on polycrystalline gold electrodes via three attachment methods in an attempt to investigate the effect, if any, that orientation of 2C9 on an electrode has on the direct electrochemistry of 2C9 and whether or not a particular orientation led to a viable 2C9 biosensor. The attachment methods investigated included random attachment via amine coupling, oriented attachment via Ni-NTA/His-tag coupling, and oriented attachment via maleimide/thiol coupling. The mutants R125C, R132C, and K432C each contain a cysteine mutation directly at the binding site of the P450 reductase enzyme on the proximal side of the heme. Attachment of these mutants via maleimide/thiol coupling to a maleimide-coated gold electrode was therefore expected to orient the enzyme on the electrode such that electron transfer occurs in the same manner as it does *in vivo* with P450 reductase. All of these attachment methods involved the formation of a SAM on gold: an MPA SAM for the case of amine coupling and Ni-NTA/His-tag coupling and a cystamine SAM for the case of maleimide/thiol coupling. Characterization of MPA and cystamine SAM-coated gold electrodes via a QCM-D revealed a single adsorption of SAM in an overnight incubation and allowed for calculation of the surface coverages of the MPA and cystamine SAMs. Reductive desorption of the MPA and cystamine SAMs via electrochemistry led to similar values for the surface coverage and further confirmed the adsorption of the MPA and cystamine SAMs on the gold electrode. Activity assays of the 2C9 electrodes with the fluorogenic substrate Vivid® BOMCC showed that the enzymes were active on electrodes and confirmed their immobilization via all three attachment methods.

Cyclic voltammetry of 2C9 electrodes however, revealed that direct electrochemistry to immobilized wt 2C9 and the mutants R125C, R132C, and K432C is not possible via all three attachment methods. A surface redox process was observed in CVs of MPA and cystamine SAM electrodes covalently coupled to the redox molecule ferrocene, suggesting that electron transfer is possible through the alkane chains of MPA and cystamine to a molecule covalently coupled to the end of the SAM. Thus, it appears that electron transfer from the SAM terminus to the buried iron heme within 2C9 is not occurring. Similar redox peaks were observed in CVs for

2C9 electrodes and no-enzyme electrodes modified only with MPA, Ni-NTA, and maleimide, suggesting that the redox peaks seen in the CVs of 2C9 electrodes are related to the underlying monolayer. Plots of the peak anodic and cathodic currents versus scan rate for CVs of the no-enzyme electrodes in aerobic buffer showed that there is a linear relationship between the two indicative of a surface redox process, providing further proof that a redox process is occurring within the SAMs.

Indirect electrochemistry with the 2C9 mutant R132C immobilized via maleimide/thiol coupling was attempted with the small molecule mediator phenosafranine. Phenosafranine had been shown previously to be an effective mediator for electron transfer to the bacterial CYP P450cin[29] and as such was chosen as a mediator for 2C9. An initial chronoamperometry experiment with the R132C electrode and PS in the presence of increasing concentrations of the 2C9 substrate tolbutamide showed that PS was not acting as a mediator to shuttle electrons from the electrode to immobilized R132C. Plots of current versus time for the chronoamperometry experiment exhibited exponential decay to the same steady-state current value after each addition of tolbutamide, suggesting that the reduction of phenosafranine at the electrode surface is not rate-limited by the enzymatic reaction and instead is occurring according to classical diffusion-limited reduction of a redox compound in an unstirred solution. To confirm whether or not this was the case, samples of the electrolyte were taken during electrolysis with the R132C electrode, PS, and tolbutamide for HPLC analysis. The product 4-hydroxytolbutamide was not detected although there was a sharp drop in the tolbutamide concentration during the first 10 minutes of electrolysis, suggesting again that the PS mediator experiment is not working. It is unclear however, what is causing the disappearance of tolbutamide in the electrolyte solution; an electrochemical process may be destroying or altering the tolbutamide.

3.5 References

1. Ying, M., Kabulski, J.L., Wollenberg, L. Chen, X., Subramanian, M., Tracy, T.S., Lederman, D., Gannett, P.M., Wu, N. Electrocatalytic drug metabolism by CYP2C9 bonded to a self-assembled monolayer-modified electrode. *Drug Metab. Disp.* (2009) 37:892-899.
2. Panicco, P., Dodhia, V.R., Fantuzzi, A., Gilardi, G. Enzyme-based amperometric platform to determine the polymorphic response in drug metabolism by cytochromes P450. *Anal. Chem.* (2011) 83:2179-2186.
3. Nikki, K., Gregory, B. Electrochemistry of redox-active protein films immobilized on self-assembled monolayers of organothiols. In: Rusling, James, ed. Surfactant Science Series. Biomolecular Films. Vol. 111. New York, NY. Marcel Dekker Inc. (2003)
4. Lewis, D.F.V., Hlavica, P. Interactions between redox partners in various cytochrome P450 systems: functional and structural aspects. *Biochim. Biophys. Acta* (2000) 1460:353-374.
5. Hlavica, P., Schulze, J., Lewis D.F.V. Functional interaction of cytochrome P450 with its redox partners: a critical assessment and update of the topology of predicted contact regions. *J. Inorg. Biochem.* (2003) 96: 279-297.
6. Kazlauskaite, J., Westlake, A.C.G., Wong, L., Hill, H.A.O. Direct electrochemistry of cytochrome P450cam. *Chem. Commun.* (1996) 18:2189-2190.
7. Kam-Wing Lo, K., Wong, L., Hill, A.O. Surface-modified mutants of cytochrome $P450_{cam}$: enzymatic properties and electrochemistry. *FEBS Letters* (1999) 451:342-346.
8. Ferroro, V.E.V., Andolfi, L., Di Nardo, G., Sadeghi, S.J., Fantuzzi, A., Cannistraro, S., Gilardi, G. Protein and electrode engineering for the covalent immobilization of P450 BMP on gold. *Anal. Chem.* (2008) 80:8438-8446.
9. Mak, L.H., Sadeghi, S.J., Fantuzzi, A., Gilardi, G. Control of human cytochrome P450 2E1 electrocatalytic response as a result of unique orientation on gold electrodes. *Anal. Chem.* (2010) 82:5357-5362.
10. Fantuzzi, A., Fairhead, M., Gilardi, G. Direct electrochemistry of immobilized human cytochrome P450 2E1. *JACS* (2004) 126:5040-5041.
11. Vela, M.E., Salvarezza, R.C., Arvia, A.J. The electroreduction kinetics of the hydrous gold oxide layers and growth modes and roughness of the electroreduced gold overlayers. *Electrochim. Acta* (1990) 35:117-125.
12. Laibinis, P.E., Palmer, B.J., Lee, S., Jennings, G.K. The synthesis of organothiols and their assembly into monolayers on gold. In: Rossnagel, S., Ulman, A., Francombe, M. ed. Thin Films. Vol. 24. Maryland Heights, MO. Academic Press (1998)
13. Mie, Y., Ikegami, M., Komatsu, Y. Gold sputtered electrode surfaces enhance direct electron transfer reactions of human cytochrome P450s. *Electrochem. Commun.* (2010) 12:860-683.
14. Ikegami, M., Mie, Y., Hirano, Y., Suzuki, M., Komatsu, Y. Size-controlled fabrication of gold nanodome arrays and its application to enzyme electrodes. *Colloids and Surfaces A: Physicochem. Eng. Aspects* (2011) 384:388-392.
15. O'Sullivan, C.K., Guilbault, G.G. Commercial quartz crystal microbalances — theory and applications. *Biosens. Bioelectron.* (1999) 14:663-670.

16. Sauerbrey, G. Verwendung von schwingquarzen zur wagung dunner schichten und zur mikrowagung. *Phys.* (1959) 155:206-222.
17. Mokrani, C., Fatisson, J., Guérente, L., Labbé, P. Structural characterization of (3-mercaptopropyl)sulfonate monolayer on gold surface. *Langmuir* (2005) 21:4400-4409.
18. Poirier, G. Characterization of organosulfur molecular monolayers on Au(111) using scanning tunneling microscopy. *Chem. Rev.* (1997) 97:1117-1127.
19. Walczak, M.M., Popenoe, D.D., Deinhammer, R.S., Lamp, B.D., Chung, C., Porter, M.D. Reductive desorption of alkanethiolate monolayers at gold: a measure of surface coverage. *Langmuir* (1991) 7:2687-2693.
20. Widrig, C.A., Chung, C., Porter, M.D. The electrochemical desorption on n-alkanethiol monolayers from polycrystalline Au and Ag electrodes. *J. Electroanal. Chem.* (1991) 310:335-339.
21. Weisshaar, D.E., Walczak, M.M., Porter, M.D. Electrochemically induced transformations of monolayers formed by self-assembly of mercaptoethanol at gold. *Langmuir* (1993) 9:323-329.
22. Walczak, M.M., Alves, C.A., Lamp, B.D., Porter, M.D. Electrochemical and X-ray photoelectron spectroscopic evidence for differences in the binding sites of alkanethiolate monolayers chemisorbed at gold. *J. Electroanal. Chem.* (1995) 396:103-114.
23. Arrondo, J.L.R., Muga, A., Castresana, J., Goñi, F.M. Quantitative studies of the structure of proteins in solution by fourier-transform infrared spectroscopy. *Prog. Biohys. Molec. Biol.* (1993) 59:23-56.
24. Eckermann, A.L., Feld, D.J., Shaw, J.A. Meade, T.J. Electrochemistry of redox-active self-assembled monolayers. *Coord. Chem. Rev.* (2010) 254:1769-1802.
25. Shumyantseva, V.V., Bulko, T.V., Archakov, A.I. Electrochemical reduction of cytochrome P450 as an approach to the construction of biosensors and bioreactors. *J. Inorgan. Biochem.* (2005) 99:1051-1063.
26. Bistolas, N., Wollenberger, U., Jung, C., Scheller, F.W. Cytochrome P450 biosensors—a review. *Biosens. Bioelectron.* (2005) 20:2408-2423.
27. Fleming, B.D., Johnson, D.L., Bond, A.M., Martin, L.L. Recent progress in cytochrome P450 enzyme electrochemistry. Expert Opin. Drug Metab. Toxicol. (2006) 2:581-589.
28. Johnson, D.L., Lewis, B.C., Elliot, D.J., Miners, J.O., Martin, L.L. Electrochemical characterization of the human cytochrome P450 CYP2C9. *Biochem. Pharmacol.* (2005) 69:1533-1541.
29. Cekic, S., Holtmann, D., Guven, G., Mangold, K., Schwaneberg, U., Schrader, J. Mediated electron transfer with P450cin. *Electrochem. Commun.* (2010) 12:1547-1550.
30. Bard, A.J., Faulkner, L. Electrochemical Methods: Fundamentals and Applications. New York, NY. John Wiley & Sons. (2001).

Chapter 4. Closing Summary and Future Directions

4.1 Closing Summary

Based on the results from CV experiments with the 2C9 electrodes and no-enzyme (MPA, Ni-NTA, and maleimide surfaces only) electrodes it appears that the direct electrochemistry of 2C9 on a gold electrode is not possible via attachment to a short-chain alkanethiol SAM by amine coupling, Ni-NTA/His-tag coupling, or maleimide/thiol coupling. The electrochemical evidence suggests that there is a surface redox process occurring on the SAM-modified electrodes but it is unclear what this redox process is. As mentioned earlier in Chapter 3, it is possible that the underlying MPA and cystamine SAMs are being 'lifted-off' of the gold electrode during electrochemical potential cycling via reductive desorption. This process was shown to occur in alkaline pH at approximately -0.8 to -1.2 V vs. Ag/AgCl (3 M NaCl); however, the reduction peaks seen in the CV scans of the 2C9 and no-enzyme electrodes were at much more positive potentials (approximately -0.45 V vs Ag/AgCl, 3 M NaCl). It is possible though that reductive desorption of the MPA and cystamine SAMs occurs at a less negative potential at a lower pH, which would explain this difference in the reduction peak potentials. More protons are present at a less basic pH; thus, reductive desorption would occur at more positive potentials at a lower pH because there is a higher probability of charge neutralization for the resulting thiolate anions in solution. Further studies are needed to test this hypothesis. A QCM-D with an electrochemical cell could be used to monitor adsorption and desorption of the MPA and cystamine SAMs during electrochemical potential cycling, and results from such a study would confirm whether or not the redox process observed in CVs of both the 2C9 and no-enzyme electrodes is due to reductive desorption of the underlying SAM.

There are very few studies in the literature on the direct electrochemistry of CYPs covalently attached to short chain alkanethiol SAMs and no studies, to our knowledge, of CYP2C9 covalently attached to a short chain alkanethiol SAM—the difficulties our laboratory has experienced working with 2C9 and electrodes modified with the short chain SAMs MPA and cystamine may be one reason why. Gilardi and co-workers have been the most successful in creating CYP biosensors with short chain alkanethiol SAMs[1-3]. In 2004, they published a communication in *JACS* on the direct electrochemistry of the drug-metabolizing CYP 2E1 covalently attached via maleimide/thiol coupling to a cystamine SAM on gold but they did not disclose the amine-reactive maleimide used to functionalize the cystamine SAM with maleimide[1]. In a follow-up study published in 2010 they used native cysteine residues on the proximal side of 2E1 to attach the enzyme to a gold electrode via maleimide/thiol coupling and used the maleimide-containing thiol dithio-bismaleimidoethane (DTME) to functionalize the gold electrode with maleimide groups[2]. Interestingly, the same research group published a study two years earlier in 2008 comparing the direct electrochemistry of the heme domain of the bacterial CYP P450 BM-3 (BMP) on gold electrodes modified by either a DTME SAM or cystamine SAM modified by N-succinimidyl-3-maleimidopropionate and found that the shorter of the two SAMs (DTME) resulted in poor attachment and electrochemistry of the immobilized enzyme[3]. This study hints at the problems associated with immobilizing CYPs on short-chain SAMs and perhaps sheds some light on why, in their recent papers, the Gilardi group appears to have abandoned short chain SAMs such as cystamine and DTME altogether in favor of longer chain SAMs such as 6-aminohexanethiol (6AHT) and 7-mercaptoheptanoic acid (7MHA)[4,5]. In addition, a curious statement in their most recent paper published this year in *Analytical*

Chemistry suggests that attachment of 2C9 to a gold electrode via maleimide/thiol coupling may not lead to electroactive enzyme[5]. In the study, the authors coupled recombinant 3A4 and 2C9 to the flavodoxin (FLD) from *Desulfovibrio vulgaris* and attached the resulting 3A4 and 2C9 fusion proteins to long-chain SAMs on gold electrodes via maleimide/thiol and amine coupling, respectively. In explaining their decision to use amine coupling and not maleimide/thiol coupling for 2C9 the authors noted, "P450 2C9 gave poor performance bound to the maleimido terminated linker and therefore a SAM specific for amino terminated groups was employed"[5]. It is unclear exactly what the authors meant as they did not give any evidence to back up their claim. However, it is clear from the progression of their work from the short chain SAMs DTME and cystamine to longer chain SAMs such as 6AHT and 7MHA that long chain SAMs are preferable and produce more stable CYP biosensors.

The general consensus in the literature on short chain SAMs is that they are less stable and more diffuse than long chain SAMs[5] but exhibit higher electron transfer rate constants across their chains[6,7]. Thus, there is a trade-off when using longer-chain SAMs for creating CYP biosensors: long-chain SAMs may be well-ordered and stable and prevent enzyme denaturation on the surface but hinder fast electron transfer to and from the electrode surface. In fact, it is well-documented that the electron transfer rate constant across alkanethiol SAMs decays exponentially as the chain number, *n*, of the SAM increases[7,8]. In light of this it is surprising that there are so many examples in the literature of attachment of CYPs to electrodes modified with long chain SAMs. In the aforementioned studies Gilardi and co-workers used long-chain SAMs of six and seven methylene units; using SAM chains that are even longer than this may be detrimental to electron transfer and result in non-functional CYP biosensors. Yang et al. claimed in their publication in *Drug Metabolism and Disposition* to have observed the direct electrochemistry of 2C9 bound to an 11-mercaptoundecanoic acid (MUA) SAM on gold. A plot of current versus concentration of the 2C9 substrate warfarin taken with the 2C9 electrode in the presence of increasing concentrations of warfarin showed nearly perfect—nay perfect—agreement with the Michaelis-Menten equation for enzyme catalysis and thus the authors also claimed to have observed electrochemically-driven 2C9 catalysis[9]. Although their work was reviewed by the scientific community and therefore accepted in the literature, our laboratory was unable to repeat their results and remains suspicious of their findings. Indeed, a surface-enhanced resonance Raman scattering (SERRS) study of the drug-metabolizing enzyme CYP 2D6 adsorbed on silver electrodes coated with an MUA SAM showed that much of the immobilized 2D6 is in an inactive P420 form, and the authors were unable to electrochemically reduce the enzyme[10], calling into question the results published by Yang et al[9]. It is possible though, that 2D6 behaves differently on an MUA-coated electrode than 2C9, which would explain the discrepancy between the results from the SERRS study with 2D6/MUA[10] and the electrochemical study by Yang et al.[9] with 2C9/MUA[9].

There is also evidence in the literature that suggests short chain alkane thiol SAMs expose immobilized CYPs to higher electric fields closer to the electrode surface, leading to conformation changes and/or the formation of inactive P420. This could be an additional reason why 2C9 electrodes made with the short chain SAMs MPA and cystamine were not electroactive. Daniel Murgida and Peter Hildebrandt have been jointly studying the conformation of CYPs immobilized on SAM-coated electrodes by SERRS and have concluded that short chain SAMs result in a decrease in the redox potential due to stabilization of the ferric (Fe^{3+}) heme and the formation of more P420[11-13]. In a study with P450 BM-3, they immobilized

BM-3 separately on SAMs with increasing chain lengths and investigated the conformation of the heme via SERRS[11]. Not only did they find evidence for the formation of inactive P420 for all of the SAM chain lengths tested, but they found that the redox potential of the immobilized BM-3 decreased with shorter-chain SAMs. These results suggest that immobilization of CYP to short chain SAMs results in stabilization of the ferric (Fe^{3+}) form of the enzyme and formation of inactive enzyme, both of which are most likely due to the high electric field that exists closer to the surface of the electrode. This electric-field induced conformation change was also found to occur with the heme-containing enzyme cytochrome c, on SAM-modified silver electrodes, suggesting that these electric field-induced conformational changes are not specific to CYP electrodes[14,15].

4.2 Future Directions

The evidence from the present studies in our laboratory and those in the literature points to the use of longer chain SAMs on gold as a better alternative for creating functional CYP biosensors. Thus, for future work we propose investigating the oriented attachment of 2C9 to a maleimide-functionalized gold electrode modified with a long-chain SAM. In particular, we propose immobilizing 2C9 via maleimide/thiol coupling to gold electrodes modified first with a mixed SAM of 6-hexanethiol (6HT) and 7MHA and then gold-nanoparticles (AuNPs) functionalized with maleimide groups (Figure 4.1). Gold nanoparticles functionalized with primary amines can be readily attached to the carboxyl groups on 7MHA via the amine-coupling reagents EDC/NHS, and the unreacted amines on the AuNPs will then react with the amine-reactive maleimide N-succinimidly-3-maleimidopropionate to form maleimide-coated AuNPs. The mixed SAM of 6HT and 7MHA is longer than the short-chain MPA and cystamine SAMs used in the present study and thus should be more stable. In addition, these same alkanethiols were used by Gilardi and co-workers in the aforementioned study on the direct electrochemistry of the fusion protein 2C9-FLD and therefore should result in electroactive enzyme[5]. Two key differences between the surface chemistry used in their study and that which we are proposing for future work in Figure 4.1 are the inclusion of AuNPs and the oriented attachment of 2C9 to the gold nanoparticles via maleimide/thiol coupling. Gold nanoparticles[16-19] and nanostructured surfaces in general[20,21] have been shown in several CYP biosensor studies to enhance electron transfer to the immobilized CYP and allow for more intimate electrical contact with the enzyme. Thus, the AuNPs should act as electron transfer relays to the surface of immobilized 2C9. In addition, coupling of one of the single Cys 2C9 mutants (R125C, R132C, or K432C) to the maleimide-coated AuNPs will ensure that the binding site for P450 reductase and the proximal side of the heme faces the electrode and the AuNPs such that electron transfer occurs in the same manner as it does *in vivo*. To our knowledge, there are no published examples of such an electrode system in the literature for the oriented attachment of 2C9 to AuNP-modified SAMs on gold and thus the proposed future work would be a significant advancement to the CYP biosensor field.

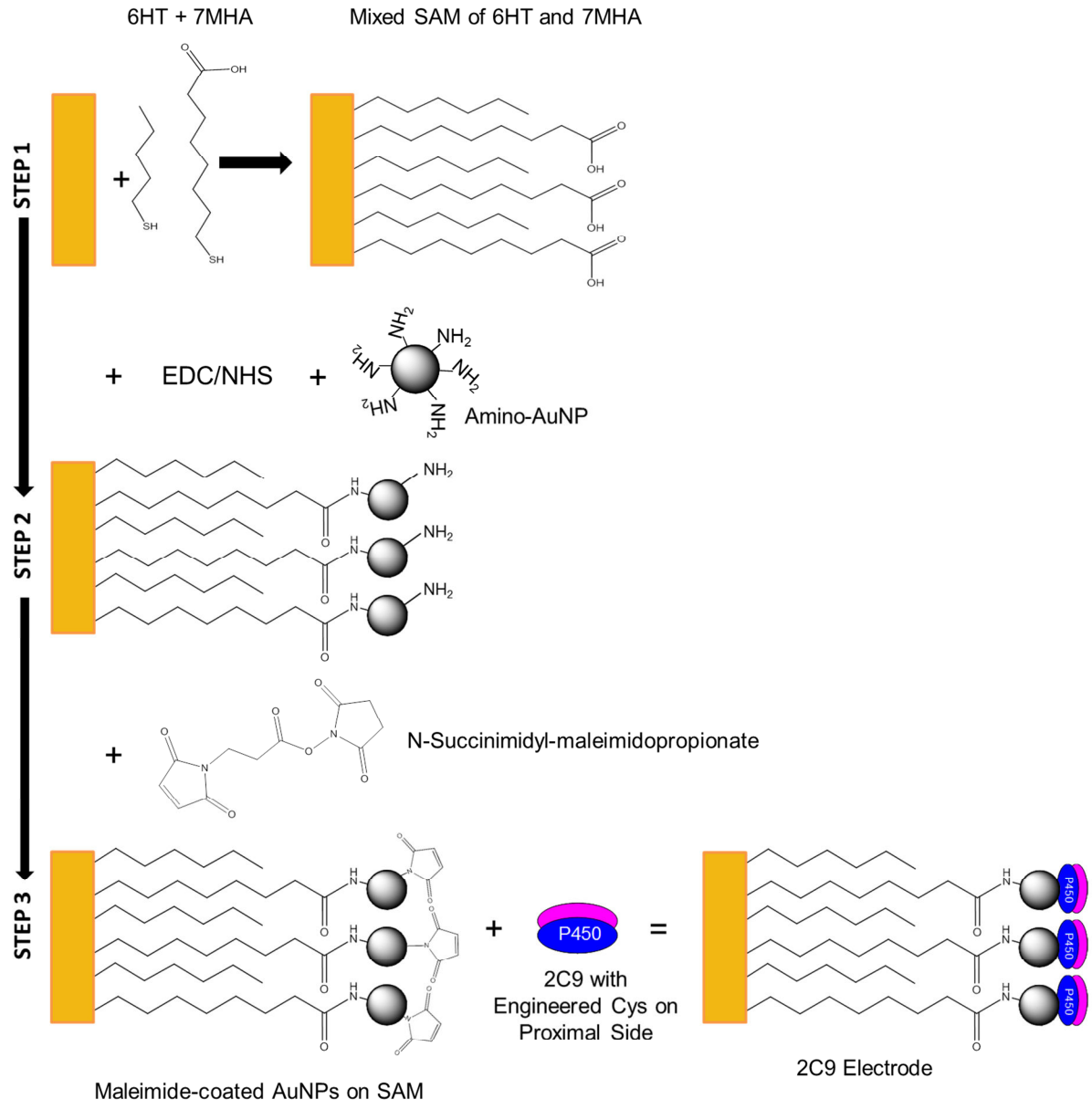

Figure 4.1 Schematic of Oriented Attachment of 2C9 to Maleimide-Functionalized AuNPs on a Mixed SAM of 6HT and 7MHA on a Gold Electrode. Step 1: Incubation of a gold electrode in a mixed solution of 6HT and 7MHA leads to the formation of a mixed SAM of 6HT and 7MHA on the electrode. Step 2: Amine coupling of amine-coated AuNPs to the carboxy-terminated SAM via the reagents EDC/NHS leads to a SAM bearing amino-functionalized AuNPs. Step 3: Reaction of the amine groups on the AuNP-SAM with N-succinimidyl-3-maleimidopropionate functionalizes the AuNPs with maleimide groups and incubation of the maleimide-AuNP electrode with a mutant 2C9 bearing a cysteine mutation on the proximal side orients the enzyme such that the binding site for P450 reductase—where electron transfer occurs *in vivo*—faces the AuNPs and the electrode.

4.3 References

1. Fantuzzi, A., Fairhead, M., Gilardi, G. Direct electrochemistry of immobilized human cytochrome P450 2E1. *JACS* (2004) 126:5040-5041.
2. Mak, L.H., Sadeghi, S.J., Fantuzzi, A., Gilardi, G. Control of human cytochrome P450 2E1 electrocatalytic response as a result of unique orientation on gold electrodes. *Anal. Chem.* (2010) 82:5357-5362.
3. Ferroro, V.E.V., Andolfi, L., Di Nardo, G., Sadeghi, S.J., Fantuzzi, A., Cannistraro, S., Gilardi, G. Protein and electrode engineering for the covalent immobilization of P450 BMP on gold. *Anal. Chem.* (2008) 80:8438-8446.
4. Fantuzzi, A., Capria, E., Mak, L.H., Dodhia, V.R., Sadeghi, S.J., Collins, S., Somers, G., Huq, E., Gilardi, G. An electrochemical microfluidic platform for human P450 drug metabolism profiling. *Anal. Chem.* (2010) 82:10222-10227.
5. Panicco, P., Dodhia, V.R., Fantuzzi, A., Gilardi, G. Enzyme-based amperometric platform to determine the polymorphic response in drug metabolism by cytochromes P450. *Anal. Chem.* (2011) 83:2179-2186.
6. Ulman, A. Formation and structure of self-assembled monolayers. Chem. Rev. (1996) 96:1533-1554.
7. Nikki, K., Gregory, B. Electrochemistry of redox-active protein films immobilized on self-assembled monolayers of organothiols. In: Rusling, James, ed. Surfactant Science Series. Biomolecular Films. Vol. 111. New York, NY. Marcel Dekker Inc. (2003)
8. Eckermann, A.L., Feld, D.J., Shaw, J.A., Meade, T.J. Electrochemistry of redox-active self-assembled monolayers. *Coord. Chem. Rev.* (2010) 254:1769-1802.
9. Yang, M., Kabulski, J.L., Wollenberg, L. Chen, X., Subramanian, M., Tracy, T.S., Lederman, D., Gannett, P.M., Wu, N. Electrocatalytic drug metabolism by CYP2C9 bonded to a self-assembled monolayer-modified electrode. *Drug Metab. Disp.* (2009) 37:892-899.
10. Bonifacio, A., Millo, D., Keizers, P.H.J., Boegschoten, R., Commandeur, J.N.M., Vermeulen, NPE., Gooijer, C., van der Zwan, G. Active-site structure, binding and redox activity of the heme-thiolate enzyme CYP2D6 immobilized on coated Ag electrodes: a surface-enhanced resonance Raman scattering study. *J. Biol. Inorg. Chem.* (2008) 13:85-96.
11. Todorovic, S., Jung, C., Hildebrandt, P., Murgida, P. Conformational transitions and redox potential shifts of cytochrome P450 induced by immobilization. *J. Biol. Inorg. Chem.* (2006) 11:119-127.
12. Murgida, D.H., Hildebrandt, P. Redox and redox-coupled processes of heme proteins and enzymes at electrochemical interfaces. *Phys. Chem. Chem. Phys.* (2005) 7:3773-3784.
13. Murgida, D.H., Hildebrandt, P. Disentangling interfacial redox processes of proteins by SERR spectroscopy. *Chem. Soc. Rev.* (2008) 37:937-945.
14. Murgida, D.H., Hildebrandt, P. Electron-transfer processes of cytochrome *c* at interfaces. New insights by surface-enhanced resonance raman spectroscopy *Acc. Chem. Res.* (2004) 37:854-861.
15. Murgida, D.H., Hildebrandt, P. Heterogeneous electron transfer of cytochrome *c* on coated silver electrodes. Electric field effects on structure and redox potential *J. Phys. Chem. B* (2001) 105:1578-1586.

16. Shumyantseva, V.V., Carrara, S., Bavastrello, V. Riley, J.D., Bulko, T.V., Skryabin, K.G., Archakov, A.I., Nicolini, C. Direct electron transfer between cytochrome P450scc and gold nanoparticles on screen-printed rhodium-graphite electrodes.
17. Shumyantseva, V.V., Bulko, T.V., Rudakov, Y.O., Kuznetsova, G.P., Samenkova, N.F., Lisitsa, A.V., Karuzina, I.I., Archakov, A.I. Electrochemical properties of cytochroms P450 using nanostructured electrodes: direct electron transfer and electro catalysis. *J. Inorgan. Biochem.* (2007) 101:859-865.
18. Shumyantseva, V.V., Bulko, T.V., Suprun, E.V., Chalenko, Y.M., Yu.Vagin, M., Rudakov, YO., Shatskaya, MA., Archkov, AI. Electrochemical investigations of cytochrome P450. *Biochim. Biophys. Acta Proteins & Proteomics* (2011) 1814:94-101.
19. Liu, S., Peng, L., Yang, X., Wu, Y., He, L. Electrochemistry of cytochrome P450 enzyme on nanoparticle-containing membrane-coated electrode and its applications for drug sensing. *Anal. Biochem.* (2008) 375:209-216.
20. Mie, Y., Ikegami, M., Komatsu, Y. Gold sputtered electrode surfaces enhance direct electron transfer reactions of human cytochrome P450s. *Electrochem. Commun.* (2010) 12:860-683.
21. Ikegami, M., Mie, Y., Hirano, Y., Suzuki, M., Komatsu, Y. Size-controlled fabrication of gold nanodome arrays and its application to enzyme electrodes. *Colloids and Surfaces A: Physicochem. Eng. Aspects* (2011) 384:388-392.